Phage Display as a Tool for Probing Lipid A Biosynthesis

by

Ronald J. Jenkins

A dissertation submitted in partial fulfillment
of the requirements for the degree of
Doctor of Philosophy
(Medicinal Chemistry)
in The University of Michigan
2013

Doctoral Committee:

Assistant Professor Garry D. Dotson, Chair
Professor Carol A. Fierke
Assistant Professor Matthew B. Soellner
Professor Ronald W. Woodard

To my family,
Katie, Mom, Dad, Jamie and Keegan

Acknowledgements

There are far too many individuals who have been influential in my life to thank in just two pages. I've been blessed to have some of the greatest teachers and mentors from grade school through my Ph.D. work. I would like to thank my undergraduate mentor at Temple, Dr. Jonathan Shackman for encouraging me to come to the University of Michigan. I would like to thank my mentor Connie Azumaya at AstraZeneca pharmaceuticals who has always been both a great influence and a great person. I owe a world of gratitude to my Ph.D. mentor and friend, Dr. Garry D. Dotson for all that he has done for me over the past four years. Garry's mentorship went beyond the classroom and lab. While he has challenged me as a scientist, he has taught me to be a better person. His scientific vision and hard-working attitude are only matched by his patience as a teacher. I hope one day I can become the mentor to students that you were to me. Thank you for everything, Garry. I would like to thank Dr. Cherie Dotson who has been a mentor outside of the classroom to me and so many students in the College of Pharmacy. I would also like to thank my thesis committee, Dr. Carol Fierke, Dr. Matthew Soellner and Dr. Ronald W. Woodard for all of their advice and support.

I would like to thank my old friends Ben Schreiber, Nick Stanavitch, and Mike and Matt Figured for everything they've done for me over the years; keeping me balanced or at least trying. I would like to acknowledge the brothers of Pi Lambda Phi fraternity for great years and all they've done for me. To the Dotson lab, I would like to thank Dr. James Patrone, Dr. Jiangwei Yao, and Kyle Heslip for fostering an

environment of scientific rigor and hard work, yet always finding a way to incorporate laughter and fun into science. I would personally like to my friends who have made the long journey to a Ph.D. easier Dr. Caleb Bates, Dr. Katrina Lexa, Dr. James Patrone, Dr. Bob Rarig, Kyle Heslip, Doug Hansen, Kris Brandvold, Scotty Barraza, Bryan Yestrepsky and Frank Kwarcinski. I would like to thank the Royal's Baseball team for four great summers in Ann Arbor.

Last, but not least, I would like to thank the most important and influential people in my life, my family. To my wife, Katie, thank you for patience and understanding of the long hours at work, listening to our chemistry conversations when we were outside of work and absolutely everything you've done for me. I would not have been able to complete my Ph.D. without your love and support. I would like to acknowledge and thank my parents, Ron and Linda Jenkins, my sister Jamie, and all of the Stevens and Jenkins families (it would take a full thesis chapter to list all of them!). Without their guidance and support I wouldn't be the person I am today. I would like to give a special thanks to our long-time family friends the Komar's, Burak's, and Pencek's. Finally I would like to acknowledge the O'Connor family (Pat, Cheryl, Michelle, Ben Dobil, Melissa, Pat, Kristin, Sean, and Kira) for all of their support.

Table of Contents

List of Figures

List of Tables

Abstract

The lipid A biosynthetic pathway is exclusive to gram-negative bacteria, thus making it an ideal target for antimicrobial drug discovery. Furthermore, two distinct acyltransferases, UDP-GlcNAc acyltransferase (LpxA) and UDP-3-*O*-(Acyl)-GlcN acyltransferase (LpxD), display structural and functional similarities within the pathway. Such similarities offer the potential to design inhibitors capable of targeting both active sites. This provides a unique paradigm to combating antimicrobial resistance by decreasing the likelihood that the bacteria would obtain resistance, through increasing the number of mutations necessary for the microbe to survive the therapeutic.

Phage display was used to identify several LpxD-inhibitory peptides, one of which (RJPXD33) also inhibited LpxA (LpxD K_d = 7 μM; LpxA K_d = 22 μM) and one which was found to be selective for LpxD (RJPXD34; K_d = 31 μM). Both peptides displayed antimicrobial activity when expressed as N-terminal fusions to thioredoxin. A fluorescence polarization (FP) binding assay was developed for LpxD utilizing a fluorescein-labeled RJPXD33 (K_d = 600 nM) and for LpxA using a fluorescein-labeled Peptide 920 (K_d = 200 nM). With the FP binding assay, RJPXD33 was shown to bind competitively with acyl-ACP. RJPXD33 was co-crystallized with LpxA, in order to gain an understanding of how RJPXD33 binds to LpxA. The structural data suggested that RJPXD33 mimics the acyl-phosphopantetheine moiety of acyl-acyl carrier protein (ACP), the native substrate of LpxA. Biochemical characterization of truncated variations of RJPXD33 confirmed this model and showed that smaller peptides could be

synthesized that could inhibit LpxA with similar potency. While RJPXD33 could not be crystallized with LpxD, a crosslinking strategy using photo-affinity derivatives of RJPXD33 was developed for mapping the peptide-protein interactions. Finally, the FP binding assay was employed to screen a small molecule library (~120,000 compounds) against LpxD. The hits were reconfirmed with a continuous, fluorescent enzyme assay developed for both LpxA and LpxD. Eleven compounds ranging in potency (IC_{50}'s = 0.1 – 30 μM) were identified, three of which demonstrated in vivo toxicity in *Escherichia coli* lacking the multidrug efflux pump, *TolC*. These molecules provide a foundation for the future development of more potent small molecule inhibitors of LpxD.

Chapter 1

Introduction

Current Trends in Antimicrobial Chemotherapy.

The discovery and clinical utilization of antimicrobial chemotherapeutic agents in the late 1930's was a monumental feat towards combating bacterial pathogenesis world-wide (1). However, increases in clinical antimicrobial resistance to most of the currently used therapeutics has threatened to offset such advances (2). In addition, increases in the number of immune-compromised populations owing to advances in organ transplants, individuals with acquired immune deficiency disease (AIDs), and advances in treating burn victims has seen an emergence of new pathogenic organisms and the reemergence of microbial pathogens long thought to be completely curable (3). The constant threat of "deliberate emergence" of pathogens released into society through bioterrorism plots, further poses a significant threat to public health and welfare. Despite the necessity for novel chemotherapeutics to thwart these trends, only two antibacterial drugs with novel scaffolds and modes of action have been clinically approved from the late 1960's to 2008 (4). It has been hypothesized that lower profit margins, owing to decreased life-span of compounds, have effectively lessened pharmaceutical impact on development of antimicrobial chemotherapies (5). The aforementioned dilemma has prompted a call for the design of novel antibacterial treatments along with development of novel paradigms to combat and potentially deplete the unrelenting rise of resistance.

One such paradigm includes the design of agents that target virulence factors. The overarching hypothesis is that virulence factors are not essential to the growth or survival of the pathogen, and thus inhibition of these virulence factors should reduce selective pressures on the pathogen, ultimately decreasing the likelihood of resistance. Some bacterial toxins have been shown to induce toxicity through effects on mammalian cell signaling pathways. The Anthrax lethal factor (LF) has been shown to proteolytically cleave kinases within the mitogen activated protein kinase (MAPK) pathway (6). Forino *et. al*. have successfully identified hydroxamate-containing small molecule inhibitors of LF which prevented MAPK Kinase (MAPKK) degradation and decreased cytotoxicity to murine macrophages in the presence of LF (7). Such molecules offer the potential to combat the rapid toxicity associated with this bioterrorism agent, despite the fact that LF is not essential to the survival of Anthrax strains. *Vibrio cholerae*, an infectious pathogen which causes diarrhea and water loss, releases cholera toxin (CT) that has been shown to ADP-ribosylate regulatory G-proteins preventing the $G_s\alpha$ subunit from hydrolyzing GTP, leaving the G-protein in a permanent "on state" (8). This state increases intracellular Ca^{2+} concentration in the intestinal tract, which is followed by a release of H_2O and Na^+ from the epithelial lining. Utilizing a whole-cell screen, Hung *et. al*. were able to target a transcriptional regulator of CT (9). Though the molecules did not inhibit growth in culture media, they protected mice from colonization of the *V. cholerae*. This suggested that targeting gene expression of toxins is another way to decrease virulence.

While this paradigm offers much potential, there are disadvantages. One disadvantage is that immune-compromised patients lack the ability to clear infections, requiring continual dosing regimens or combinatorial therapy with a bactericidal agent.

Furthermore, while the small molecules are not directly affecting survival of the pathogen, inhibition of virulence factors allows the immune system to eradicate the infection. This, by definition, is a selective pressure for survival and growth of the pathogen. Further investigation is warranted to conclude that the original hypothesis is correct.

There has been much focus around the paradigm of designing novel classes of antimicrobials which include novel chemical scaffolds and subcellular targets (10). Natural products and semi-synthetic derivatives, from underexplored niches, are potential examples for finding novel scaffolds with diverse effects. This approach comes with no surprise as natural products and their analogues account for ~68% of the antibacterial novel chemical entities from 1981 – 2006 (11). One dilemma in screening libraries of natural products, especially in whole cell assays, is the risk of re-identification of compounds previously identified. This "re-inventing" of the wheel is time consuming and offers no new advances in antibacterial drug discovery. Furthermore, producing large quantities of natural products can be a daunting task in its own right. Strategies to genetically engineer microbes to produce large-scale and novel antimicrobials have been an active area of research to address these two problems (12-14). However, to properly perform these genetic manipulations a thorough understanding of the biosynthetic pathways and the microorganisms are prerequisites, which may require many years of basic research.

More recent approaches towards identifying novel scaffolds have included repurposing chemical libraries to screen for antimicrobial inhibitors, as well as synthesizing complex combinatorial libraries to expand beyond the chemical space of

existing libraries. Miller *et. al*. identified novel biotin synthase inhibitors from a pre-existing small molecule library designed to identify protein kinase inhibitors (15). This strategy provides a plethora of compounds at the grasp of pharmaceutical companies. However, one might question the utilization of compounds targeted towards eukaryotic proteins, owing to the potential for adverse side effects. Approaches towards diversifying chemical libraries through combinatorial synthetic strategies have been pioneered by Stuart Schreiber and colleagues (16). While stereospecific properties of molecules may enhance binding, skeletally diverse products may contain a vast number of stereocenters. When chemically synthesizing such libraries, one must take into account that the total number of isomers of a single molecule synthesized is 2^n, where n is the number of stereocenters. For example, if a single molecule contains 5 stereocenters, and only one isomer is active, the library would include 31 unwanted isomers of a single molecule. While this disadvantage is time consuming and unproductive, these studies do increase our chemical screening space and our fundamental understanding of chemical reactivity, and therefore should not be disregarded.

The strategies mentioned thus far all offer a great contribution towards design and identification of novel chemotherapeutic agents against microbial pathogenesis. Furthermore, multiple paradigms and strategies should be pursued in order to prevent a bottleneck in scientific discovery. A strategy that has not received much attention is the design of chemotherapeutics to target multiple proteins on the basis of similar structure and functionality. Inhibition of two enzymes decreases the likelihood of target mutation-mediated resistance by increasing the minimal number of essential gene mutations required for the pathogen to obtain resistance to the therapeutic (17). While most efforts

have been aimed at the ATPase domains of DNA transcription machinery (gyrase and topoisomerase), other classes such as peptidoglycan ligases are beginning to emerge as potential targets (18-21). However, this strategy is not without disadvantage, as difficulty in targeting two similar proteins could result in unwanted promiscuity which could present adverse side effects. Further, identifying targets essential to microbial survival that share highly similar structure and function may prove to be considerably difficult. We felt the lipid A biosynthetic pathway could be an appropriate molecular avenue for this approach owing to the high degree of structural and functional similarity between the early acyltransferases in the pathway. Furthermore, lipid A is essential and exclusive to gram-negative microbes decreasing the likelihood of adverse interactions with the host organism. The results we have obtained suggest this strategy can be utilized effectively in antimicrobial drug design.

Lipid A Biosynthesis: The Hydrophobic Anchor of Lipopolysaccharide.

Lipopolysaccharide (LPS) constitutes the outer monolayer of the outer cell membrane of gram-negative bacteria (22,23). This protective sheath encapsulates the bacterial peptidoglycan wall, as opposed to gram-positive bacteria which contain an environmentally exposed peptidoglycan layer (24). LPS has been shown to act as a permeability barrier to protect gram negative pathogens from hydrophobic antibiotics (25,26). LPS is constructed of three domains (Figure 1.1): a multi-acylated oligosaccharide, known as lipid A, which is essential to growth of most gram-negative bacteria (27), a core polysaccharide region and *O*-antigen polysaccharide both of which are not essential, but play a role in virulence (22). Lipid A also plays a structural role, anchoring LPS to the outer cell membrane. Furthermore, there are many diverse

modifications to lipid A which play a functional role in protection of gram-negative bacteria from environmental stresses and the mammalian immune response (22).

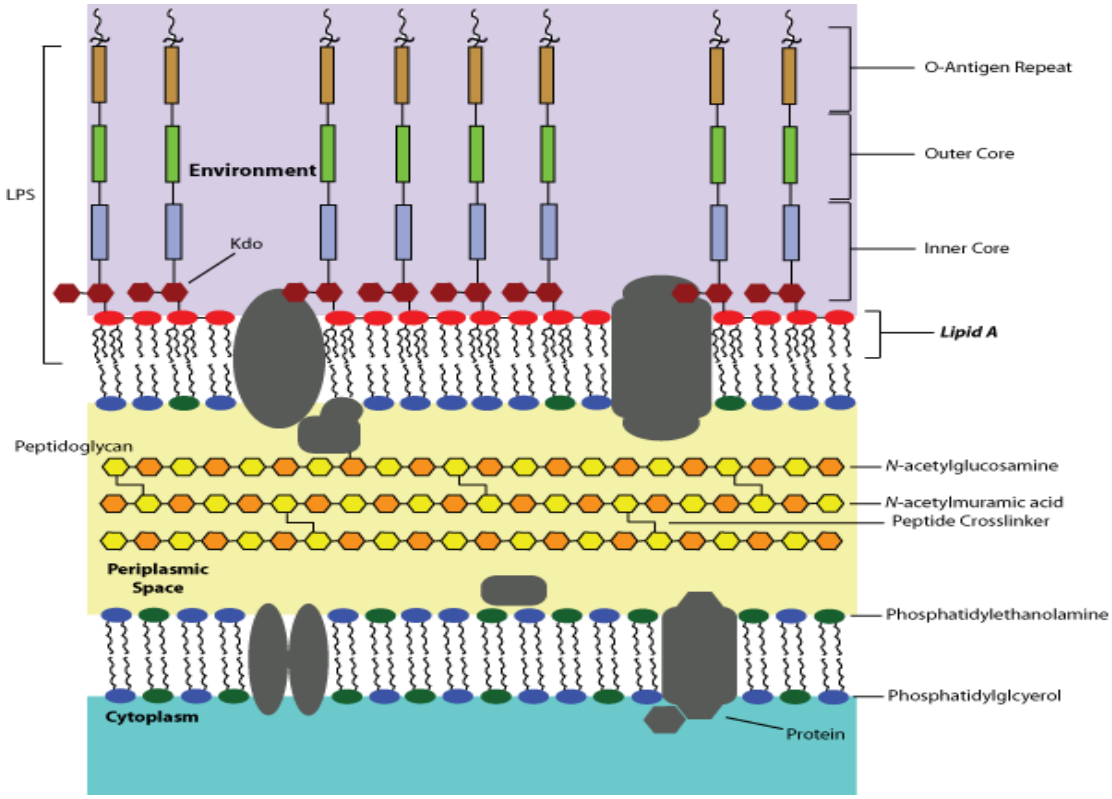

Figure 1.1. The inner and outer membranes of gram-negative bacteria**.**

Lipid A initiates the host-cell immune response by stimulating the release of Tumor Necrosis Factor (TNF) and IL-β through activation of the Toll-Like Receptor 4 (TLR-4) and a co-receptor MD-2 (28-31). Though necessary for the host immune response to clear bacterial infections, over-stimulation of these responses can lead to septic shock and ultimately death (32). The biological significance of lipid A in relation to the host-immune response further makes lipid A biosynthesis an attractive target for discovery and design of antimicrobial therapeutics.

Lipid A biosynthesis is comprised of nine constitutive steps as shown in Figure 1.2. The pathway begins with the catalytic acylation of UDP-*N*-acetylglucosamine (UDP-

GlcNAc) via LpxA which utilizes an acyl-acyl carrier protein (ACP) donor (33,34). The formation of UDP-3-*O*-(*R*-3-hydroxymyristoyl)-*N*-acetylglucosamine in *Escherichia coli* has been shown to be a thermodynamically unfavorable reaction with a K_{eq} = 0.01 (35). The deacylation of the *N*-acetyl moiety, catalyzed by LpxC, has been shown to be the first irreversible step in lipid A biosynthesis and a key regulatory step of the pathway in *E. coli* (36-38). A subsequent acylation of the free amine by the acyltransferase LpxD, constitutes the third reaction step in the pathway (39). UDP is catalytically hydrolyzed to UMP and a diacyl-glucosamine-1-phosphate moiety (lipid X) by LpxH (40,41). Lipid X is subsequently linked to the product of LpxD via LpxB to form a disaccharide with a 1,6-β-linkage (42). The lipid A kinase, LpxK, phosphorylates the 4'-OH of the β-linked tetra acylated disaccharide (43). KdtA, also known as WaaA, adds two Kdo moieties onto the 6'-hydroxyl, which is followed by the addition of two acyl-chains by two separate membrane bound acyltransferases, LpxL and LpxM (44-48). With the exception of the first three soluble cytosolic enzymes (LpxA, LpxC and LpxD), the latter steps are all catalyzed on the cytosolic face of the inner membrane. The mature Kdo_2-lipid A species is subsequently flipped to the periplasmic face of the inner membrane by an ATP-dependent transporter, MsbA (49). The translocation of LPS to the outer membrane is carried out by a trans-envelope complex stretching from the inner membrane to the outer membrane by a series of lipopolysaccharide transport proteins (LptA–G) (50). However, the complete mechanism of lipid A transport remains an active area of research.

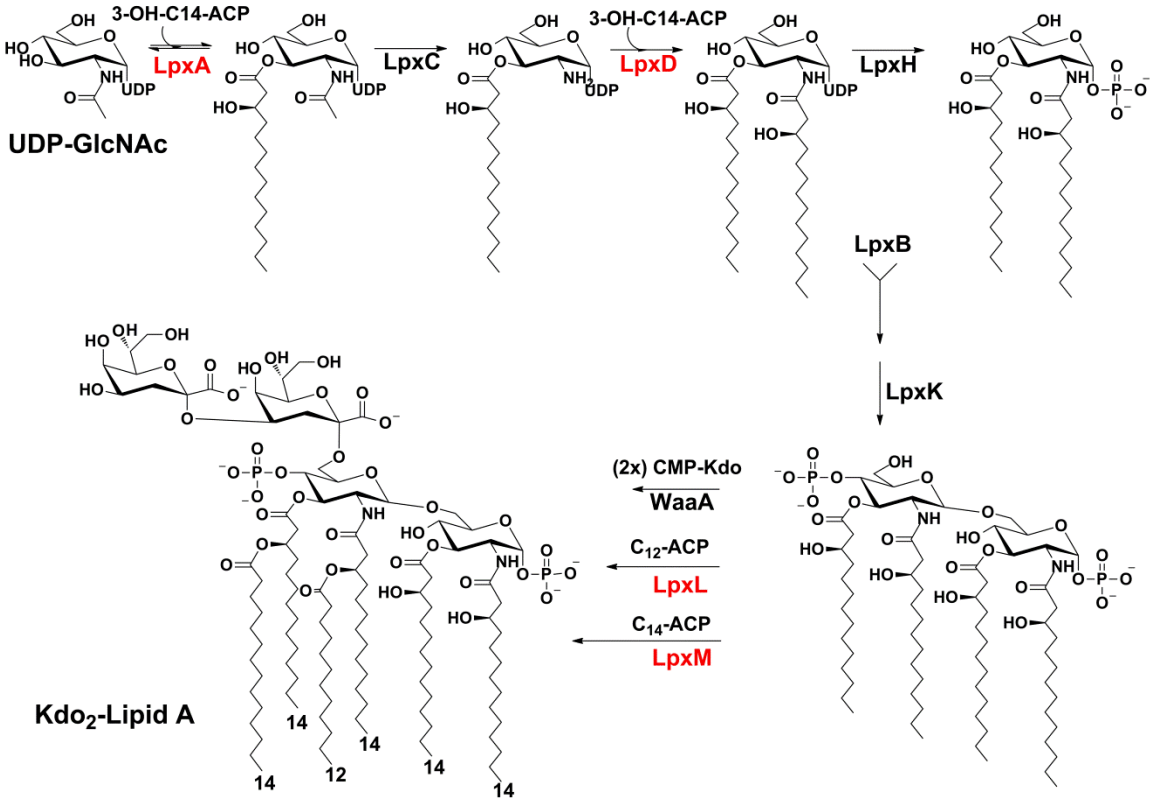

Figure 1.2. Representative scheme of lipid A biosynthesis in *E. coli*. Acyltransferases are highlighted in red.

The core of lipid A tends to be relatively conserved through the glucosamine moiety, though there are organisms such as *Leptospira interrogans* which catalytically convert the 3-hydroxyl of UDP-GlcNAc to an amine (51,52). Beyond the glucosamine backbone, one of the more highly variable moieties is the length of the acyl chains (53-56). Differences in acyl chains play an important role in recognition by the host-immune system (ref 8 and those within). Further variations come about by modifications of mature lipid A such as hydrolysis of an acyloxyacyl chain, dephosphorylation of the 1'- or 4'-phosphates, and masking of negative charges on the phosphates that different organisms use to evade the host immune system (22,57-61). It has been postulated that modified lipid A molecules could be utilized for potential vaccination, though discovery

of therapeutics that target the early steps of the pathway may provide for a more direct route in preventing bacterial sepsis (8).

Temperature sensitive mutants of early steps of lipid A biosynthesis have demonstrated that lipid A is required for viability of the microbe (36,39,62). However, the essentiality of a gene target is not always indicative of a good drug target. The discovery of *E. coli* LpxC inhibitors provided validation that the committed step of lipid A biosynthesis was a viable drug target (63). This initial discovery of the first LpxC inhibitor led to a concerted effort towards optimizing the compound in order to find broad spectrum LpxC inhibitors (63-67). More recently Benson *et. al*. have demonstrated that overexpression of an inhibitory peptide targeting LpxA displayed toxicity in *E. coli* (68), thus chemically validating LpxA as a antimicrobial target.

LpxA is a trimeric enzyme and the first discovered to contain the unique left-handed β-helical (LβH) fold (69,70). The active site of LpxA has been shown to be comprised of a catalytic histidine (His125 in *E. coli*) which deprotonates the 3-OH of the UDP-GlcNAc moiety allowing for nucleophilic attack into the thioester of the acyl-ACP substrate (71). Wyckoff and Raetz also demonstrated that all three active sites of the trimer are active. LpxA from several species have been co-crystallized with substrates UDP-GlcNAc and acyl-methylphosphopantethenine as well as products UDP-3-*O*-(*R*-3-hydroxyacyl)-GlcNAc (51,72,73). The acyl chains of both ligands were shown to bind in the hydrophobic pocket between two monomeric subunits of the LpxA trimer, highlighting the acyl chain binding region of LpxA. The α-helical C-terminal region of LpxA was further implicated in binding of the UDP moiety of both substrate and product,

and thus termed the UDP binding domain. The binding modalities of these ligands will be further discussed in chapter 4.

Though LpxA has been extensively studied, only more recently the second acyltransferase, LpxD has begun finding attention in literature. LpxD displays high sequence homology to LpxA (27.2% from a Clustal Pairwise Analysis). Hunter and coworkers were able to crystallize LpxD from *C. trachomatis* (74). Interestingly, it was not previously known that LpxD could bind UDP-GlcNAc, but Hunter and coworkers effectively demonstrated crystallographic evidence of the ligand•protein interaction, albeit at concentrations above physiological conditions. LpxD is comprised of an α-helical UDP binding domain, a LβH motif highly similar to that of LpxA (Figure 1.3), and a C-terminal α-helical extension region. Structural differences arise at the C-terminus of the LβH domain between *C. trachomatis* LpxD and *E. coli* LpxD, which account for the differences in acyl chain selectivity of the two proteins (75). The profound similarity between the structure and function of LpxA and LpxD, combined with the knowledge that they could bind similar ligands, led us to the hypothesis that LpxD and LpxA could potentially be exploited to discover dual-targeting inhibitory probes for the future design of inhibitory small molecules.

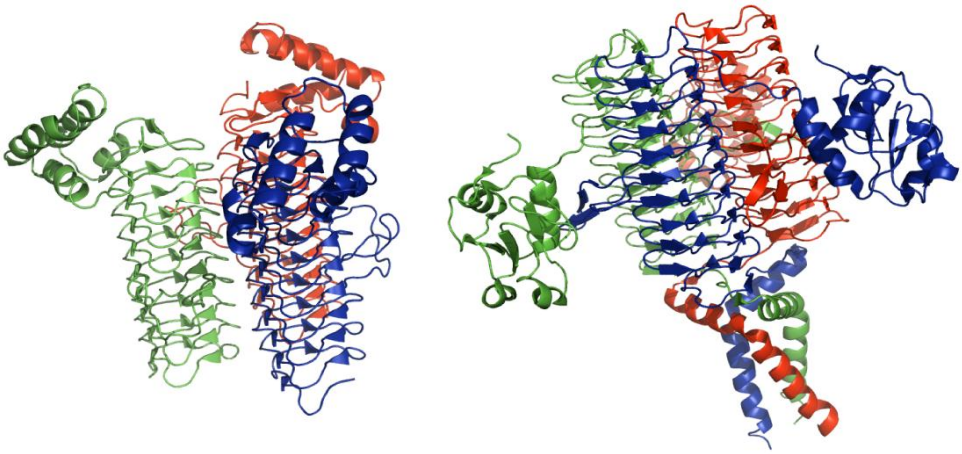

Figure 1.3. Structures of *E. coli* LpxA (left; PDB 1LXA) and *E. coli* LpxD (right; PDB 3EH0) (70,75).

Phage Display as a Tool for Probe Design.

Filamentous phage, such as M13, have the ability to display foreign, small peptides on their coat surface (76). Two of the M13 coat proteins are the major coat protein (pVIII) and a minor coat protein (pIII). Both of these have demonstrated the ability to display foreign peptides at the ends of their sequences (77). The pIII coat is more widely utilized today as there are only five copies expressed on the cellular surface compared to the pVIII protein which contains nearly 2700 copies per phage particle (77-80). This provides for lower valency and ultimately higher binding affinity of identified ligands. M13 phage are lysogenic and thus are not plaque forming, requiring a method for selection and detection. This was overcome by equipping the M13 with a lacZΔ15 α-complementation factor which permits for blue-white selection in lacZΔ15 *E. coli* strains that are commercially available (New England BioLabs).

Phage display has been a potent tool in the design and discovery of novel peptide ligands that disrupt protein-protein interactions (77,81). Peptide probes are widely applicable due to the synthetic ease incurred by advances in solid-phase synthesis methodology first pioneered by R. Bruce Merrifield (82). The fundamental premise of

phage display is the genetic manipulation of bacteriophage to display a random array of peptide ligands on their coat protein (Figure 1.4). Panning, or screening, the library against an immobilized target can then be used identify bound phage. Phage particles that remain unbound can be washed away, where bound phage can be eluted by various techniques such as a high acid wash or competitive ligand elution strategies to disrupt peptide•target interactions (81,83). Following elution of the bound phage, one can titer the eluent to determine the plaque forming units (pfu) and subsequently amplify the phage pool by infecting an *E. coli* culture. Generally three to four rounds are undertaken before individual phage are tittered and the individual "plaque" or colony is selected for DNA isolation and sequence identification. From the DNA sequence identification, the peptide sequence can be determined. This strategy offers unique advantages from the standpoint that little knowledge of the target is necessary to perform the screen. One is only limited by the ability to purify and immobilized the target of interest, as commercially available libraries of phage expressing random peptides are widely available.

Phage display experiments identified the LpxA-binding peptide, peptide 920 (P920), which was then used to demonstrate that overexpression of phage display-selected peptides could function as chemical knockout tools of essential microbial enzymes (68). Later, LpxA inhibition studies suggested that the peptide was a competitive inhibitor of acyl-ACP, providing the molecular basis for its antimicrobial activity (84). However, crystallization studies of the LpxA•P920 and LpxA•UDP-GlcNAc complexes demonstrated that P920 overlaps with portions of the fatty acid binding pocket and the UDP-GlcNAc binding domain (72).

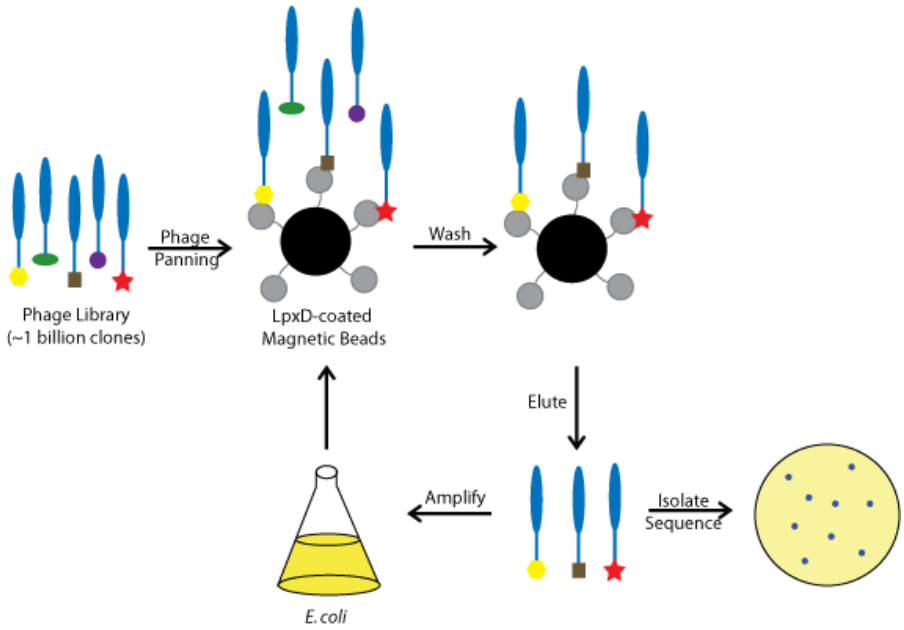

Figure 1.4. General schematic of the phage display screening process.

Thesis Outline and Significance.

Acyltransferases within the lipid A pathway are attractive targets for antimicrobial chemotherapy. However, hurdles such as lack of non-radioactive enzyme assays and difficulties in obtaining large quantities of substrates have prevented chemical genomics approaches towards identifying inhibitory small molecules. This thesis work encompasses the development of novel chemical and biological tools to address these challenges for studying the early acyltransferases of lipid A biosynthesis.

One of the first issues addressed was the development of a non-radioactive enzyme assay for both LpxA and LpxD (85). Acyl-ACP is a valuable substrate and necessary for the chemoenzymatic production of UDP-3-*O*-(*R*-3-hydroxyacyl)-GlcN, the LpxD substrate. Currently employed methods for generating acyl-ACP are arduous and require large amounts of *E. coli* due to toxicity associated with the overexpression of apo-ACP (86-89). This challenge is addressed in chapter 2 with an overexpression and purification system for *E. coli* holo-ACP. The production of holo-ACP combined with the

utilization of a soluble acyl-ACP synthetase recently characterized by Cronan and coworkers allowed for large production of acyl-ACP (90,91). Once the substrates were obtained, a continuous fluorescent enzyme assay was developed by exploiting the lone thiol unveiled on ACP during LpxA and LpxD catalysis. The reaction can be monitored by labeling the free thiol with a thiol-specific labeling reagent, ThioGlo1 for continuous monitoring of product turnover.

The development of a continuous enzyme assay marked a platform for testing inhibitory probes identified from a phage display screen against LpxD (92). As hypothesized, dual targeting peptides were discovered along with a more selective LpxD inhibitory peptide. Chapter 3 discusses the discovery of these peptides and the development of a fluorescence polarization (FP) assay for high-throughput screening (HTS) efforts. The development of the FP assay was essential to minimize the need for large quantities of substrates to perform an HTS assay. We further elaborated on the potential of P920 and utilized this as a tool for probing LpxA. Furthermore, this FP assay was used to demonstrate that the peptides were binding to LpxD and/or LpxA exclusive of *R*-3-hydroxymyristoyl-ACP highlighting a potential basis for the dual inhibitory functionality.

The discovery of the dual targeting inhibitor, RJPXD33 laid the foundation for a multi-faceted approach to identify small molecule acyltransferase inhibitors capable of penetrating the cellular membrane of gram-negative bacteria (Figure 1.5). One approach would be the rational design and synthesis of RJPXD33 peptidomimetics with enhanced bioavailability, decreased susceptibility to proteolysis, and the ability to maintain secondary structure necessary for inhibition. However, in order to identify

peptidomimetics it is essential to understand the fundamental mechanism of how the inhibitor binds to the target protein. To address this issue a structural and biochemical study was undertaken to provide molecular insights into RJPXD33 mechanism of binding (chapter 4). A second approach, discussed in chapter 5, was the use of an FP binding assay to screen a large library of small molecular weight compounds (~120,000) against LpxD. These experiments led to the identification of several small molecule LpxD inhibitors, some with antimicrobial activity against *E. coli*.

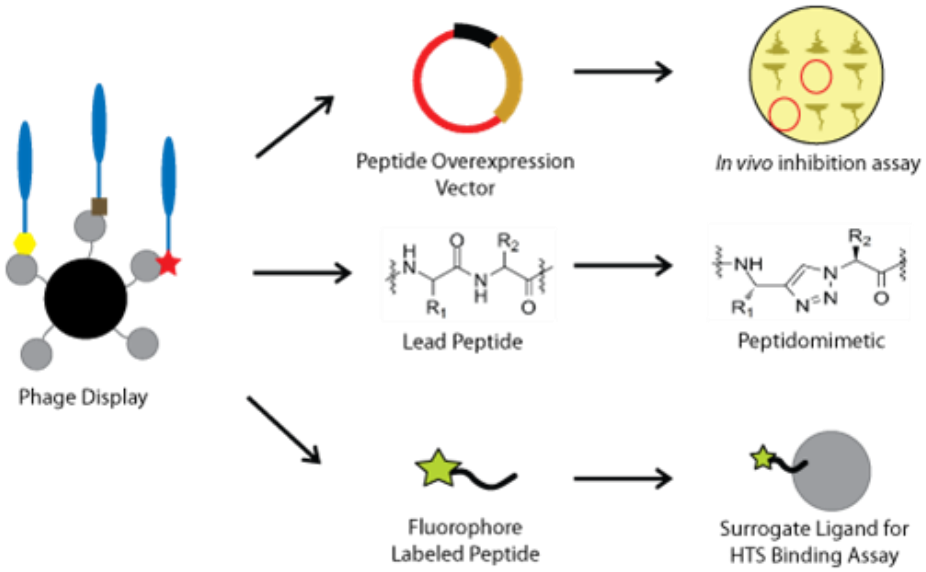

Figure 1.5. Use of peptides to probe lipid A biosynthesis. Phage display led directly to the discovery of the dual targeting inhibitor RJPXD33. This allowed for an in vivo overexpression assay, a lead peptide which can be further developed into peptidomimetics, and a surrogate ligand used in a high-throughput binding assay to identify small molecule inhibitors.

This thesis work has provided a novel toolset for future investigations into the early acyltransferases of lipid A biosynthesis. Furthermore, it establishes the proof-of-principle that dual targeting inhibitory molecules can be identified against LpxA and LpxD. The probes and techniques established herein should provide a lasting impact on the field of lipid A biosynthesis, as well as the field of antimicrobial chemotherapeutic drug discovery.

References.

1. Cohen, M. L. (1992) *Science* **257**, 1050-1055
2. Neu, H. C. (1992) *Science* **257**, 1064-1073
3. Boucher, H. W., Talbot, G. H., Bradley, J. S., Edwards, J. E., Gilbert, D., Rice, L. B., Scheld, M., Spellberg, B., and Bartlett, J. (2009) *Clinical Infectious Diseases* **48**, 1-12
4. Clatworthy, A. E., Pierson, E., and Hung, D. T. (2007) *Nat Chem Biol* **3**, 541-548
5. Nathan, C., and Goldberg, F. M. (2005) *Nature Reviews Drug Discovery* **4**, 887-891
6. Duesbery, N. S., Webb, C. P., Leppla, S. H., Gordon, V. M., Klimpel, K. R., Copeland, T. D., Ahn, N. G., Oskarsson, M. K., Fukasawa, K., Paull, K. D., and Vande Woude, G. F. (1998) *Science* **280**, 734-737
7. Forino, M., Johnson, S., Wong, T. Y., Rozanov, D. V., Savinov, A. Y., Li, W., Fattorusso, R., Becattini, B., Orry, A. J., Jung, D., Abagyan, R. A., Smith, J. W., Alibek, K., Liddington, R. C., Strongin, A. Y., and Pellecchia, M. (2005) *Proc. Natl. Acad. Sci. U. S. A.* **102**, 9499-9504
8. Cassel, D., and Pfeuffer, T. (1978) *Proc. Natl. Acad. Sci. U. S. A.* **75**, 2669-2673
9. Hung, D. T., Shakhnovich, E. A., Pierson, E., and Mekalanos, J. J. (2005) *Science* **310**, 670-674
10. Fischbach, M. A., and Walsh, C. T. (2009) *Science* **325**, 1089-1093
11. Newman, D. J., and Cragg, G. M. (2007) *Journal of Natural Products* **70**, 461-477
12. Ajikumar, P. K., Xiao, W.-H., Tyo, K. E. J., Wang, Y., Simeon, F., Leonard, E., Mucha, O., Phon, T. H., Pfeifer, B., and Stephanopoulos, G. (2010) *Science* **330**, 70-74
13. Pfeifer, B. A., Admiraal, S. J., Gramajo, H., Cane, D. E., and Khosla, C. (2001) *Science* **291**, 1790-1792
14. McDaniel, R., Thamchaipenet, A., Gustafsson, C., Fu, H., Betlach, M., and Ashley, G. (1999) *Proc. Natl. Acad. Sci. U. S. A.* **96**, 1846-1851
15. Miller, J. R., Dunham, S., Mochalkin, I., Banotai, C., Bowman, M., Buist, S., Dunkle, B., Hanna, D., Harwood, H. J., Huband, M. D., Karnovsky, A., Kuhn, M., Limberakis, C., Liu, J. Y., Mehrens, S., Mueller, W. T., Narasimhan, L., Ogden, A., Ohren, J., Prasad, J. V. N. V., Shelly, J. A., Skerlos, L., Sulavik, M., Thomas, V. H., VanderRoest, S., Wang, L., Wang, Z., Whitton, A., Zhu, T., and Stover, C. K. (2009) *Proc. Natl. Acad. Sci. U. S. A.* **106**, 1737-1742
16. Schreiber, S. L. (2000) *Science* **287**, 1964-1969
17. Charifson, P. S., Grillot, A.-L., Grossman, T. H., Parsons, J. D., Badia, M., Bellon, S., Deininger, D. D., Drumm, J. E., Gross, C. H., LeTiran, A., Liao, Y., Mani, N., Nicolau, D. P., Perola, E., Ronkin, S., Shannon, D., Swenson, L. L., Tang, Q., Tessier, P. R., Tian, S.-K., Trudeau, M., Wang, T., Wei, Y., Zhang, H., and Stamos, D. (2008) *Journal of Medicinal Chemistry* **51**, 5243-5263
18. Cheng, J., Thanassi, J. A., Thoma, C. L., Bradbury, B. J., Deshpande, M., and Pucci, M. J. (2007) *Antimicrob. Agents Chemother.* **51**, 2445-2453

19. Grossman, T. H., Bartels, D. J., Mullin, S., Gross, C. H., Parsons, J. D., Liao, Y., Grillot, A.-L., Stamos, D., Olson, E. R., Charifson, P. S., and Mani, N. (2007) *Antimicrob. Agents Chemother.* **51**, 657-666
20. Hossion, A. M. L., Zamami, Y., Kandahary, R. K., Tsuchiya, T., Ogawa, W., Iwado, A., and Sasaki, K. (2011) *Journal of Medicinal Chemistry* **54**, 3686-3703
21. Tomasic, T., Sink, R., Zidar, N., Fic, A., Contreras-Martel, C., Dessen, A., Patin, D., Blanot, D., Mueller-Premru, M., Gobec, S., Zega, A., Kikelj, D., and Masic, L. P. (2012) *Acs Medicinal Chemistry Letters* **3**, 626-630
22. Raetz, C. R. H., Reynolds, C. M., Trent, M. S., and Bishop, R. E. (2007) *Annu. Rev. Biochem.* **76**, 295-329
23. Raetz, C. R. H., and Whitfield, C. (2002) *Annu. Rev. Biochem.* **71**, 635-700
24. Barreteau, H., Kovac, A., Boniface, A., Sova, M., Gobec, S., and Blanot, D. (2008) *Fems Microbiol. Rev.* **32**, 168-207
25. Vaara, M. (1993) *Antimicrob. Agents Chemother.* **37**, 354-356
26. Vuorio, R., and Vaara, M. (1992) *Antimicrob. Agents Chemother.* **36**, 826-829
27. Meredith, T. C., Aggarwal, P., Mamal, U., Lindner, B., and Woodard, R. W. (2006) *ACS Chem. Biol.* **1**, 33-42
28. Beutler, B., and Cerami, A. (1988) *Annu. Rev. Biochem.* **57**, 505-518
29. Poltorak, A., He, X., Smirnova, I., Liu, M.-Y., Huffel, C. V., Du, X., Birdwell, D., Alejos, E., Silva, M., Galanos, C., Freudenberg, M., Ricciardi-Castagnoli, P., Layton, B., and Beutler, B. (1998) *Science* **282**, 2085-2088
30. Hoshino, K., Takeuchi, O., Kawai, T., Sanjo, H., Ogawa, T., Takeda, Y., Takeda, K., and Akira, S. (1999) *The Journal of Immunology* **162**, 3749-3752
31. Visintin, A., Halmen, K. A., Latz, E., Monks, B. G., and Golenbock, D. T. (2005) *The Journal of Immunology* **175**, 6465-6472
32. Russell, J. A. (2006) *New England Journal of Medicine* **355**, 1699-1713
33. Anderson, M. S., Bulawa, C. E., and Raetz, C. R. (1985) *J. Biol. Chem.* **260**, 15536-15541
34. Anderson, M. S., Robertson, A. D., Macher, I., and Raetz, C. R. H. (1988) *Biochemistry* **27**, 1908-1917
35. Anderson, M. S., Bull, H. G., Galloway, S. M., Kelly, T. M., Mohan, S., Radika, K., and Raetz, C. R. H. (1993) *J. Biol. Chem.* **268**, 19858-19865
36. Young, K., Silver, L. L., Bramhill, D., Cameron, P., Eveland, S. S., Raetz, C. R. H., Hyland, S. A., and Anderson, M. S. (1995) *J. Biol. Chem.* **270**, 30384-30391
37. Jackman, J. E., Raetz, C. R. H., and Fierke, C. A. (1999) *Biochemistry* **38**, 1902-1911
38. Ogura, T., Inoue, K., Tatsuta, T., Suzaki, T., Karata, K., Young, K., Su, L.-H., Fierke, C. A., Jackman, J. E., Raetz, C. R. H., Coleman, J., Tomoyasu, T., and Matsuzawa, H. (1999) *Molecular Microbiology* **31**, 833-844
39. Kelly, T. M., Stachula, S. A., Raetz, C. R. H., and Anderson, M. S. (1993) *J. Biol. Chem.* **268**, 19866-19874
40. Babinski, K. J., Kanjilal, S. J., and Raetz, C. R. H. (2002) *J. Biol. Chem.* **277**, 25947-25956
41. Babinski, K. J., Ribeiro, A. A., and Raetz, C. R. H. (2002) *J. Biol. Chem.* **277**, 25937-25946
42. Metzger, L. E., and Raetz, C. R. H. (2009) *Biochemistry* **48**, 11559-11571

43. Garrett, T. A., Que, N. L. S., and Raetz, C. R. H. (1998) *J. Biol. Chem.* **273**, 12457-12465
44. Reynolds, C. M., and Raetz, C. R. H. (2009) *Biochemistry* **48**, 9627-9640
45. Carty, S. M., Sreekumar, K. R., and Raetz, C. R. H. (1999) *J. Biol. Chem.* **274**, 9677-9685
46. Vorachek-Warren, M. K., Ramirez, S., Cotter, R. J., and Raetz, C. R. H. (2002) *J. Biol. Chem.* **277**, 14194-14205
47. Heinrichs, D. E., Monteiro, M. A., Perry, M. B., and Whitfield, C. (1998) *J. Biol. Chem.* **273**, 8849-8859
48. Isobe, T., White, K. A., Allen, A. G., Peacock, M., Raetz, C. R. H., and Maskell, D. J. (1999) *J. Bacteriol.* **181**, 2648-2651
49. Zhou, Z., White, K. A., Polissi, A., Georgopoulos, C., and Raetz, C. R. H. (1998) *J. Biol. Chem.* **273**, 12466-12475
50. Freinkman, E., Okuda, S., Ruiz, N., and Kahne, D. (2012) *Biochemistry* **51**, 4800-4806
51. Robins, L. I., Williams, A. H., and Raetz, C. R. H. (2009) *Biochemistry* **48**, 6191-6201
52. Sweet, C. R., Williams, A. H., Karbarz, M. J., Werts, C., Kalb, S. R., Cotter, R. J., and Raetz, C. R. H. (2004) *J. Biol. Chem.* **279**, 25411-25419
53. Dotson, G. D., Kaltashov, I. A., Cotter, R. J., and Raetz, C. R. H. (1998) *J. Bacteriol.* **180**, 330-337
54. Odegaard, T. J., Kaltashov, I. A., Cotter, R. J., Steeghs, L., vanderLey, P., Khan, S., Maskell, D. J., and Raetz, C. R. H. (1997) *J. Biol. Chem.* **272**, 19688-19696
55. Wyckoff, T. J. O., Lin, S. H., Cotter, R. J., Dotson, G. D., and Raetz, C. R. H. (1998) *J. Biol. Chem.* **273**, 32369-32372
56. Sweet, C. R., Lin, S., Cotter, R. J., and Raetz, C. R. H. (2001) *J. Biol. Chem.* **276**, 19565-19574
57. Kanistanon, D., Hajjar, A. M., Pelletier, M. R., Gallagher, L. A., Kalhorn, T., Shaffer, S. A., Goodlett, D. R., Rohmer, L., Brittnacher, M. J., Skerrett, S. J., and Ernst, R. K. (2008) *PLoS Pathog.* **4**
58. Kawasaki, K., Ernst, R. K., and Miller, S. I. (2004) *J. Biol. Chem.* **279**, 20044-20048
59. Reynolds, C. M., Ribeiro, A. A., McGrath, S. C., Cotter, R. J., Raetz, C. R. H., and Trent, M. S. (2006) *J. Biol. Chem.* **281**, 21974-21987
60. Zhou, Z. M., Lin, S. H., Cotter, R. J., and Raetz, C. R. H. (1999) *J. Biol. Chem.* **274**, 18503-18514
61. Zhou, Z. M., Ribeiro, A. A., Lin, S. H., Cotter, R. J., Miller, S. I., and Raetz, C. R. H. (2001) *J. Biol. Chem.* **276**, 43111-43121
62. Galloway, S. M., and Raetz, C. R. H. (1990) *J. Biol. Chem.* **265**, 6394-6402
63. Onishi, H. R., Pelak, B. A., Gerckens, L. S., Silver, L. L., Kahan, F. M., Chen, M. H., Patchett, A. A., Galloway, S. M., Hyland, S. A., Anderson, M. S., and Raetz, C. R. H. (1996) *Science* **274**, 980-982
64. Barb, A. W., Jiang, L., Raetz, C. R. H., and Zhou, P. (2007) *Proc. Natl. Acad. Sci. U. S. A.* **104**, 18433-18438
65. Barb, A. W., Leavy, T. M., Robins, L. I., Guan, Z. Q., Six, D. A., Zhou, P., Bertozzi, C. R., and Raetz, C. R. H. (2009) *Biochemistry* **48**, 3068-3077

66. Jackman, J. E., Fierke, C. A., Tumey, L. N., Pirrung, M., Uchiyama, T., Tahir, S. H., Hindsgaul, O., and Raetz, C. R. H. (2000) *J. Biol. Chem.* **275**, 11002-11009
67. McClerren, A., Endsley, S., Bowman, J., Andersen, N., Guan, Z., and Rudolph, J. (2005) *Biochemistry* **44**, 16574-16583
68. Benson, R. E., Gottlin, E. B., Christensen, D. J., and Hamilton, P. T. (2003) *Antimicrob. Agents Chemother.* **47**, 2875-2881
69. Pfitzner, U., Raetz, C. R. H., and Roderick, S. L. (1995) *Proteins* **22**, 191-192
70. Raetz, C. R. H., and Roderick, S. L. (1995) *Science* **270**, 997-1000
71. Wyckoff, T. J. O., and Raetz, C. R. H. (1999) *J. Biol. Chem.* **274**, 27047-27055
72. Ulaganathan, V., Buetow, L., and Hunter, W. N. (2007) *Journal of Molecular Biology* **369**, 305-312
73. Williams, A. H., and Raetz, C. R. H. (2007) *Proc. Natl. Acad. Sci. U. S. A.* **104**, 13543-13550
74. Buetow, L., Smith, T. K., Dawson, A., Fyffe, S., and Hunter, W. N. (2007) *Proc. Natl. Acad. Sci. U. S. A.* **104**, 4321-4326
75. Bartling, C. M., and Raetz, C. R. H. (2009) *Biochemistry* **48**, 8672-8683
76. Smith, G. P. (1985) *Science* **228**, 1315-1317
77. Smith, G. P., and Petrenko, V. A. (1997) *Chemical Reviews* **97**, 391-410
78. Cwirla, S. E., Peters, E. A., Barrett, R. W., and Dower, W. J. (1990) *Proc. Natl. Acad. Sci. U. S. A.* **87**, 6378-6382
79. Scott, J. K., and Smith, G. P. (1990) *Science* **249**, 386-390
80. Devlin, J. J., Panganiban, L. C., and Devlin, P. E. (1990) *Science* **249**, 404-406
81. Sparks, A. B., Adey, N. B., Cwirla, S., and Kay, B. K. (1996) *Phage display of peptides and proteins: A laboratory manual*, 227-253
82. Merrifield, R. B. (1963) *J. Am. Chem. Soc.* **85**, 2149-&
83. Oldenburg, K. R., Loganathan, D., Goldstein, I. J., Schultz, P. G., and Gallop, M. A. (1992) *Proc. Natl. Acad. Sci. U. S. A.* **89**, 5393-5397
84. Williams, A. H., Immormino, R. M., Gewirth, D. T., and Raetz, C. R. H. (2006) *Proc. Natl. Acad. Sci. U. S. A.* **103**, 10877-10882
85. Jenkins, R. J., and Dotson, G. D. (2012) *Analytical Biochemistry* **425**, 21-27
86. Keating, D. H., Carey, M. R., and Cronan, J. E. (1995) *J. Biol. Chem.* **270**, 22229-22235
87. Rock, C. O., and Cronan, J. E., Jr. (1979) *J. Biol. Chem.* **254**, 7116-7122
88. Rock, C. O., and Cronan, J. E., Jr. (1979) *J. Biol. Chem.* **254**, 9778-9785
89. Byers, D. M., and Gong, H. S. (2007) *Biochemistry and Cell Biology-Biochimie Et Biologie Cellulaire* **85**, 649-662
90. Jiang, Y. F., Chan, C. H., and Cronan, J. E. (2006) *Biochemistry* **45**, 10008-10019
91. Jiang, Y. F., Morgan-Kiss, R. M., Campbell, J. W., Chan, C. H., and Cronan, J. E. (2010) *Biochemistry* **49**, 718-726
92. Jenkins, R. J., and Dotson, G. D. (2012) *ACS Chem. Biol.* **7**, 1170-1177

Chapter 2

A Continuous Fluorescent Enzyme Assay for LpxA and LpxD[1]

Introduction

The enzymes in early lipid A biosynthesis are highly conserved in Gram-negative pathogens and represent potential targets for antibacterial development. Both biochemical and genetic studies have demonstrated the essential nature of LpxA and LpxD acyltransferases in Gram-negative organisms (1-3). For the most part, current assays utilized for assaying enzymes within the lipid A biosynthetic pathway use radiolabeled substrates coupled with thin layer chromatography and phosphorimaging development. These assays have endured over the years due to their reliability and the inherent need for sensitivity as a result of scarcity and solubility of substrates. Fluorescence-based enzymatic assays have proven to be highly sensitive and robust, and unlike radioactivity-based assays, have been used widely for high throughput screening (HTS) (4). The continuous fluorescent assays established herein are initial efforts to facilitate the identification and evaluation of LpxA/D inhibitors to be used as research probes and/or antimicrobial leads.

The thermodynamically unfavorable reaction catalyzed by LpxA presented one of the main difficulties in developing an assay (5). In order to circumvent this problem, it was envisioned that labeling of one of the products would allow the reaction to proceed

[1]The work described in this chapter has been published. Jenkins, RJ and Dotson, GD. "A continuous fluorescent enzyme assay for early steps of lipid A biosynthesis." *Analytical Biochemistry* **425** (2012), 21-27.

continuously in the forward direction. The lone thiol unveiled upon ACP directly following acyl transfer to the core glucosamine ring offered the greatest feasibility to perform such a reaction. As an added benefit, this assay would also be amenable for use with the reaction catalyzed by LpxD (6,7).

In order to develop this assay, the thiol specific labeling reagent, ThioGlo1, was utilized to continuously monitor the generation of free ACP over the course of the LpxA or LpxD reactions (Figure 2.1). ThioGlo1 contains a coumarin ring covalently linked to a fluorescence quenching maleimide (8). Upon thiol addition into the maleimide, the coumarin ring fluoresces at λ_{ex} = 379 nm and λ_{em} = 513 nm, allowing the generation of holo-ACP to be monitored in real time. These assays marked the first non-radioactive assay for either acyltransferase and allowed for rapid and sensitive analysis of catalytic turnover for both LpxA and LpxD.

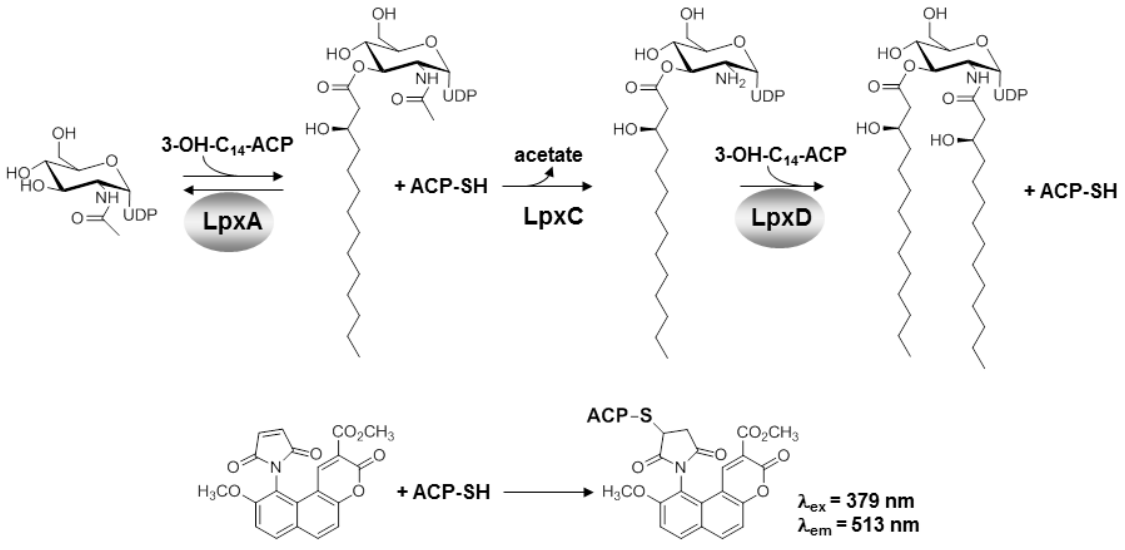

Figure 2.1. Methodology for monitoring catalysis of LpxA and LpxD. Early enzymatic steps of LPS biosynthesis in *E. coli* (top). Formation of the ThioGlo-ACP conjugate formed from holo-ACP produced in the acyltransferases reaction (bottom).

Materials and Methods

Materials. *R*-3-hydroxymyristic acid was purchased from Wako Chemicals. Tris(2-carboxyethyl)phosphine hydrochloride (TCEP), isopropanol, magnesium chloride and buffer reagents were purchased from Thermo Fisher Scientific. L-arabinose, ATP, and UDP-*N*-acetylglucosamine were purchased from Sigma-Aldrich. Benzonase, ThioGlo®1, and *E. coli* Rosetta(DE3)/pLysS cells were purchased from EMD Chemicals (Novagen). *E. coli* XL-1 Blue cells were purchased from Strategene. Isopropyl β-D-1-thiogalactopyranoside (IPTG), *E. coli* BL21-AI cells were purchased from Invitrogen. Bio-Gel P2 was purchased from Bio-Rad. All DNA modifying and restriction enzymes were purchased from New England Biolabs.

Cloning of E. coli lpxA, lpxC, lpxD, acpP, acpS and Vibrio harveyi aasS. PCR protocols were carried out under standard conditions utilizing Pfu DNA polymerase and DNA obtained from the *E. coli* K-12 strain MG1655 or the *V. harveyi* ATCC14126 strain. To perform the amplifications of the individual genes the following primers were used: *lpxA* (forward 5'-GCGCCATATGATTGATAAATCCGCCTTTGTGCATCCAACCGC, reverse 5'-CGCGCTCGAGTTAACGAATCAGACCGCGCGTTGAGCG); *lpxC* (forward 5'-GCGCCATATGATGATCAAACAAAGGACACT , reverse 5'-GCGCCTCGAGTGCCAGTACAGCTGAAGGCG); *lpxD* (forward 5'-CATCACCATCACCATCACGCTCAATTCGACTGGCTGATTTAGCG , reverse 5'-CGCGCTCGAGTTAGTCTTGTTGATTAACCTTGCGCTC); *acpP* (forward 5'-GCGCCATATGAGCACTATCGAAGAACGCGTTAAGAAAATTATC, reverse 5'-GCGCCTCGAGTTAACTTTCAATAATTACCGTGGCAC); *acpS* (forward 5'-

CGCGTGGCATATGGCAATATTAGGTTTAG, reverse 5'-GCGCCTCGAGACTTTCAATAATTACCGTGGCACAAGC); *V. harveyi aasS* (forward 5'-GCGCCATATGAACCAGTATGTAAAT, reverse 5'-GCGCCTCGAGCAGATGAAGTTTACGCAG).

The PCR products for both *lpxA*, and *acpP* were cloned into pET24a using *Nde*I and *Xho*I restriction sites (underlined). The *Xho*I-restricted PCR product for *lpxD* was cloned into pET23d which had been *Nco*I restricted, T4 DNA polymerase filled-in, and then restricted with *Xho*I. Each of the PCR products for *lpxC, acpS* and *aasS* were cloned into pET23a using *Nde*I and *Xho*I restriction sites. All plasmids were transformed into *E. coli* XL-1 Blue cells for amplification and plasmids isolated from these cell lines were sequenced at the University of Michigan Sequencing Core Facility. From these confirmed plasmids the following *E. coli* expression strains were constructed: BL21-AI/pET24a::*lpxA*, Rosetta (DE3)/pLysS/pET23a::*lpxC-his*$_6$, Rosetta (DE3)/pLysS/pET23d::*his*$_6$*-lpxD*, BL21-AI/pET24a::*acpP*/pET23a::*acpS-his*$_6$, BL21-AI/pET23a::*aasS-his*$_6$. Genes containing a 6 histidine tag coding region are indicated by *his*$_6$ in the above construct names. The *his*$_6$ in front of the gene name denotes a 5' histidine coding region, whereas the *his*$_6$ after the gene name denotes a 3' histidine coding region.

Cell cultures. Strains of interest were used to inoculate 500 mL LB (Lennox) or TB media containing the appropriate antibiotic(s), and incubated while shaking (250 rpm) at 37 °C until an OD_{600} of 0.6-1.0 was reached. The cultures were then induced with either 1 mM IPTG (Rosetta DE3/pLysS strains) or 0.2% L-arabinose/1 mM IPTG (BL21-AI strains). Unless otherwise noted, cells were induced at 37 °C and allowed to incubate

at 37 °C for 4 hours post-induction. Cells were harvested by centrifugation at 5,000 x g for 10 min at 4 °C, suspended in 10 mL of buffer and stored at -80 °C. Cell suspensions were thawed and disrupted by French press at 20,000 psi. Cellular debris was removed by centrifugation at 20,000 x g for 30 min at 4 °C and the resultant crude cytosol used for protein purification.

Purification of LpxA. For LpxA purification, 10 mL of crude cytosol in 20 mM potassium phosphate (KPhos) buffer, 20% glycerol pH 7.0 was applied to a 10 mL Reactive Green 19 column, which had been pre-equilibrated in the same buffer. The column was washed successively with 50 mL of loading buffer containing 0 M, 0.5 M, and 1 M NaCl. LpxA eluted with the 1 M NaCl fractions and was dialyzed overnight at 4 °C against 4 L of 20 mM Tris-HCl, 10% glycerol pH 8.0. The enzyme was then loaded onto an 8 mL Source 15Q column, washed with 24 ml of loading buffer and eluted with a gradient from 0-500 mM NaCl. LpxA was desalted on a Bio-Gel P2 column equilibrated in 20 mM HEPES pH 8.0. The purified LpxA was analyzed by SDS-PAGE and its concentration determined by UV absorbance at 280 nm (ε = 9190 M^{-1} cm^{-1}). The molecular weight of LpxA was confirmed by MALDI-TOF Mass spectrometry (MS) at the University of Michigan Protein Structure Facility.

Purification of LpxC-His_6 and His_6-LpxD. For His_6-LpxD purification, Benzonase (Novagen) was added after cell lysis and the lysate was incubated for 30 min on ice prior to centrifugation at 20,000 x g. Ten milliliters of crude cytosol in 20 mM HEPES, 50 mM imidazole pH 8.0 was loaded onto 3 mL of Ni-NTA resin (Qiagen) equilibrated in the same buffer. The resin was washed with 10 column volumes of loading buffer containing 500 mM NaCl and then eluted with 20 mM HEPES, 250 mM imidazole pH 8.0. Purified

His_6-LpxD and LpxC-His_6 were desalted on a Bio-Gel P2 column and analyzed by SDS-PAGE. Concentrations were determined by UV absorbance at 280 nm (ε = 22920 M^{-1} cm^{-1} for LpxC; ε = 27305 M^{-1} cm^{-1} for LpxD).

Purification of holo-ACP. A slightly modified protocol from Broadwater and Fox was utilized to prepare holo-ACP (9). Holo-ACP was produced in cells expressing both apo-ACP (*acpP* gene product) and holo-ACP synthetase (*acpS* gene product). Protein was expressed as describe above (Cell culture) except cells were cooled to 18 °C prior to induction and then allowed to grow overnight at 18 °C. To the cellular lysate, in 20 mM HEPES, 1 mM TCEP pH 8.0 (20 mL), 20 mL of cold isopropanol was added slowly and while gently mixing for 1 hour at 4 °C. The resulting suspension was centrifuged at 20,000 x g for 30 min at 4 °C. The supernatant was removed and to this 40 mL of 20 mM HEPES, 1 mM TCEP pH 8.0 was added. This solution was loaded onto a Source 15Q column (8 mL). A gradient of 20 mM HEPES, 1 mM TCEP, pH 8.0 containing 0 - 500 mM NaCl was performed and holo-ACP eluted at approximately 300 mM NaCl as judged by SDS-PAGE analysis. The protein was subsequently desalted on a P2 Bio-Gel column in 20 mM HEPES, 1 mM TCEP, pH 8.0. The protein was freeze dried and stored at -20 °C. Protein concentrations were measured via BioRad protein assay. The molecular weight of holo-ACP was confirmed by MALDI-TOF Mass spectrometry (MS) at the University of Michigan Protein Structure Facility.

Purification of V. harveyi AasS-His_6. Expression and purification of the soluble acyl-ACP synthetase (AasS) was carried out under the same conditions as His_6-LpxD and LpxC-His_6. Following elution from the Ni-NTA resin, AasS was desalted on a Bio-Gel P2 column in 20 mM Tris-HCl pH 7.5, 10% glycerol, 1 mM EDTA, 0.1 mM TCEP and

0.002% Triton-X100 as previously described for optimal storage (10). The desalted protein was aliquoted into microcentrifuge tubes and stored at -80 °C. Protein concentration was determined by UV absorbance 280 nm (ε = 65780 M^{-1} cm^{-1}).

Acylation of holo-ACP. Acylation was carried out as previously described with slight modifications (10). Holo-ACP was reduced for 1 hour at room temperature in the presence of two equivalence of TCEP prior to the loading of the fatty acid. The acylation reaction contained, in a final volume of 10 ml, 40 μM reduced holo-ACP, 5 mM ATP, 5 mM $MgCl_2$, 100 μM TCEP, 0.01% Triton X-100, 100 μg of AasS, and 150 μM *R*-3-hydroxymyristic acid in 100 mM Tris, pH 7.5. The reaction was incubated at 30 °C for 45 min and another 50 μg of AasS was added. After 20 min of additional incubation at 30 °C, the reaction was cooled and loaded directly onto a Source 15Q column (8 mL) equilibrated in 20 mM HEPES pH 8.0. The column was washed with 3 column volumes of equilibration buffer and eluted with an 80 mL linear gradient of 0 - 500 mM NaCl. Acyl-ACP eluted at approximately 300 mM NaCl and was subsequently desalted via a Bio-Gel P2 column and lyophilized.

Synthesis and purification of ThioGlo-ACP conjugate. 1 mL of holo-ACP (100 μM) was incubated with 1 mM TCEP and 132 μM of ThioGlo for 25 min (5% DMSO final concentration). Following the 25 min, an additional 132 μM of ThioGlo was added and mixed by pipetting up and down multiple times. The solution was incubated for an additional 35 min. The mixture was desalted on a Bio-Rad P2 size-exclusion column equilibrated in 20 mM HEPES pH 8. Protein concentrations were determined using Bio-Rad Protein assay with *R*-3-hydroxymyristoyl-ACP as a standard.

Synthesis of UDP-3-O-(R-3-hydroxmyristoyl)-GlcN. 50 μM holo-ACP was reduced for 1 hour at room temperature with 3 mM TCEP in 100 mM Tris-HCl pH 7.6 containing 0.01% Triton-X100. Following reduction of ACP, 3 mM ATP, 3 mM $MgCl_2$, 150 μM *R*-3-hydroxymyristic acid, and 150 μg of AasS were added to the centrifuge tube at a final volume of 5 mL and the tube was incubated at 37 °C for 15 min. Substrate synthesis was initiated by the addition of LpxA, LpxC and UDP-GlcNAc at concentrations of 30 μg/mL, 50 μg/mL and 500 μM and the solution was incubated for 45 min at 37 °C. Following the 45 min incubation, 100 μM of *R*-3-hydroxmyristic acid, 30 μg/mL LpxA, 30 μg/mL AasS, and 50 μg/mL LpxC were added and incubated for an additional 30 min. The solution was added to a round bottom flask containing silica gel (20 mg) and the water removed by rotary evaporation. The dried silica gel was added to a silica column (2 g) pre-equilibrated in 75:25 hexanes/ethyl acetate (EtOAc). The silica was washed with 100 mL 75:25 hexanes/EtOAc to remove the *R*-3-hydroxmyristic acid. The plug was subsequently washed with 50 mL of 25:15:4:2 v/v/v/v dichloromethane (DCM)/methanol (MeOH)/water/acetic acid. The solvent was evaporated off and the resulting solid was resuspended in 1 mL of DMSO and filtered through a .2 micron filter to remove any silica gel. UDP-3-*O*-(*R*-3-hydroxmyristoyl)-GlcN was purified by HPLC using 0.05% ammonium acetate and acetonitrile on a reverse phase C18 semi-prep column as reported by Anderson and Raetz (11). Purified UDP-3-*O*-(*R*-3-hydroxymyristoyl)-GlcN was lyophilized, dissolved in water and frozen at -80 °C until further use. The concentration was measured by UV absorbance at 262 nm (ε = 9900 M^{-1} cm^{-1}) (6). The purified product was subjected to analytical HPLC and negative ion electrospray ionization mass spectrometry (ESI-MS) for characterization.

Fluorescent enzyme assay for LpxA and LpxD. Assays were performed at 25 °C in Corning black, 96-well half-area plates and all solutions were made up in 20 mM HEPES pH 8.0 with a final assay volume of 100 μL. A SpectraMax M5 (Molecular Devices) plate reader was used to monitor fluorescence, with PMT sensitivity set at low to prevent saturation and number of readings set to 100. First, 50 μL of 20 μM ThioGlo solution was added to 20 μL of various concentrations of 3-hydroxymyristoly-ACP and 20 μL of various concentrations of UDP-GlcNAc or UDP-3-*O*-(*R*-3-hydroxymyristolyl)-GlcN. This mixture was incubated in the dark at 25 °C for 5 min to allow any unacylated ACP to react with the ThioGlo solution. To initiate the reaction, 10 μL of 100 nM acyltransferase solution was added directly to the well, mixed gently and the plate was read continuously at λ_{ex} = 379 nm and λ_{em} = 513 nm for 10 min at 15 s intervals. It should be noted that 100 nM LpxA or LpxD solutions were made fresh between each run from 1 mg/mL stock solution of purified enzymes. All reactions were performed in triplicate.

Data Analysis. Initial velocities were calculated through linear regression analysis during the first 2 min of the assay. K_m's were determined by non-linear regression analysis using KaleidaGraph software, from plots of initial velocities versus substrate concentrations, while holding the other substrate at saturating conditions (eq. 1). Control reactions lacking individual substrate or enzyme components were performed to demonstrate that increase in fluorescence was both enzyme and substrate dependent, and that no individual substrate or enzyme was causing an increase in relative fluorescence over time. Linear dependence of enzyme concentration with respect to initial velocity

was established through altering enzyme concentration while holding both substrates constant.

$$v = \frac{V_{max}\,[S]}{K_m + [S]} \tag{1}$$

Results & Discussion

ThioGlo®1 (methyl 10-(2,5-dioxo-2,5-dihydro-1H-pyrrol-1-yl)-9-methoxy-3-oxo-3*H*-benzo[*f*]chromene-2-carboxylate) has been used in the fluorescent detection of free thiol containing compounds in analytical HPLC, biological tissue samples, cell free extracts, and HTS (4,12-14). This reagent has been used to determine protein thiol concentrations as low as 10 nM (15). Therefore, we sought to utilize this reagent to monitor holo-ACP generation during LpxA and LpxD catalysis. With this assay the rate of holo-ACP production can be monitored continuously by detection of the fluorescent ThioGlo-ACP conjugate (λ_{ex} = 379 nm and λ_{em} = 513 nm). A standard fluorescent curve was generated by reading the fluorescence of various concentrations (0.1-16 μM; 100 μL) of ThioGlo-ACP conjugate in a Corning black, 96-well half-area plate (Figure 2.2). No deviation from linearity was noted upon adding ThioGlo at concentrations up to 10 μM. Under these conditions 1 μM ThioGlo-ACP gives 99.8 RFU.

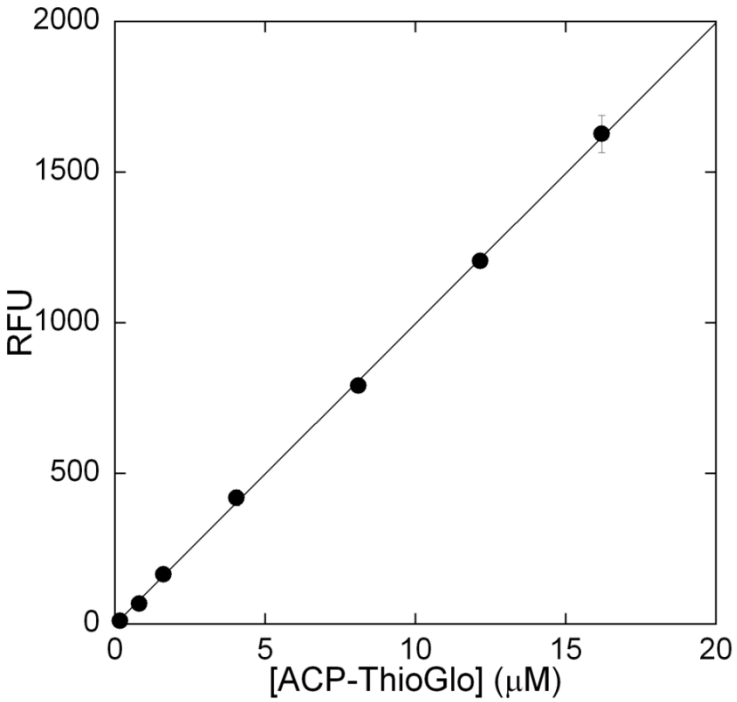

Figure 2.2. Fluorescence vs. [ThioGlo-ACP] plot. The fluorescence of various concentrations of purified ThioGlo-ACP conjugate, in 20 mM HEPES pH 8 (total volume 100 μL), was determined at 25 °C using a SpectraMax M5 plate reader.

Optimization of the reagents utilized for the kinetic analysis needed to be performed prior to kinetic characterization of LpxA. Final concentrations of LpxA were found to be optimal at 10 nM, where linear velocities could be measured within the first 2 min of a 10 min assay. It should be noted that when LpxA was diluted in assay buffer alone to 100 nM stock solution, the enzyme lost activity over time while on ice. Therefore, enzyme from a 1 mg/mL stock was diluted fresh to 100 nM for each assay and used immediately.

Since the free thiol generated upon holo-ACP generation is prone to oxidation and disulfide formation, which would interfere with ThioGlo conjugation, initially TCEP (a reducing agent) was employed to mitigate this possibility. However, TCEP proved to interfere with the reproducibility of labeling holo-ACP with ThioGlo in agreement with previous protein labeling studies with maleimide reagents in the presence of TCEP (16).

Exclusion of reducing agent resulted in greatly enhanced reproducibility and robustness of the assay, and thiol oxidation over the course of the assay time was not an issue.

Once conditions were optimized, time dependent-turnover of LpxA catalyzed acyl group transfer was demonstrated (Figure 2.3). Control reactions where individual components were omitted showed no increase in fluorescence, demonstrating that the generation of holo-ACP was being measured. The assay shows a linear dependence on enzyme concentration up to 20 nM which further establishes that the kinetics of LpxA are being measured, rather than the kinetics of ThioGlo conjugation to ACP (Figure 2.4). The specific activity for LpxA under our reaction conditions (25 °C) is 7.7 μmol/min/mg (k_{cat} = 3.6 s^{-1}). This value is reasonably lower (36 %) than literature values where assays were performed at a higher temperature (30 °C) (17).

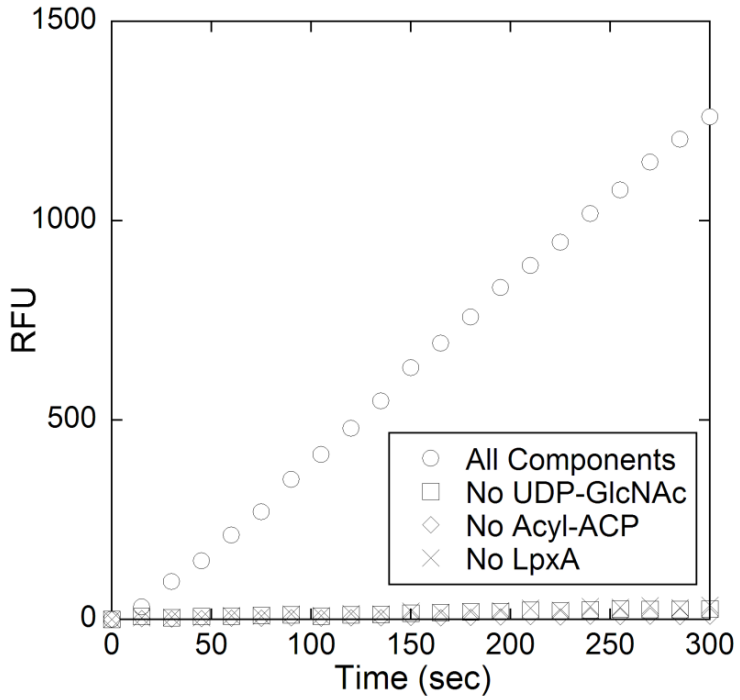

Figure 2.3. Reaction progress curves of the complete LpxA reaction (○), and control reactions without either nucleotide (□), acyl-ACP (◊), or acyltransferase (x). The complete LpxA assay mixture contained 20 mM HEPES (pH 8), 40 μM *R*-3-hydroxymyristoyl-ACP, 4 mM UDP-GlcNAc, 10 μM ThioGlo, and 10 nM LpxA (added 5 minutes after ThioGlo) in a final volume of 100 μL. The reaction was incubated at 25 °C and its progress was monitored continuously at λ_{ex} = 379 nm and λ_{em} = 513 nm for 10 min at 15 s intervals. Control reactions were run in similar fashion with the omission of substrate or enzyme, as indicated.

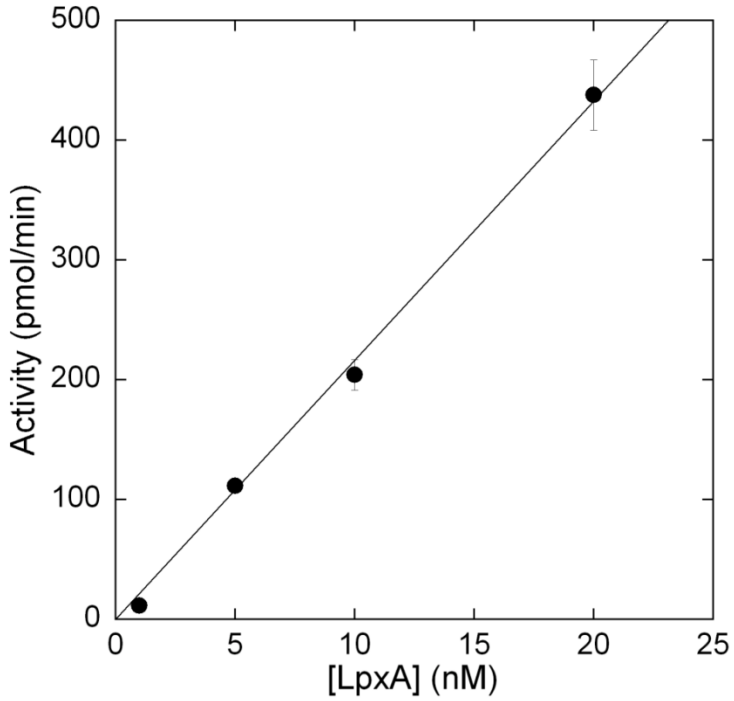

Figure 2.4. Linear dependence of initial reaction velocity with varying LpxA concentrations using the ThioGlo coupled fluorescence assay. The assays were run as described under Figure 3 caption, with varying amounts of LpxA being added. The assay showed a linear relationship between activity and enzyme concentration up to 20 nM LpxA.

The steady state kinetic parameters of LpxA were analyzed to determine the utility of the assay. The Michaelis-Menten constant for UDP-GlcNAc was established by holding acyl-ACP constant at 40 μM and varying UDP-GlcNAc between concentrations of 150 μM – 4.0 mM (Figure 2.5A). The K_m was found to be 600 ± 80 μM, which was in good accordance with the previously published values of 100-800 μM (17,18). Next the K_m for acyl-ACP was established by holding UDP-GlcNAc constant at 4.0 mM concentration, while varying acyl-ACP between 1-40 μM and plotting the initial velocity versus acyl-ACP concentration (Figure 2.5B). The K_m of acyl-ACP was determined to be 10 ± 1 μM. Estimates of acyl-ACP K_m using the radioactivity assay ranged from 1.5-5 μM (17,19). However, LpxA has an unfavorable equilibrium constant in the forward direction (K_{eq} = 0.01), and this has made it difficult to precisely measure the conversion

of radiolabeled UDP-GlcNAc to acylated product under high nucleotide and low acyl-ACP concentrations (18). With our current assay ThioGlo is able to sequester the holo-ACP product, thus mitigating the unfavorable K_{eq} and allowing accurate determination of the K_m of acyl-ACP.

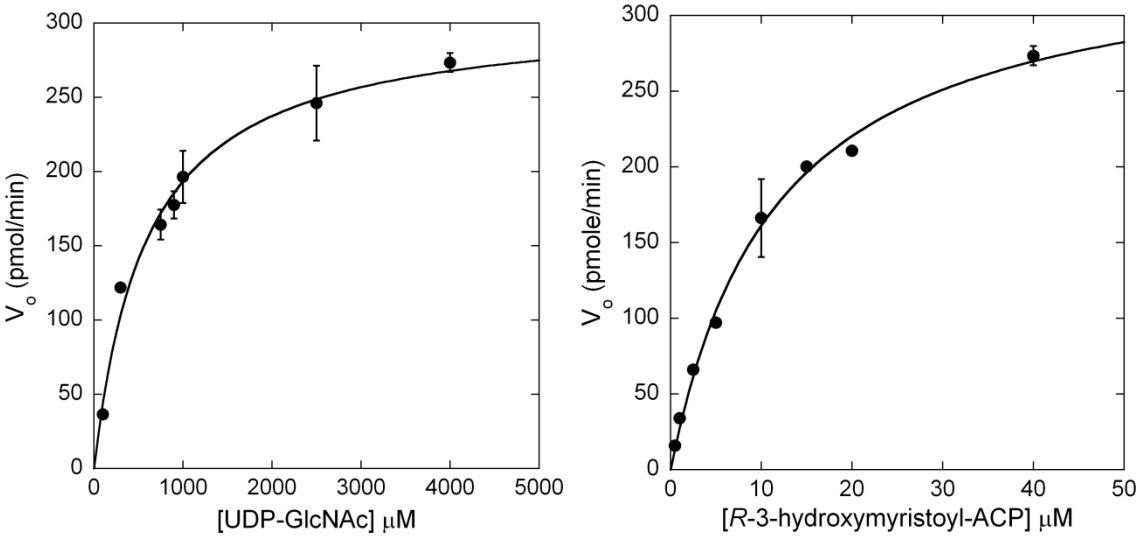

Figure 2.5. Saturation kinetics of LpxA for (A; left) UDP-GlcNAc and (B; right) *R*-3-hydroxymyristoyl-ACP. A) UDP-GlcNAc was varied between 150-4000 μM, while holding acyl-ACP constant at 40 μM. B) *R*-3-hydroxymyristoyl-ACP was varied over a concentration range of 1-40 μM, while holding UDP-GlcNAc constant at 4000 μM. Assays were run in triplicate.

In order to assay LpxD, the nucleotide substrate, UDP-3-*O*-(*R*-3-hydroxymyristoyl)-GlcN, needed to be synthesized. The current method for obtaining LpxD substrate is through an LpxA and LpxC coupled enzymatic process, utilizing acyl-ACP and UDP-GlcNAc as substrates (2,6). To decrease the amount of acyl-ACP necessary for this coupled assay, the soluble *V. harveyi* acyl-ACP synthetase was utilized to produce and continuously regenerate *R*-3-hydroxymyristoyl-ACP in situ from holo-ACP within the LpxA/LpxC coupled reaction (Figure 2.6).

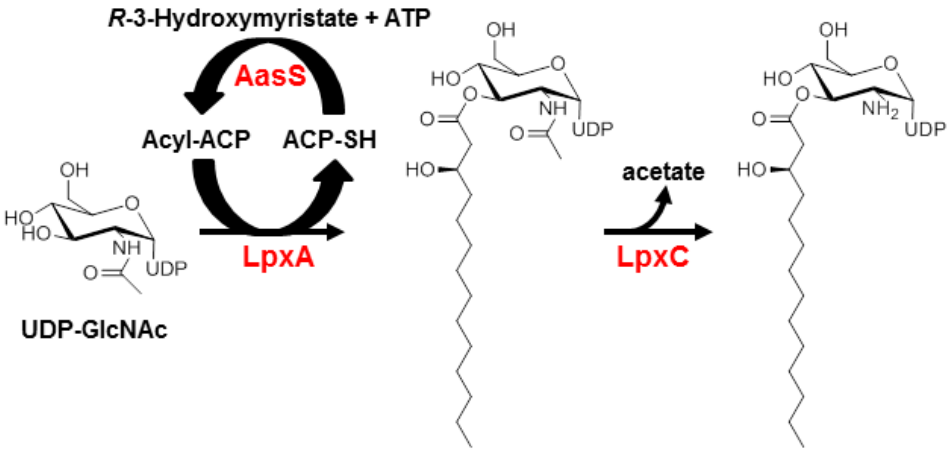

Figure 2.6. Schematic representation of UDP-3-*O*-(*R*-3-hydroxymyristoyl)-GlcN enzymatic preparation. The LpxA catalyzed formation of UDP-3-*O*-(*R*-3-hydroxyacyl)-GlcNAc is coupled directly to LpxC to form UDP-3-*O*-(*R*-3-hydroxymyristoyl)-GlcN, while AasS catalyzes the acylation of holo-ACP to regenerate acyl-ACP.

Upon obtaining UDP-3-*O*-(*R*-3-hydroxymristoyl)-GlcN, the kinetic parameters of His_6-LpxD were next established. It should be noted that previous literature precedent has established there is no difference in activity between His_6-LpxD and native LpxD (6). Acyl-ACP was varied between 2.5-40 μM while holding UDP-3-*O*-(*R*-3-hydroxymyristoyl)-GlcN at 19 μM to determine the K_m of acyl-ACP (Figure 2.7A). The K_m was 12 ± 2 μM which is higher than the previously published literature value of 3 μM (6). This discrepancy could be attributed to various reasons such as cysteine labeling of free thiols on LpxD which may interfere with acyl-ACP binding, differences in substrate quantitation between the two studies or a combination of the two. To determine the K_m of UDP-3-*O*-(*R*-3-hydroxymyristoyl)-GlcN, the substrate was varied between 0.35-19 μM, while holding acyl-ACP constant at 40 μM (Figure 2.7B). Again the K_m established, 4 ± 0.5 μM, correlated well to the reported value of 2.5 μM. The LpxD specific activity calculated from the V_{max} and protein concentration used in the steady state analysis was determined to be 5.0 μmol/min/mg (k_{cat} = 3.0 s^{-1}). Previously determined specific activity

for LpxD was 8.9 μmol/min/mg (30 °C) (6). These results demonstrated the reproducibility and robustness for the ThioGlo assay for LpxD.

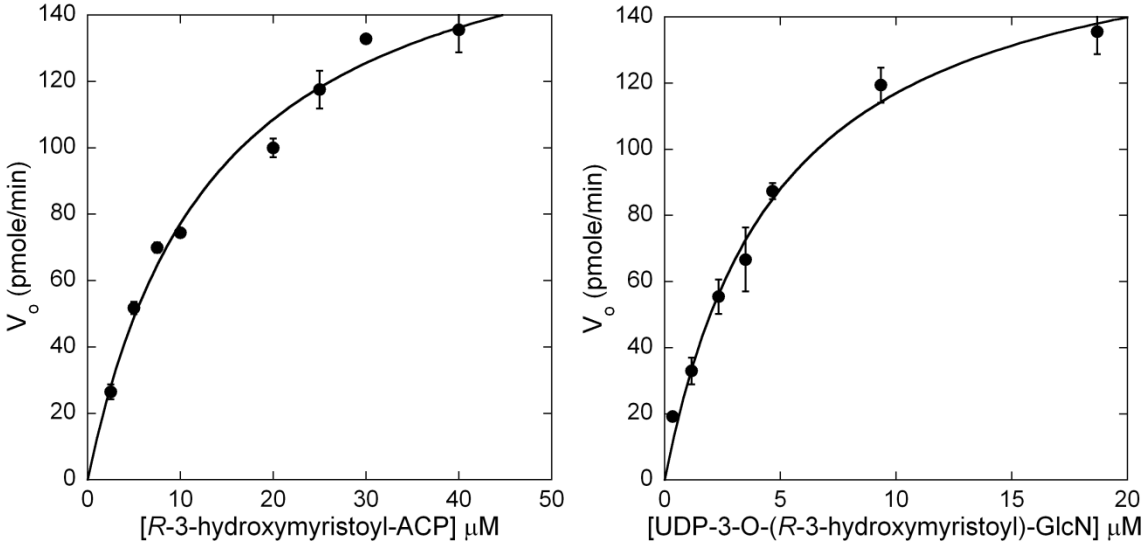

Figure 2.7. Saturation kinetics of LpxD for (A; left) *R*-3-hydroxymyristoyl-ACP and (B; right) UDP-3-*O*-(*R*-3-hydroxymyristoyl)-GlcN. A) acyl-ACP was varied over a concentration range of 1-40 μM while holding UDP-3-*O*-(*R*-3-hydroxymyristoyl)-GlcN constant at 19 μM. B) UDP-3-*O*-(*R*-3-hydroxymyristoyl)-GlcN was varied over a range of 0.35-19 μM while holding acyl-ACP constant at 40 μM. Assays were run in triplicate.

We have developed the first non-radioactive kinetic assay for both LpxA and LpxD. The above results demonstrate the utility of the thiol-specific reagent ThioGlo for use in kinetic assays involving turnover of acyl-ACP to holo-ACP. We have established and optimized the conditions essential to monitor turnover, and with these optimized conditions have determined the Michaelis-Mentin constants for both *E. coli* LpxA and LpxD substrates. These values are in good agreement with previously reported literature values. The assay is fast, continuous, and can be adapted to 384-well plates for high-throughput screening, depending on the readiness of non-commercially available substrates (acyl-ACP and UDP-3-*O*-(*R*-3-hydroxymyristoyl)-GlcN). This assay will be instrumental in the discovery and characterization of small-molecule inhibitors of LpxA and LpxD. Beyond LPS biosynthesis, holo-ACP is involved in a multitude of

biochemical pathways such as membrane phospholipid biosynthesis (20), fatty acid biosynthesis (21), polyketide biosynthesis (22), and quorum sensing (23), to name but a few. Therefore, this assay may find broad utility across various research communities.

Acknowledgements/Contributions

This research was supported in part by a Valteich Research Award administered by the College of Pharmacy, University of Michigan and by a Pre-Doctoral Research Grant administered by the University of Michigan Rackham Graduate School. R.J.J. was supported in part by the University of Michigan Chemistry-Biology Interface (CBI) training program (NIH), grant number 5T32GM008597-14, an American Foundation for Pharmaceutical Education fellowship and a Rackham Predoctoral Research Fellowship.

Experiments were planned by R.J.J. and Dr. Garry D. Dotson. Experiments were performed by R.J.J. The original manuscript was written by R.J.J. and G.D.D.

References

1. Vuorio, R., and Vaara, M. (1995) *FEMS Microbiol. Lett.* **134**, 227-232
2. Kelly, T. M., Stachula, S. A., Raetz, C. R., and Anderson, M. S. (1993) *J. Biol. Chem.* **268**, 19866-19874
3. Galloway, S. M., and Raetz, C. R. (1990) *J. Biol. Chem.* **265**, 6394-6402
4. Bulfer, S. L., McQuade, T. J., Larsen, M. J., and Trievel, R. C. (2011) *Anal. Biochem.* **410**, 133-140
5. Anderson, M. S., Bull, H. G., Galloway, S. M., Kelly, T. M., Mohan, S., Radika, K., and Raetz, C. R. (1993) *Journal of Biological Chemistry* **268**, 19858-19865
6. Bartling, C. M., and Raetz, C. R. (2008) *Biochemistry* **47**, 5290-5302
7. Wyckoff, T. J., and Raetz, C. R. (1999) *Journal of Biological Chemistry* **274**, 27047-27055
8. Yang, J.-R., and Langmuir, M. E. (1991) *Journal of Heterocyclic Chemistry* **28**, 1177-1180
9. Broadwater, J. A., and Fox, B. G. (1999) *Protein Expr. Purif.* **15**, 314-326
10. Jiang, Y., Chan, C. H., and Cronan, J. E. (2006) *Biochemistry* **45**, 10008-10019
11. Anderson, M. S., and Raetz, C. R. (1987) *J. Biol. Chem.* **262**, 5159-5169
12. Wu, J., Ferrance, J. P., Landers, J. P., and Weber, S. G. (2010) *Anal. Chem.* **82**, 7267-7273
13. Mi, Z., Hong, B., Mirnics, Z. K., Tyurina, Y. Y., Kagan, V. E., Liang, Y., and Schor, N. F. (2006) *Cancer Chemother. Pharmacol.* **57**, 357-367
14. Mare, S., Penugonda, S., and Ercal, N. (2005) *Biomed. Chromatogr.* **19**, 80-86
15. Wright, S. K., and Viola, R. E. (1998) *Anal. Biochem.* **265**, 8-14
16. Getz, E. B., Xiao, M., Chakrabarty, T., Cooke, R., and Selvin, P. R. (1999) *Anal. Biochem.* **273**, 73-80
17. Anderson, M. S., Bull, H. G., Galloway, S. M., Kelly, T. M., Mohan, S., Radika, K., and Raetz, C. R. (1993) *J. Biol. Chem.* **268**, 19858-19865
18. Wyckoff, T. J., and Raetz, C. R. (1999) *J. Biol. Chem.* **274**, 27047-27055
19. Williams, A. H., Immormino, R. M., Gewirth, D. T., and Raetz, C. R. H. (2006) *Proc. Natl. Acad. Sci. U. S. A.* **103**, 10877-10882
20. Zhang, Y. M., and Rock, C. O. (2008) *J. Lipid Res.* **49**, 1867-1874
21. Campbell, J. W., and Cronan, J. E., Jr. (2001) *Annu. Rev. Microbiol.* **55**, 305-332
22. Staunton, J., and Weissman, K. J. (2001) *Nat. Prod. Rep.* **18**, 380-416
23. Parsek, M. R., Val, D. L., Hanzelka, B. L., Cronan, J. E., Jr., and Greenberg, E. P. (1999) *Proc. Natl. Acad. Sci. U. S. A.* **96**, 4360-4365

Chapter 3

Dual Targeting Antibacterial Peptide Inhibitor of Early Lipid A Biosynthesis[1]

Introduction

LpxA and LpxD acyltransferases have been touted as novel subcellular targets for antimicrobial development (1,2), and while in vivo chemical inhibition of the *lpxA* gene product has been shown to display antimicrobial activity (2), there are no known in vivo active LpxD inhibitors. Of the two acyltransferases, LpxD is thought to be the better target due to the build-up of UDP-3-*O*-(*R*-3-hydroxyacyl) glucosamine that occurs in LpxD mutants grown at non-permissive temperatures (1,3). This compound has detergent-like properties and its accumulation is potentially toxic.

Peptides that bind to and inhibit essential enzymes have been invaluable as chemical probes used to validate intracellular targets, modulate biosynthetic pathways, develop target-specific binding assays, as well as serve as templates for the development of more pharmacologically relevant peptidomimetic agents (4-6). Therefore, as a prelude to small molecule inhibitor discovery, here we describe the use of a random phage-bound peptide library, combined with ligand-competitive phage elution, to identify bioactive LpxD inhibitory peptides. One bioactive peptide in particular was identified that binds to and inhibits both purified recombinant LpxD and LpxA. A single peptide with the ability to inhibit two steps in early lipid A biosynthesis represents a unique finding and serves as a new example of a dual targeting antimicrobial agent.

[1]The work described in this chapter has been published. Jenkins, RJ and Dotson, GD. "Dual targeting antibacterial peptide of early lipid A biosynthesis." *ACS Chemical Biology* **7** (2012), 1170-1177.

Materials and Methods

Materials. All DNA primers and Dynabeads M-270 Streptavidin were purchased from Invitrogen. Ph.D.-12 phage peptide library, pTYB2, pTYB3, Chitin beads, and all restriction enzymes were purchased from New England BioLabs (NEB). Plasmid pBirAcm was purchased from Avidity. Bio-Rad Protein Assay and Bio-Gel P2 size-exclusion resin were purchased from Bio-Rad. LB (Lennox) Broth and Agar, and dextrose were purchased from Difco. Peptide synthesis reagents and resins were purchased from Anaspec. Fluorescein isothiocyanate (FITC) was purchased from Acros Organics. ThioGlo1 reagent was purchased from Calbiochem. *R*-3-hydroxymyristic acid was obtained from Wako Chemicals. All antibiotics and other chemicals were purchased in the highest grade from Fisher Scientific or Sigma-Aldrich. SpectraMax M5 spectrophotometer was from Molecular Devices. DNA sequencing was performed at the University of Michigan DNA Sequencing Core.

Cell culture. A list of all bacteria strains and plasmids are described in Table 3.1. All LB-containing agar plates were incubated at 37 °C unless otherwise indicated. For protein expression and purification, all recombinant *E. coli*/T7 RNA polymerase promoter constructs were grown in 1 L baffled flask containing 250 mL of LB media supplemented with the appropriate antibiotics. The flasks were shaken (250 rpm) at 37 °C until the cells reached an optical density of OD_{600} = 0.6. To the cultures were added either 1 mM isopropyl β-D-1-thiogalactopyranoside (IPTG) (Rosetta (DE3)) or 1 mM IPTG and 0.2% L-arabinose (BL21-AI), and the cultures allowed to incubate at 37 °C for an additional 4 hours. Cells were harvested at 4 °C by centrifugation at 6,000 x g, and lysed

by French press. Crude cytosol was prepared by centrifugation of the lysate at 20,000 x g for 30 min at 4 °C.

Biotinylation of E. coli LpxD. The *lpxD* gene was amplified (pfu DNA polymerase) from *E. coli* MG1655 (ATCC) genomic DNA by standard PCR protocols with two primers corresponding to the 5' and 3' ends of the *lpxD* open reading frame. The forward primer was CCTTCAATTCGACTGGCTGATTTAGCG and the reverse primer was ATATCTCGAGGTCTTGTTGATTAACCTTGCGCTCAAGCG. The forward primer begins at the second codon of the *lpxD* reading frame, while the reverse primer contains an *XhoI* restriction site (underlined) in place of the *lpxD* stop codon. The purified PCR product was restricted with *XhoI* and inserted into pTYB3, which had undergone digestion with *NcoI*, a fill-in reaction with T4 DNA polymerase, and restriction with *XhoI*. The resulting construct, pUMGD13, contained *lpxD* with a 3'-intein coding tag.

In a second *lpxD*-intein construct, a coding region for a 15-amino acid biotin ligase-recognition motif was inserted in frame with, and upstream of, the intein tag coding region in pTYB2 (5,7,8). The following complimentary primer pair, 5'-GGGCTGAACGATATTTTTGAAGCGCAGAAAATTGAATGGCATGAACCG-3' and 5'-CGGTTCATGCCATTCAATTTTCTGCGCTTCAAAAATATCGTTCAGCCC-3', coding for the biotin ligase-recognition motif (underlined), was blunt-end cloned into the *SmaI* restriction site of pTYB2 to give pTYB2btc. The *XbaI*/*XhoI* restriction fragment from pUMGD13, containing the *lpxD* open reading frame, was ligated into *XbaI*/*XhoI* restricted pTYB2btc to give pUMRJ4 and the insert was confirmed by DNA sequencing.

The resulting pUMRJ4 construct contained *lpxD* with a 3'-biotin ligase recognition motif coding region followed by the intein coding region.

E. coli BL21-AI harboring the plasmids pUMRJ4 and pBirAcm was grown in a 250 mL culture, as indicated above, with D-biotin (12 mg/L) added along with IPTG and L-arabinose during induction. Crude cytosol (10 mL) was applied to a 5 mL Chitin bead column, and the column wash with 10 column volumes of 20 mM Tris-HCl pH 8.0. Immobilized LpxD was cleaved from the intein fusion tag by washing the column with 15 mL of 50 mM mercaptoethane sulfonic acid (MESNA), stopping the flow, and allowing the resin to sit overnight at 4 °C. Fresh buffer was then added to the top of the column and biotinylated LpxD eluted in the first 4 mL. The protein was desalted through a 12 mL Bio-Gel P2 column in 20 mM Tris-HCl pH 8.0. The purified biotinylated LpxD was analyzed by SDS-PAGE and its concentration determined by UV absorbance at 280 nm (ε = 32805 M^{-1} cm^{-1}). Molar ratio of biotin was determined by 4'-hydroxyazobenzene-2-carboxylic acid (HABA) assay per manufacturer's protocol (Thermo Scientific).

Phage Display. Streptavidin-conjugated Dynabeads (10 μL) were washed three times with 100 μL of 50 mM Tris-HCl, pH 7.5, 150 mM NaCl (TBS). Biotinylated LpxD (4 pmol) in 100 μL of TBS was added to Dynabeads (10 μL) and the mixture was allowed to incubate at room temperature for 30 min. The beads were magnetically separated from the supernatant and washed five times with 100 μL TBS. To the affinity captured biotinylated LpxD, 100 μM biotin (100 μL) was added and incubated at room temperature for 10 min to block any excess streptavidin sites. The beads were again washed five times with 100 μL TBS. Phage-bound peptide library (Ph.D.-12), at a

concentration of 1 x 10^9 – 1 x 10^{10} plaque forming units (pfu), was added to the immobilized LpxD in a total volume of 100 μL TBS. This suspension was allowed to incubate for 45 min at room temperature with gentle mixing. Following the incubation period the supernatant was removed and the beads were washed ten times with 100 μL TBS. Bound phage were eluted by incubating for 15 min with gentle mixing with either 50 μM acyl carrier protein (ACP) or 500 μM UDP-GlcNAc in 100 μL TBS buffer. The phage were then amplified by direct infection with *E. coli* XL1 Blue, isolated and tittered as previously described, and used in the next cycle (9). In subsequent rounds of panning 0.1% Tween 20 was added to all TBS buffer containing solutions. Following rounds three and four, individual plaques were selected at random, phage purified, and the DNA from each was sequenced.

*Bioactivity Assay***.** pACYC184, isolated from *E. coli* JM110 (*dam*$^-$), was restricted with *HindIII*/*BclI* and the fragment containing the p15A origin of replication and chloramphenicol resistance marker was isolated from a 1% agarose gel. The *araC* and thioredoxin genes were individually amplified using pBAD-thio as the template in two separate PCR reactions. For the *araC* gene 5'-GCGCTGATCATTATGACAACTTGACGGCTACATCATTC-3' was used as the forward primer and 5'-GCGCCATATGTATGTATATCTCCTTCTTAAAGTTAAAC-3' was used as the reverse primer. The forward primer contains a *BclI* restriction site (underlined) and the reverse primer contains an *NdeI* restriction site (underlined). The thioredoxin gene was cloned using 5'-GCGCCATATGGGGCCCGGATCTGATAAAATTATTCATCTGACTG-3' as the forward primer (*NdeI* site underlined) and 5'-CCGAGGAGAGGGTTAGGGATAGGC-3'

as the reverse primer. The *araC* PCR product was restricted with *BclI* and *NdeI*, while the thioredoxin containing PCR fragment was restricted with *NdeI* and *HindIII*. These two inserts were ligated together with the *BclI*/*HindIII* restricted pACYC184 fragment, resulting in the formation of pUMRJ100.

Complementary DNA oligonucleotides coding for peptides identified from phage display were purchased in the following format, *NdeI*-(dodecapeptide coding region)-*ApaI*. Complementary oligos were mixed in equal molar ratios, heated to 94 °C for 2 min, and allowed to cool to room temperature over several minutes. The hybridized oligos were restricted with *NdeI* and *ApaI*, pooled, and ligated into pUMRJ100 restricted with the same enzymes. The ligation mixture was used to transform competent *E. coli* XL1 Blue and the transformed cells selected on LB agar containing 1% dextrose and 10 μg/mL chloramphenicol (LB-cam/dex) at 37 °C overnight. Seventy-two random colonies were selected and streaked onto both LB-cam/dex and LB-cam/0.2% L-arabinose (8 replica plates). Colonies which grew on the dextrose containing plates, but not on the arabinose containing plates were indicative of bioactive peptide expression. Plasmids were isolated from colonies on the LB-cam/dex plates having the desired phenotype and the peptide coding regions determined by DNA sequencing. Empty plasmid vector was used as a negative control and showed no toxicity.

E. coli LpxA and LpxD expression constructs. *E. coli* His_6-LpxD and LpxA were expressed and purified as previously described (10). The pUC18::*lpxD* construct was made from a previously described wild-type pET expression construct (10). The *lpxD* gene was excised from the pET construct by *XhoI* restriction/T4 DNA polymerase fill-in, followed by *XbaI* restriction. The insert was then ligated into pUC18 which had been

restricted with *HindIII*, filled-in with T4 DNA polymerase, and restricted with *XbaI*. The resulting *lpxD* pUC18 construct was designated pUMRJ45. All constructs were verified by DNA sequencing.

Synthesis of Acytransferase substrates. *R*-3-hydroxymyristoyl-ACP and UDP-3-*O*-(*R*-3-hydroxymyristoyl)-glucosamine were synthesized and purified as previously described in chapter 2 (10).

Fluorescence polarization protein binding assay. Peptides FITC-RJPXD33 (FITC-(βA)TNLYMLPKWDIP-NH_2), RJPXD33 (TNLYMLPKWDIP-NH_2), RJPXD31 (QHFMVPDINDMQ-NH_2), RJPXD34 (SENNFMLPLLPL-NH_2), and FITC-P920 (FITC-(βA)SSGWMLDPIAGKWSR-NH_2) were synthesized using rink-amide resin (0.4 mmol/g capacity) by established peptide coupling procedures. Labeled peptides contained an N-terminal β-alanine (βA) linker coupled to fluorescein using fluorescein isothiocyanate (FITC). Peptides were purified via RP-HPLC and analyzed by electrospray ionization mass spectrometry (ESI-MS) at the University of Michigan Chemistry Mass Spectrometry Services. Purified peptides were suspended in DMSO and diluted to a concentration of 200 nM in 20 mM HEPES, pH 8.0 (~0.1% DMSO). LpxA and His_6-LpxD were serially diluted to appropriate concentrations in 20 mM HEPES, pH 8.0 and 45 μL of the dilutions were added to 354-well black Costar plates. To this, 5 μL of labeled peptide was added for a final concentration of 20 nM FITC-peptide. The wells were gently mixed and incubated at 30 °C for 15 min. Polarization was measured on a SpectraMax M5 plate reader in triplicate with readings taken at λ_{ex} = 485 nm and λ_{em} = 525 nm. The data for FITC-RJPXD33 binding to LpxD was normalized to the

experimentally determined polarization of the fully bound peptide (mP_b), and the resulting binding curves fit to Hill equation (1) using KaleidaGraph software.

$$\alpha = \frac{\left(\frac{[P]}{K_d}\right)^h}{1 + \left(\frac{[P]}{K_d}\right)^h} \quad (1)$$

Where α is the fraction of FITC-peptide bound, h is the Hill coefficient, [P] is the concentration of protein, and K_d is the dissociation constant of protein•peptide complex. For RJPXD33 binding to LpxA the polarization values of the fully bound labeled peptide (mP_b) and K_d were determined by nonlinear fit of the polarization versus [Acyltransferase] plots to Eq. (2). Where mP is the experimentally determined polarization, mP_f is the polarization of free FITC-RJPXD33, P is the total amount of acyltransferase, and K_d is the dissociation constant of the protein•peptide complex. The calculated mP_b was then used to normalize the experimental data and the resulting binding curves fit to Eq. (1).

$$mP = mP_f + \left[\left(mP_b - mP_f\right) * \left([P]/([P] + K_d)\right)\right] \quad (2)$$

For competition binding assays, 220-660 nM of acyltransferase was incubated in the presence of varying concentrations of unlabeled peptides or acyl-ACP for 10 min at 30 °C. FITC-labeled peptide (20 nM) was added and incubated in the dark at 30 °C for 15 min before reading. The $[I]_{50}$ was determined from the competition binding curve and the dissociation constant of the unlabeled ligand was calculated as previously described using Eq. (3) (11):

$$K_i = \frac{[I]_{50}}{\frac{[L]_{50}}{K_d} + \frac{[P]_0}{K_d} + 1} \quad (3)$$

Where $[I]_{50}$ is the free unlabeled ligand (inhibitor) concentration at 50% inhibition, $[L]_{50}$ is the free ligand (fluorescent tracer) concentration at 50% inhibition, and $[P]_0$ is the free protein concentration at 0% inhibition, K_d is the dissociation constant of the ligand (fluorescent tracer), and K_i is the calculated dissociation constant for the unlabeled ligand.

Acyltransferase inhibition assays. The acyltransferase reaction was observed in the forward direction using a continuous fluorescent assay. The fluorescent assay detects holo-ACP liberation via conjugation with ThioGlo1 reagent, which could be monitored as an increase in fluorescence from excitation and emission wavelengths set to λ_{ex} = 379 nm and λ_{em} = 513 nm. Assays were performed on a SpectraMax M5 microplate reader (auto cutoff set to λ = 495 nm, PMT set to low and precision set to 40 scans per well) using Corning black, 96-well half-area plates. The assay mixture in a final volume of 100 μL contained 20 mM HEPES pH 7.5, 10 μM ThioGlo, 600 μM UDP-GlcNAc (LpxA assay) or 4.5 μM UDP-3-*O*-(*R*-3-hyrdoxymyristoyl)-GlcN (LpxD assay), 9 μM *R*-3-hydroxymyristoyl-ACP, 10 nM acyltransferase and varying concentrations of peptide (200 μM – 1 μM). Assays contained a final concentration of 2% (*v/v*) DMSO from peptide stock solutions. All components with the exception of enzyme were mixed and incubated in the dark at 30°C for 5 min. To initiate the reaction, a fresh dilution of acyltransferase was added and the reaction was monitored for 10 min. Assays were run in triplicate with the average IC_{50} being reported. A negative control containing no inhibitor

and a positive control containing no acyltransferase were used for 100% and 0% relative activity, respectively.

Multicopy suppression. Competent *E. coli* XL1 Blue/pUMRJ45 were transformed separately with pUMRJ40 (pUMRJ100::*rjpxd34*), pUMRJ41 (pUMRJ100::*rjpxd33*), or pUMRJ100 (control). The transformed cells were grown overnight at 37 °C on LB agar containing 1% dextrose, 100 μg/mL ampicillin, and 10 μg/mL chloramphenicol (LB-amp/cam/dex). Single colonies were selected and streaked onto both LB-amp/cam/dex and LB-amp/cam/0.2% L-arabinose plates. These plates were incubated overnight at 37 °C.

Results and Discussion

Table 3.1. Plasmids and bacterial strains used in this study

Bacterial strain or plasmid	Relevant characteristics	Source
Plasmids		
pACYC184	*p15A ori*, Tet^r, Cam^r	NEB
pBAD-Thio	P_{araBAD}, *trxA*, Amp^r	Invitrogen
pUC18	P_{lac}, Amp^r	Invitrogen
pBIRAcm	*birA*	Avidity
pTYB2	*intein*	NEB
pUMGD13	pTYB2::*lpxD*	This Study
pTYB2btc	pTYB2::*birA* recognition sequence	This Study
pUMRJ4	pTYB2btc::*lpxD*	This Study
pUMRJ100	*p15A ori*, P_{araBAD}, *trxA*, Cam^r	This Study
pUMRJ40	pUMRJ100::*rjpxd34-trxA*	This Study
pUMRJ41	pUMRJ100::*rjpxd33-trxA*	This Study
pUMRJ45	pUC18::*lpxD*	This Study
Strains		
E. coli		
MG1655	Wild type	ATCC
XL-1 Blue	*recA1 endA1 gyrA96 thi-1 hsdR17 supE44 relA1 lac [F´ proAB lacIqZΔM15 Tn10 (*Tet^r*)]*	Stratagene
XD33	*E. coli* XL1 Blue/pUMRJ41	This Study
XD34	*E. coli* XL1 Blue/pUMRJ40	This Study
BL21-AI	*araB::T7RNAP-tetA*	Invitrogen
JM110	*dam dcm*	Strategene

Phage display was employed to identify LpxD-binding peptides. LpxD contains a C-terminal helical extension spanning 45 Å from the active site contained within its LβH

core structure that proved to be an ideal position to place a biotin tag for biopanning experiments (12,13). Initial attempts at labeling the C-terminus via cleavage of an LpxD-intein fusion, expressed from pUMGD13, using cysteine-biotin or ethylenediamino-biotin failed to generate biotinylated protein (14). As well, other nucleophiles known to cleave intein protein fusions, such as mercaptoethane sulfonic acid (MESNA) and/or DTT, also failed to cleave the LpxD-intein fusion protein. Therefore, a biotin ligase recognition (BLR) motif coding region was cloned upstream of the intein coding region in pTYB2 to allow for in vivo biotinylation of protein fusions (7,8). The construct pUMRJ4 contains *lpxD* cloned upstream of the BLR coding region and upon induction in *E. coli* BL21-AI/pBirAcm/pUMRJ4, allows for the expression of a 96 kDa protein fusion (LpxD-BLR motif-intein-chitin binding domain). The 96 kDa biotinylated-LpxD intein fusion was bound to chitin resin and the intein linkage cleaved using MESNA, resulting in elution of biotinylated LpxD (38 kDa). The purified protein contained 0.97 moles of biotin per mole of LpxD.

Phage display screening was performed using the Ph.D.-12 random peptide library (NEB), which contains approximately 1.9 billion phage-bound, random 12-amino acid peptides fused to the N-terminus of the M13 phage pIII coat protein. Biopanning experiments were carried out against biotinylated LpxD immobilized on magnetic beads coated with streptavidin (Dynabeads M-270). Bound phage were eluted from immobilized LpxD with either UDP-GlcNAc, previously shown to bind to *Chlamydia trachmoatis* LpxD (13), or ACP as competitive ligands. Peptide coding sequences from ten randomly selected phage were obtained after rounds three and four of panning. The twenty DNA sequences isolated encoded 17 unique peptides. Peptide sequences were

aligned in Clustal W (15) to determine sequence homology (Figure 3.1). A consensus YMLP motif was heavily conserved (Figure 3.2, panel a) and identified among a third of the sequences, which is similar to the WMLDP motif located within the LpxA-specific peptide, peptide 920 (P920; SSGWMLDPIAGKWSR) (5). The aromatic-Met-hydrophobic motif is heavily conserved among 50% of the sequences, with variations between tyrosine and phenylalanine in the lead position. Also, the sequences TNLYMLPKWDIP (RJPXD33) and AWWEFNPFAWPY were identified multiple times among the twenty isolated phages.

RJPXD31	QH**FMVP**DINDMQ
RJPXD32	**FMLP**YHHPYMNY
RJPXD33	TNL**YMLP**KWDIP
RJPXD34	SENN**FMLP**LLPL
RJPXD35	HPWNMLSQMWWW
RJPXD36	QE**YMI**G**P**YQAEW
RJPXD37	QPYGLDPMTHQW
RJPXD38	TAFNWNPLRSGL
RJPXD39	SPS**FML**NDAMLS
RJPXD40	TQL**YMW**D**P**VHYM
RJPXD51	FPSK**YML**ITHML
RJPXD52	TNL**YMLP**KWDIP
RJPXD53	TNL**YMLP**KWDIP
RJPXD54	YFGMTDHMWWPV
RJPXD55	TTFYWDHPQYSR
RJPXD56	FPFWWPDQNSIW
RJPXD57	AWWEFNPFAWPY
RJPXD58	AWWEFNPFAWPY
RJPXD59	YYDDFLWWRSPW
RJPXD60	FYEYDDLLFWEH

Figure 3.1. Multiple sequence alignment of dodecapeptides identified from competition phage display experiments. Twenty sequences were aligned using Clustal W (15). Peptides highlighted in bold showed antibacterial activity upon expression in *E. coli* XL1 Blue. Amino acids highlighted in bold reveal a consensus motif (Y/FMLP) identified within many of the peptides. RJPXD33 was identified among three of the twenty randomly selected colonies, representing 15% of total colonies selected.

The M13 pIII coat protein containing the N-terminal peptide is expressed in the *E. coli* host with a signal sequence immediately upstream of the peptide library site. This signal sequence targets the modified pIII protein to the *E. coli* periplasm wherein the signal peptide is cleaved (16). While this compartmentalization away from the cytoplasm is ideal for amplifying and expressing phage displaying inhibitory peptides to essential

cytosolic enzymes, bioactivity of such peptides cannot be ascertain within this context. Therefore, a general strategy utilized for bioactivity screening of LpxD-binding peptides identified from phage display was worked out (Figure 3.2, panel b). A low copy, tightly controlled expression construct was employed to promote stringent conditions for bioactivity assays. DNA oligonucleotides, coding for the 17 peptides identified in the phage display screen were cloned into a low-copy (p15A ori) plasmid, pUMRJ100, upstream of the thioredoxin (*trxA*) coding region (Figure 3.3). The expression of the peptide-TrxA fusions were under the control of the L-arabinose promoter (P_{araBAD}). The resultant constructs were pooled and transformed into *E. coli* XL-1 Blue cells and selected on LB-chloramphenicol (LB-cam) plates containing dextrose to suppress basal expression of the peptide fusions from the araBAD promoter. Individual colonies were then re-streaked onto both LB-cam/dextrose (non-induction) and LB-cam/L-arabinose (induction) plates to probe for toxicity (Figure 3.2, panel c). No toxicity was seen on dextrose containing media. However, individual constructs expressing peptides RJPXD31, RJPXD33, or RJPXD34 displayed in vivo toxicity (no growth) when plated on LB-cam/arabinose media. These three peptides had a more extensive N/QXYMLP motif in common, again with variations in their respective aromatic and hydrophobic amino acids. Plasmids from random colonies not displaying toxicity were sequenced and demonstrated representation of all of the pooled constructs and proper orientation of the peptide coding regions.

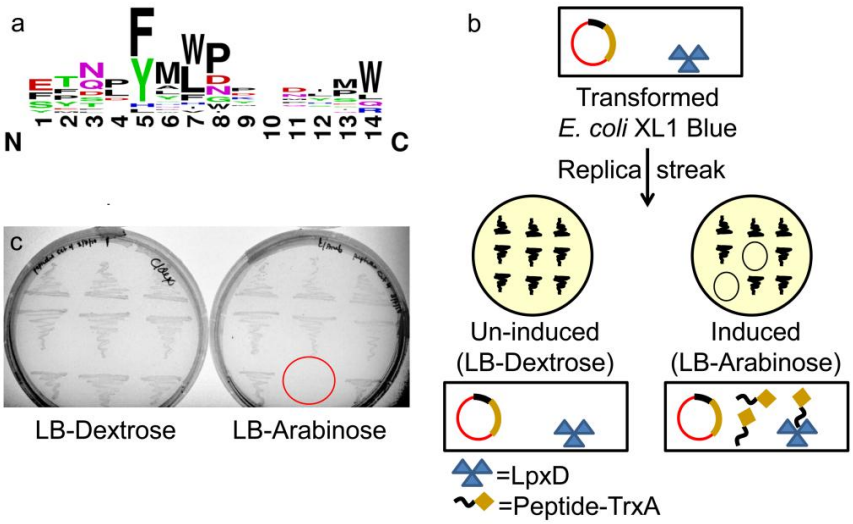

Figure 3.2. Identification and selection of bioactive peptides. a) Sequences of the peptides identified from phage display after rounds 3 and 4 of selection. The figure was generated by WebLogo (weblogo.berkeley.edu) subsequent to alignment in Clustal W. The size of the characters at any given position denotes the frequency of an amino acid, while the height of the stack is indicative of sequence conservation. b) Outline of bioactivity screen for peptides from phage display: *E. coli* XL1 Blue was transformed with a pool of plasmids coding for the expression of peptides identified from phage display (under the control of the P_{araBAD}) and evaluated under peptide induction and non-induction conditions. c) Representative replica plates from bioactivity screen: LB-Dextrose (non-induction of peptide), LB-Arabinose (induction of peptide). Red circle indicates no growth of bacteria upon in vivo peptide expression.

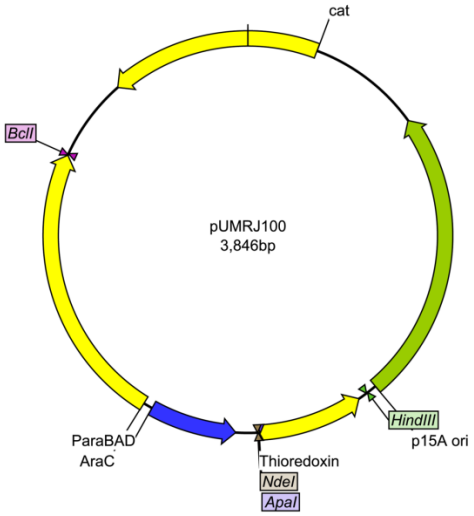

Figure 3.3. Bioactivity screening plasmid. Peptide coding sequences identified from phage display were cloned separately into the *NdeI*/*ApaI* sites of pUMRJ100. Upon induction with L-arabinose in *E. coli* XL1 Blue the cloned peptides are expressed as protein fusions with thioredoxin.

Purified native LpxA and His_6-LpxD, which has been shown in literature to exhibit equal activity to wild-type LpxD, were used in peptide binding studies (1). The

binding of fluorescein-labeled peptide to acyltransferase was assessed by measuring the changes in fluorescence polarization, which reflects changes in polarization of emitted light due to the differences in mobility between free and protein bound fluorescein-labeled peptide, when excited by polarized light. RJPXD33 was chosen for fluorescent labeling because of its bioactivity and disproportioned representation among the randomly selected phage. Increasing concentrations of acyltransferase, in the presence of fixed [FITC-RJPXD33], resulted in a sigmoidal binding isotherm upon plotting fluorescence polarization (mP) versus Log [acyltransferase]. FITC-RJPXD33 exhibited a K_d = 607 ± 40 nM for His_6-LpxD with a ΔmP = 295 ± 3 (Figure 3.4, panel a). While in the presence of LpxA, FITC-RJPXD33 exhibited a K_d = 20 ± 1.5 μM and a ΔmP of 254 ± 3. As a negative control experiment, FITC-RJPXD33 was tested against *E. coli* MurA, UDP-*N*-acetylglucosamine enolpyruvyl transferase, under the same conditions as with LpxA and LpxD. At 300 μM MurA no significant polarization was observed with FITC-RJPXD33.

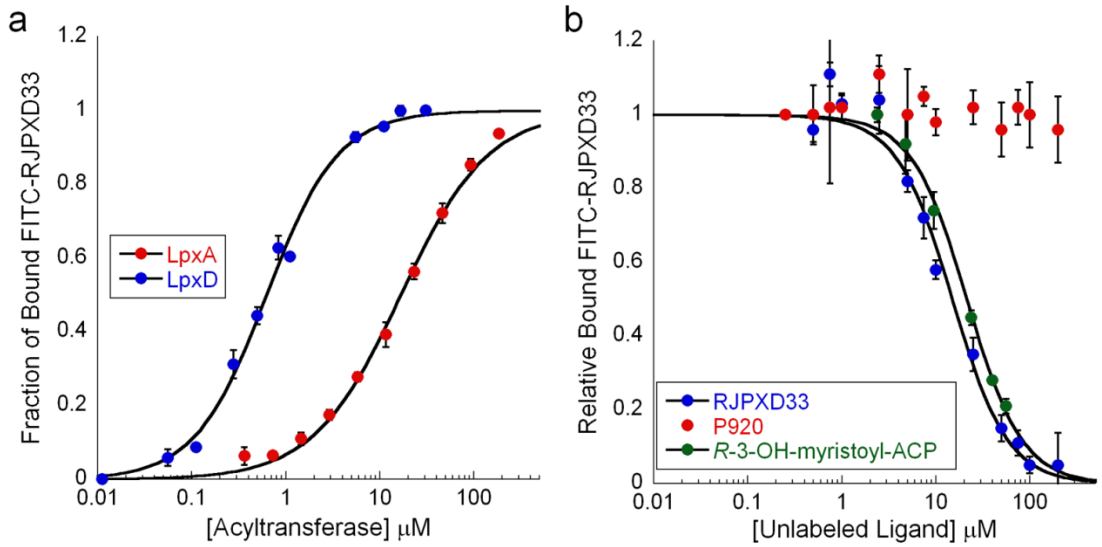

Figure 3.4. Direct and competetion binding data for bioactive peptides. a) Binding plot showing binding of FITC-RJPXD33 to both LpxD and LpxA. FITC-RJPXD33 was held constant at 20 nM while LpxD or LpxA were titrated at increasing concentrations to determine the binding isotherms. b) A fluorescent, competition LpxD binding assay, in which FITC-RJPXD33 (20 nM) and LpxD (660 nM) were held constant while unlabeled competing ligand (RJPXD33 (blue), P920 (red), or *R*-3-OH-myristoyl-ACP (green)) was titrated at various concentrations. P920 did not demonstrate binding to LpxD. All data points represent the mean of three individual experiments with error bars representing the standard deviation. The relative amount of bound labeled peptide was normalized by dividing the ΔmP obtained in the presence of competing ligand by the ΔmP obtained in the absence of competing ligand.

Competition binding experiments against unlabeled peptides were also carried out. In these experiments, the ability of labeled peptide to bind to acyltransferase, at varying concentration of unlabeled peptide, was ascertained. RJPXD33 was able to compete against FITC-RJPXD33 for binding to His_6-LpxD (K_d = 6.5 ± 0.2 μM; Figure 3.4, panel b) and against FITC-P920 for binding to LpxA (K_d = 22 ± 2.1 μM; Figure 3.5 panel a). RJPXD31 and RJPXD34 were able to displace FITC-RJPXD33 from LpxD as well, with K_ds of 41 ± 3 μM and 31 ± 1.5 μM, respectively (Table 3.2; Figure 3.5, panel c). The binding of these two peptides to LpxA were weaker than that of RJPXD33, with RJPXD31 displaying K_d = 119 ± 9 μM, while RJPXD34 did not bind at concentrations up to 300 μM (Figure 3.5, panel b). Unlike the LpxD-binding peptides, FITC-P920 showed

binding to LpxA, K_d = 187 ± 19 nM, ΔmP = 269 ± 3, but did not bind to His_6-LpxD at concentrations up to 50 μM. Unlabeled P920 demonstrated a K_d of 4.7 ± 0.2 μM for LpxA (Figure 3.5, panel a), but could not compete against FITC-RJPXD33 for binding to His_6-LpxD (Figure 3.4, panel b), as evidenced by no decrease in polarization at concentrations up to 300 μM of unlabeled P920.

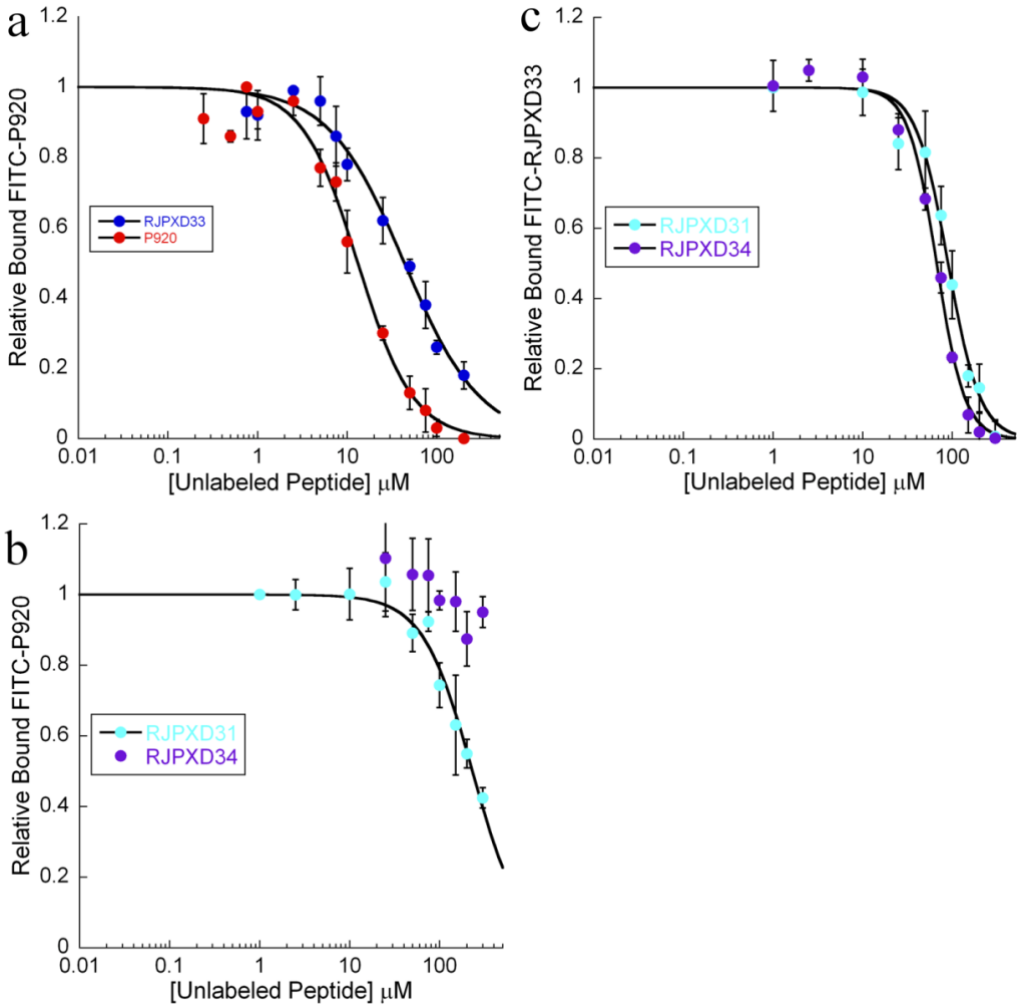

Figure 3.5. Competition FP assays with unlabeled ligands. Panel a unlabeled RJPXD33 and P920 were competed against FITC-P920 for binding to LpxA. In panel b, unlabeled RJPXD31 and RJPXD34 were competed against FITC-P920 for binding to LpxA. In panel c, RJPXD31 and RJPXD34 were competed against FITC-RJPXD33 for binding to LpxD.

The above results underscore the unique nature of peptides identified herein. Each of the bioactive peptides identified in this study bound to LpxD with dissociation

constants in the range of 6-40 μM. Despite the sequence similarities however, our studies show that RJPXD34 is specific for binding to LpxD, showing no binding to LpxA, while RJPXD31 and 33 show affinity for LpxD as well as LpxA. Those peptides having affinity for both acyltransferases bound approximately three times more tightly to LpxD than to LpxA, which is expected since they had been identified from biopanning against LpxD. Interestingly, the FITC-labeled RJPXD33 bound approximately thirty times more tightly to LpxD than to LpxA. While labeled RJPXD33 had the same affinity as the unlabeled peptide to LpxA, the labeled peptide bound ten times tighter than the unlabeled peptide to LpxD. This may indicate that the β-alanyl-fluorescein moiety is making more extensive interactions within LpxD.

Bioactive peptides were then tested for their abilities to interfere with substrate binding and acyltransferase activity. Inhibition of enzyme activity was determined for our highest affinity dual binding peptide (RJPXD33) and our LpxD-specific peptide (RJPXD34), using a recently described fluorescent acyltransferase assay (Table 3.2; Figure 3.6). RJPXD33 displayed IC_{50}s of 3.5 ± 0.08 μM and 19 ± 1.2 μM against LpxD and LpxA, respectively, which were consistent with the relative binding affinities of the unlabeled peptide for each of the acyltransferases (above). Likewise, RJPXD34 had an IC_{50} of 26 ± 3.0 μM against LpxD and did not inhibit LpxA. Next, competition binding experiments against acyl-ACP substrate was carried out. In this experiment the ability of labeled peptide to bind to acyltransferase in the presence of substrate was ascertained. Utilizing FITC-RJPXD33 as our tracer, *R*-3-hydroxymyristoyl-ACP shows competitive binding with labeled peptide to LpxD, with a dissociation constant of 8.8 ± 0.7 μM (Figure 3.4, panel b). This binding constant for acyl-ACP was in good accordance with

the published K_m value for acyl-ACP to LpxD (1). As a control, fluorescein-labeled RJPXD33 was evaluated for binding to 50 μM holo-ACP or acyl-ACP alone and displayed no significant increase in fluorescence polarization, indicating that the peptide was not binding to ACP. Recent kinetic characterization of *E. coli* LpxD described an ordered mechanism where acyl-ACP binding is the initial event (1). Peptides in this study were also selected to bind to the unbound form of LpxD and our binding studies show that RJPXD33 binds to LpxD in a mutually exclusive manner with *R*-3-hydroxymyristoyl-ACP, representing a potential basis for its inhibitory activity. Likewise, RJPXD33 binds to LpxA in a competitive fashion with P920, which has previously been shown to be a competitive inhibitor of LpxA with respect to *R*-3-hydroxymyristoyl-ACP (2). These observations are consistent with other studies in which randomly selected phage-bound peptides have been shown to bind to "hot spots" at protein•protein or protein•ligand interfaces (17,18).

Table 3.2. Binding constants of labeled and unlabeled peptides for acyltransferases.

Peptide Sequence	LpxD K_d (IC_{50}) μM	LpxA K_d (IC_{50}) μM
TNLYMLPKWDIP-NH_2 (RJPXD33)	6.5 ± 0.2 (3.5 ± 0.08)	22 ± 2.1 (19 ± 1.2)
FITC-(βa)TNLYMLPKWDIP-NH_2 (FITC-RJPXD33)	0.6 ± 0.04	17 ± 1.6
SENNFMLPLLPL-NH_2 (RJPXD34)	31 ± 1.5 (26 ± 3.0)	DNB
QHFMVPDINDMQ-NH_2 (RJPXD31)	41 ± 3	119 ± 9
SSGWMLDPIAGKWSR (P920)	DNB	4.7 ± 0.2
FITC-(βa)SSGWMLDPIAGKWSR-NH_2 (FITC-P920)	DNB	0.19 ± 0.02

(βa) - β-alanine used for the N-terminal labeling with FITC. DNB – Did Not Bind. Binding constants for FITC labeled peptides were obtained from direct binding experiments as described in Methods. Binding constants for non-labeled peptides were obtained from competition binding experiments against FITC labeled peptides. IC_{50} values were obtained using a fluorescent acyltransferase assay as described in Methods.

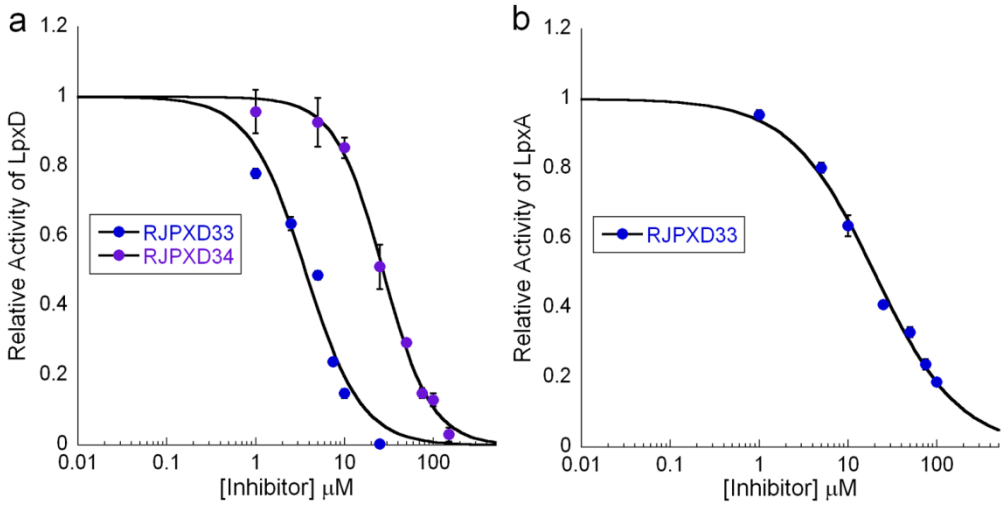

Figure 3.6. IC_{50} determination of RJPXD33 and RJPXD34. Measurements were performed in accordance with the materials and methods. IC50's were calculated using the following formula:

$$\frac{v_i}{v_o} = \frac{1}{1 + \left(\frac{[I]}{IC_{50}}\right)^h}$$

Where v_i is the initial velocity in the presence of inhibitor, v_o is the initial velocity in the absence of inhibitor, [I] is the concentration of inhibitor, IC_{50} is the concentration of inhibitor at 50% inhibition, and h is the hill slope. IC50's were determined a) for RJPXD33 (blue) and RJPXD34 (purple) against LpxD and b) for RJPXD33 (blue) against LpxA. RJPXD34 displayed no inhibition of LpxA at concentrations up to 200 μM. Data points represent the mean of three individual experiments and error bars represent the standard deviation.

Overexpression of an essential enzyme to suppress the toxicity of an antibacterial agent is a validated strategy used to identify subcellular targets (19-21). This multicopy suppression strategy was adopted to determine whether or not the antibacterial activity displayed by peptides identified in this study were due to inhibition of LpxD in vivo. Again, for this evaluation the most potent dual binding peptide, RJPXD33, as well as the LpxD-specific peptide, RJPXD34 were assessed in cells containing pUC18 or pUC18::*lpxD*. As seen previously, induction of peptide fusions alone expressing RJPXD33 or RJPXD34 showed no growth. However, as expected, suppression of antibacterial activity was seen upon induction of peptide fusions in cells containing additional extrachromasomally expressed LpxD resulting in bacterial growth (Figure

3.7). These data are consistent with the in vitro binding and inhibition studies and indicate that the bioactive LpxD-binding peptides primary mode of antibacterial activity is due to inhibition of LpxD. The stronger LpxD affinity along with the weaker LpxA binding affinity of RJPXD33 may account for the fewer number of colonies observed in the LpxD overexpression strain, as compared to RJPXD34.

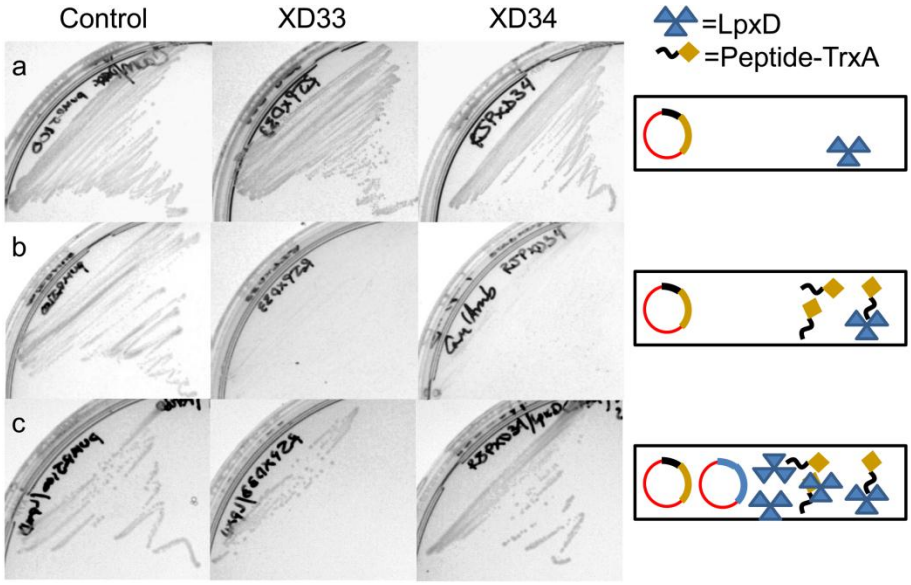

Figure 3.7. *In vivo* bioactivity assay. (A). Cells containing pUMRJ100::RJPXD33 (XD33) or pUMRJ100::RJPXD34 (XD34) were plated on LB-dextrose (1.0% *w/v*) or (B) on plates containing LB-arabinose (0.2% *w/v*). (C) Cells containing pUC18::*lpxD* and the peptide fusion constructs were further plated on LB-arabinose to demonstrate that over-expression of LpxD could suppress the toxicity induced by the peptide fusions.

In conclusion, the LpxD *N*-acyltransferase is an essential enzyme of lipid A biosynthesis and has been touted as a novel subcellular target for antimicrobial development (1). The toxicity associated with the expression of LpxD-binding peptides in *E. coli* in this current study serves as the first example of in vivo chemical inhibition of LpxD activity and further validates LpxD as an antibiotic target. With the continuing rise in resistance to current antimicrobial chemotherapy, much interest exists in finding new, less resistance-prone ways to inhibit bacterial growth. An underexplored, yet promising, niche in the field of antimicrobial development is the targeting of multiple essential

proteins with a single antimicrobial agent (22,23). Such unique agents require an organism to obtain multiple mutations in several essential targets in order to display clinically relevant resistance (24). With the identification of RJPXD33, the targeting of the structurally and functionally similar acyltransferases, LpxA and LpxD may provide another such opportunity. Moreover, protein•ACP interaction inhibitors directed against bacterial Type II ACP-dependent acyltransferases represent an untapped area for the development of unique protein•protein interaction inhibitors as potential antibacterial agents. Finally, this work has identified novel peptides that can serve as surrogate ligands for both LpxA and LpxD. Surrogate ligands such as these can serve as templates for the development of peptidomimetic based compounds more amenable to chemotherapeutic drug delivery. Furthermore, such peptides can be used to develop fluorescent binding assays, such as described above, to facilitate biological screening activities for the identification of small molecule acyltransferase inhibitors.

Acknowledgements/Contributions

This research was supported in part by a Valteich Research Award administered by the College of Pharmacy, University of Michigan and by a Pre-Doctoral Research Grant administered by the University of Michigan Rackham Graduate School. R.J.J was supported in part by the University of Michigan Chemistry-Biology Interface (CBI) training program (NIH), grant number 5T32GM008597-14 and an American Foundation for Pharmaceutical Education fellowship. The authors would like to thank the Peptide Synthesis Facility at the Division of Structural Biochemistry of the Research Center Borstel, Germany, for the gift of unlabeled P920.

Experiments were planned by R.J.J. and G.D.D. Experiments were performed by R.J.J. The original manuscript was written by R.J.J. and G.D.D.

References

1. Bartling, C. M., and Raetz, C. R. (2008) *Biochemistry* **47**, 5290-5302
2. Williams, A. H., Immormino, R. M., Gewirth, D. T., and Raetz, C. R. H. (2006) *Proc. Natl. Acad. Sci. U. S. A.* **103**, 10877-10882
3. Kelly, T. M., Stachula, S. A., Raetz, C. R., and Anderson, M. S. (1993) *J. Biol. Chem.* **268**, 19866-19874
4. Schaffer, M. L., Deshayes, K., Nakamura, G., Sidhu, S., and Skelton, N. J. (2003) *Biochemistry* **42**, 9324-9334
5. Benson, R. E., Gottlin, E. B., Christensen, D. J., and Hamilton, P. T. (2003) *Antimicrob. Agents Chemother.* **47**, 2875-2881
6. Toogood, P. L. (2002) *J. Med. Chem.* **45**, 1543-1558
7. Kwon, K., and Beckett, D. (2000) *Protein Sci.* **9**, 1530-1539
8. Beckett, D., Kovaleva, E., and Schatz, P. J. (1999) *Protein Sci.* **8**, 921-929
9. Sparks, A. B., Adey, N. B., Cwirla, S., and Kay, B. K. (1996) *Phage display of peptides and proteins: A laboratory manual*, 227-253
10. Jenkins, R. J., and Dotson, G. D. (2012) *Anal. Biochem.* **425**, 21-27
11. Nikolovska-Coleska, Z., Wang, R., Fang, X., Pan, H., Tomita, Y., Li, P., Roller, P. P., Krajewski, K., Saito, N. G., Stuckey, J. A., and Wang, S. (2004) *Anal Biochem* **332**, 261-273
12. Bartling, C. M., and Raetz, C. R. H. (2009) *Biochemistry* **48**, 8672-8683
13. Buetow, L., Smith, T. K., Dawson, A., Fyffe, S., and Hunter, W. N. (2007) *Proc. Natl. Acad. Sci. U. S. A.* **104**, 4321-4326
14. Lesaicherre, M. L., Lue, R. Y., Chen, G. Y., Zhu, Q., and Yao, S. Q. (2002) *J Am Chem Soc* **124**, 8768-8769
15. Larkin, M. A., Blackshields, G., Brown, N. P., Chenna, R., McGettigan, P. A., McWilliam, H., Valentin, F., Wallace, I. M., Wilm, A., Lopez, R., Thompson, J. D., Gibson, T. J., and Higgins, D. G. (2007) *Bioinformatics* **23**, 2947-2948
16. Wickner, W. (1988) *Biochemistry* **27**, 1081-1086
17. Sidhu, S. S., Fairbrother, W. J., and Deshayes, K. (2003) *Chembiochem* **4**, 14-25
18. DeLano, W. L., Ultsch, M. H., de Vos, A. M., and Wells, J. A. (2000) *Science* **287**, 1279-1283
19. Xu, H. H., Real, L., and Bailey, M. W. (2006) *Biochem. Biophys. Res. Commun.* **349**, 1250-1257
20. Li, X., Zolli-Juran, M., Cechetto, J. D., Daigle, D. M., Wright, G. D., and Brown, E. D. (2004) *Chem. Biol.* **11**, 1423-1430
21. Chopra, I. (1998) *J. Antimicrob. Chemother.* **41**, 584-588
22. Pucci, M. J., Podos, S. D., Thanassi, J. A., Leggio, M. J., Bradbury, B. J., and Deshpande, M. (2011) *Antimicrob. Agents Chemother.* **55**, 2860-2871
23. Charifson, P. S., Grillot, A. L., Grossman, T. H., Parsons, J. D., Badia, M., Bellon, S., Deininger, D. D., Drumm, J. E., Gross, C. H., LeTiran, A., Liao, Y., Mani, N., Nicolau, D. P., Perola, E., Ronkin, S., Shannon, D., Swenson, L. L., Tang, Q., Tessier, P. R., Tian, S. K., Trudeau, M., Wang, T., Wei, Y., Zhang, H., and Stamos, D. (2008) *J. Med. Chem.* **51**, 5243-5263
24. Charifson, P. S., Grillot, A.-L., Grossman, T. H., Parsons, J. D., Badia, M., Bellon, S., Deininger, D. D., Drumm, J. E., Gross, C. H., LeTiran, A., Liao, Y.,

Mani, N., Nicolau, D. P., Perola, E., Ronkin, S., Shannon, D., Swenson, L. L., Tang, Q., Tessier, P. R., Tian, S.-K., Trudeau, M., Wang, T., Wei, Y., Zhang, H., and Stamos, D. (2008) *Journal of Medicinal Chemistry* **51**, 5243-5263

Chapter 4

Structural and Biochemical Characterization of the Dual Targeting Acyltransferase Inhibitor of Lipid A Biosynthesis

An inhibitor (RJPXD33; TNLYMLPKWDIP-NH_2) was recently identified that demonstrated affinity for both LpxD and LpxA (1). While peptides display susceptibility to proteases and poor bioavailability, they have become a coveted tool in chemists and biologists repertoires, owing to the ease of synthesis and functional utility. Thus much attention has been given to the strategies or designing of "peptide mimics", or peptidomimetics, that display greater bioavailability, enhanced three dimensional structural characteristics and proteolytic stability compared to their natural counterparts (2). However, a structural and biochemical understanding of how the peptide interacts with its host complex is crucial to the development of peptidomimetics.

The molecular mechanism by which RJPXD33 interacts with either LpxA or LpxD is currently unknown. Herein, we have utilized x-ray crystallography and peptide photo-affinity probes to provide insights into the binding interactions between the acyltransferases and RJPXD33. Furthermore, acyltransferase binding studies utilizing truncations of RJPXD33 were undertaken in order to identify the minimal sequence necessary to inhibit both LpxA and LpxD, as well as to provide biochemical verification of the structural data obtained.

Experimental Procedures

Materials. Bio-Rad Protein assay and BioGel P2 size exclusion gel were purchased from Bio-Rad. LB (Lenox) broth and agar were purchased from Difco. Fluorescein isothiocyanate (FITC) was purchased from Acros Organics. Natural amino acids, Rink Amide Resin and Fmoc-OSu were purchased from Anaspec. Fmoc-4-Azido-L-phenylalanine was purchased from Chem-Impex. Photo-leucine (PhotoLeu) and HPDP-Biotin were purchased from Thermo Fisher/Pierce. Benzonase was purchased from Novagen. Trypsin Gold was purchased from Promega. MS grade GluC was purchased from Roche. All buffers and antibiotics were purchased in the highest grade from Sigma Aldrich or Fisher Scientific.

Protein Crystallography. Protein purification was carried out as previously described (3). Prior to crystallization, purified LpxA (10 mg/mL) was incubated for 1 h at 4 °C in the presence of 600 μM RJPXD33 (final concentration of DMSO was 2% *v/v*). The mixture was centrifuged at 10,000 x*g* for 10 min at 4 °C to pellet any insoluble material. Crystals were grown by vapor diffusion in a sitting drop tray. Droplets contained 2 μL of the LpxA-RJPXD33 solution and 2 μL of a well solution containing 0.8 – 1.8 mM Phosphate buffer (pH 6.3 – 6.8) and 31 – 34 % DMSO. Crystals formed within 24 h. Crystals were cryoprotected in well solution containing 20% glycerol and flash frozen in liquid nitrogen. X-ray data was collected at LS-CAT ID-21-F and –G lines at the Advanced Photon Source at Argonne National Laboratory. Data was processed using HKL2000 software (4). The complex was solved by molecular replacement with Phaser (5) using a previously solved structure of LpxA (containing no ligands; pdb 1LXA) as the starting model (6). Iterative rounds of refinement and model building were

completed using Buster (7) and Coot (8). MolProbity (9,10) and Parvarti (11) were used to validate the structures. Figures were generated in PyMol (Schrödinger LLC). The LpxA-RJPXD33 data collection and refinement statistics are given in Table 4.1.

Fluorescence Polarization (FP) Assay. Peptides were synthesized as previously reported for solid phase peptide synthesis (12). The FP assay was performed as previously described (1). In 384-well black Costar plates, LpxA or His_6-LpxD were serially diluted while holding the fluorescent peptide at 20 nM in a final volume of 50 μL in 20 mM HEPES pH 8.0 (~0.01% DMSO). The wells were gently mixed and incubated at 30 °C in the dark for 15 min. Polarization was measured on a SpectraMax M5 plate reader in triplicate with readings taken at λ_{ex} = 485 nm and λ_{em} = 525 nm. The binding data was first fit to a standard binding isotherm (eq 1):

$$mP = mP_f + \left[\left(mP_b - mP_f\right)\left(\frac{[P]}{[P] + K_d}\right)\right] \quad (1)$$

where mP is the experimentally determined polarization, mP_f is the polarization of free FITC-RJPXD33, [P] is the total acyltransferase concentration, K_d is the dissociation constant of peptide-protein complex, and mP_b is the polarization value of fully bound fluorescent peptide. The calculated mP_b was used to normalize the experimental data to fit the binding curves to the Hill equation (eq 2), where a is the fraction of FITC-peptide bound, h is the Hill coefficient, [P] is the total concentration of acyltransferase, and K_d is the dissociation constant of the peptide-protein complex.

$$\propto = \frac{\left(\frac{[P]}{K_d}\right)^h}{1 + \left(\frac{[P]}{K_d}\right)^h}$$

(2)

For competition binding assays, 220-660 nM of acyltransferase was incubated in the presence of varying concentrations of unlabeled peptides or acyl-ACP for 10 min at 30 °C in the dark. The $[I]_{50}$ was determined from the competition binding curve and the dissociation constant of unlabeled ligand was calculated as previously described (13) using eq. 3:

$$K_i = \frac{[I]_{50}}{\frac{[L]_{50}}{K_d} + \frac{[P]_0}{K_d} + 1}$$

(3)

where $[I]_{50}$ is the unlabeled peptide concentration (inhibitor) at 50% inhibition, $[L]_{50}$ is the free ligand (fluorescent tracer) concentration at 50% inhibition, $[P]_0$ is the free protein concentration at 0% inhibition, K_d is the dissociation constant of fluorescent peptide (tracer), and K_i is the calculated dissociation constant for unlabeled peptide.

Fmoc-Photoleucine. Fmoc-PhotoLeu was synthesized as previously described (14). In an aluminum foil covered round bottom flask, PhotoLeu (1.4 mmol, 200 mg) and sodium bicarbonate (2.8 mmol, 236 mg) were dissolved in 20 mL of H_2O and chilled to 0 °C on ice. Fmoc-OSu (2.1 mmol, 708 mg) was dissolved in 10 mL of THF and dropwise added over 15 min to the covered round bottom flask. The resulting slurry was stirred on ice for 10 min and then allowed to warm to room temperature for 8 h. The flask was placed on ice and the reaction was stopped by addition of 25 mL of H_2O and 50 mL ethyl

acetate (EtOAc) followed by acidification to pH 2 with concentrated HCl. The product was extracted (3x) with 50 mL EtOAc and concentrated by rotary evaporation. The resulting white solid was purified by flash chromatography with 1% methanol (*v/v*) and 1% acetic acid (*v/v*) in dichloromethane. The product was obtained as a white solid (464 mg, 91%). 1H NMR (400 MHz, DMSO) d 12.70 (s, 1H), 7.87 (d, J = 7.5, 2H), 7.71 (dd, J = 7.6, 4.4, 3H), 7.39 (t, J = 7.4, 2H), 7.30 (t, J = 7.4, 2H), 4.38 - 4.16 (m, 3H), 3.89 - 3.76 (m, 1H), 1.93 - 1.81 (m, 1H), 1.63 (dd, J = 14.8, 10.8, 1H), 0.99 (s, 3H). HRMS ESI^+: calculated for $[M+Na]^+$, 388.1278; observed 388.1276.

Biotinylation of Photo-affinity Peptides. Purified peptides (~2–3 mg) were resuspended in 50% DMF/10% ACN/0.1% TFA at a concentration of 0.4 mM. HPDP-Biotin was added to a concentration of 0.8 mM and the solutions were incubated overnight (~16 h) at 37 °C (15). The resulting mixture was purified by RP-HPLC, lyophilized and confirmed by high resolution ESI-MS.

Covalent Cross-linking of RJPXD33 Photo-affinity Probes to LpxD. Photo-activatable peptides (24 μM) were incubated with LpxD (10 μM), in the presence or absence of unlabeled peptide (150 μM) in 96-well half-area clear plates on ice in a final volume of 30 μL in 20 mM HEPES pH 8.0 (DMSO 1% *v/v*). Plates, remaining on ice, were irradiated using a UV lamp (UVP model UVGL-58) at λ = 365 nm for 10 min at a distance of ~2 cm. Samples were subsequently loaded and run on a 12% Tris-glycine SDS-PAGE gel. Gels were washed three times for 20 min at room temperature with deionized water to remove SDS. For fluorescein-labeled peptides, gels were analyzed for in-gel fluorescence using a Typhoon 9400 imaging system set to fluorescein wavelength (λ_{ex} = 485 nm and λ_{em} = 525 nm), PMT sensitivity at 500 and pixel size at 50 microns.

The resulting data was visualized using ImageQuant 5.2 software (RSBS-ANU). Following in-gel fluorescence analysis, gels were stained using SimplyBlue SafeStain (Invitrogen).

Peptide Enrichment for MS Analysis. Biotin-Photopeptides (200 μM) were incubated on ice with LpxD (10 μM) in a final volume of 500 μL and cross-linked as described above. Excess biotin-Photopeptide was removed by ultrafiltration in a Microcon YM-10 concentrator (Millipore) and subsequent washing (5x) with 500 μL of 100 mM $(NH_4)HCO_3$ pH 7.8. The concentrated fractions (~100 μL) of biotin-Photopeptide 1 and 3 were digested (per manufacturer's protocol) with TrypsinGold (Pierce), while biotin-Photopeptide 4 was digested with GluC (Roche). GluC digestion was necessary to avoid loss of the biotin-tag in Photopeptide 4 owing to an inherent trypsin site upstream of the cross-linking site. Digestions were carried out at 37 °C for 5 h and reactions were stopped by heating at 70 °C for 20 min followed by vortexing multiple times. Samples were loaded onto Streptavidin-conjugated DynaBeads (Invitrogen) with 1 h incubation at room temperature. The beads were washed (6x) with 100 mM $(NH_4)HCO_3$ pH 7.8 (500 μL) to remove unbound peptide. Bound peptides were eluted by incubating the beads in 100 mM $(NH_4)HCO_3$, 100 mM DTT pH 7.8 at 37 °C for 1 h (2 x 150 μL). Samples were speed vacuum dried, brought up in 50 μL of H_2O and frozen at -80 °C until analyzed by MS.

Results

The co-crystal structure of LpxA•RJPXD33 (TNLYMLPKWDIP-NH_2) diffracted to a resolution of 1.9 Å. The structure was solved by molecular replacement using a previously solved structure of LpxA (PDB code 1LXA), containing no ligands, as the

model structure (6). The structure was refined to an R_{factor} and R_{free} of 0.179 and 0.188, respectively, while maintaining a good MolProbity score and low clash score (9). The complete crystallography and refinement statistics can be found in Table 4.1.

One molecule of LpxA and RJPXD33 occupied the asymmetric unit. However, three asymmetric units form around a 3-fold crystallographic axis, which is in agreement with other structures and previous data showing that LpxA is a homotrimer (16-18). Consistent with other structures, all of the 262 amino acids of LpxA, with the exception of the first methionine side chain, were visible in the electron density map. The N-terminus of RJPXD33 binds within the region between two monomeric subunits, constituting the LpxA active site, with a portion of the M5 side chain missing (19). The six N-terminal amino acids of RJPXD33, TNLYML, run vertically up the bifurcated active site with T1 positioned at coil 6 of LpxA LβH and L6 at coil 10. Three parallel β strands make up one LβH coil. The side chains of T1, L3, and M5 all point inward toward the hydrophobic cleft between parallel β strand 3 (PB3) of the LpxA subunit within the asymmetric unit and PB2 of the adjacent subunit. The side chains of Y4 and L6 occupy separate hydrophobic pockets along PB2 of the adjacent subunit, while the N2 side chain makes a favorable amide-π center stacked interaction with the Y4 side chain (20,21). The density of the C-terminal six amino acids of RJPXD33 could not be visualized in the structure (Figure 4.1A and B) most likely due to the protrusion of this portion of the peptide away from the LpxA active site and into solvent exposed space.

Table 4.1: Crystallography data collection and refinement statistics

Data Collection	
SpaceGroup	P 2_13
Unit Cell a, b, c (Å)	96.40, 96.40, 96.40
Wavelength (Å)	0.97872
Resolution (Å)[1]	1.9 (1.93 1.90)
Rsym (%)[2]	5.7 (29.7)
<I/sI>[3]	>20 (5)
Completeness (%)[4]	99.9 (100)
Redundancy	10.6 (10.1)
Refinement	
Resolution (Å)	1.90
R-Factor (%)[5]	0.179
Rfree (%)[6]	0.188
Protein atoms	2004
Solvent Molecules	213
Unique Reflections	23,751
R.m.s.d.[7]	
Bonds	0.010
Angles	1.06
MolProbity Score[8]	1.21
Clash Score[8]	4.24

[1]Statistics for highest resolution bin of reflections in parentheses.

[2]$R_{sym} = \Sigma_h \Sigma_j \, l \, I_{hj} - \langle I_h \rangle \, l \, / \Sigma_h \Sigma_j I_{hj}$, where I_{hj} is the intensity of observation j of reflection h and $\langle I_h \rangle$ is the mean intensity for multiply recorded reflections.

[3]Intensity signal-to-noise ratio.

[4]Completeness of the unique diffraction data.

[5]R-factor = $\Sigma_h \, I \, IF_oI - IF_cI \, I \, / \, \Sigma_h IF_oI$, where F_o and F_c are the observed and calculated structure factor amplitudes for reflection h.

[6]R_{free} is calculated against a 10% random sampling of the reflections that were removed before structure refinement.

[7]Root mean square deviation of bond lengths and bond angles.

[8] Chen et al. (2010) MolProbity: all-atom structure validation for macromolecular crystallography. Acta Crystallographica D66:12-21.

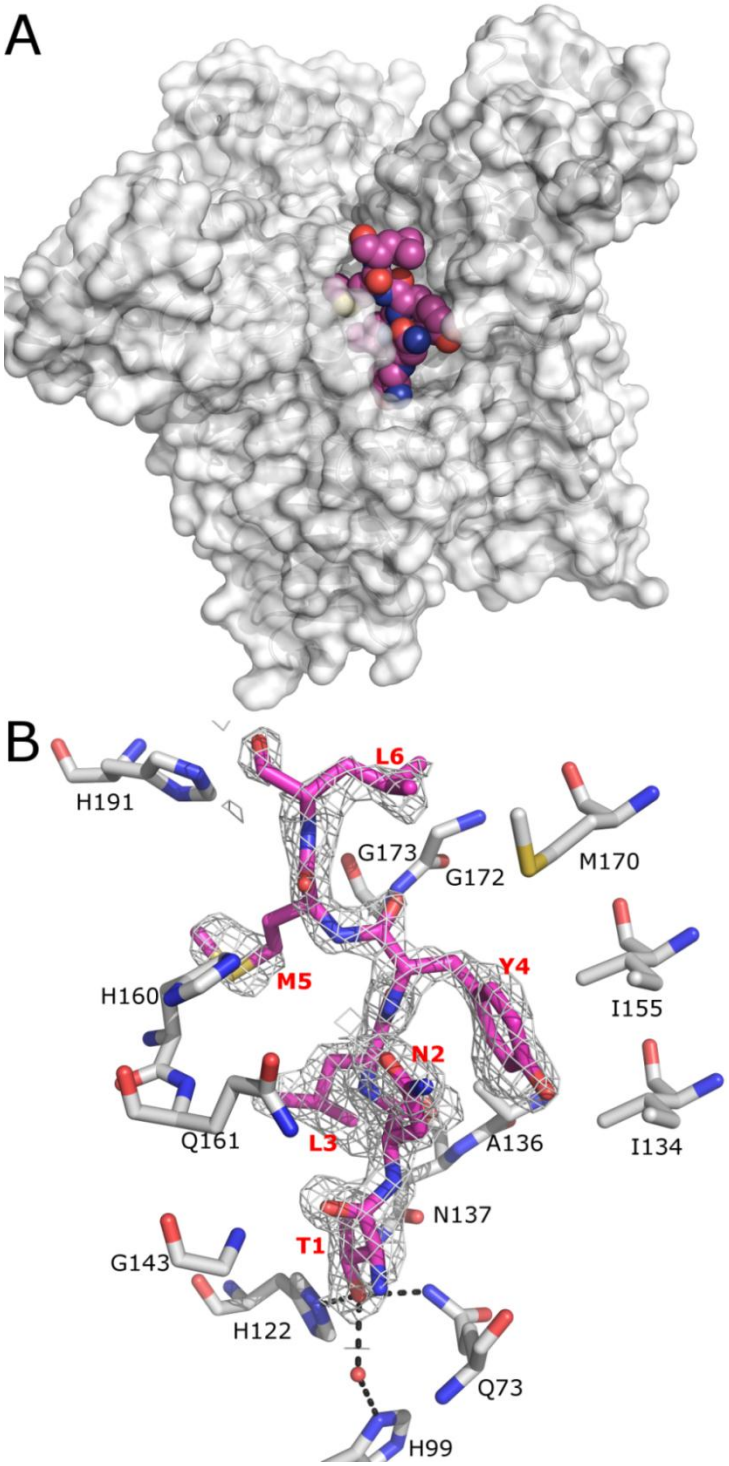

Figure 4.1. Crystal structure of RJPXD33 bound to LpxA. A. Crystal structure of RJPXD33 (magenta; spheres) in complex with LpxA (gray, surface map). Only the first six residues of RJPXD33 are modeled into the figure. RJPXD33 binds between two monomeric subunits of the trimer; only one molecule of RJPXD33 is shown. B. The $2F_o$-F_c electron density map of the RJPXD33•LpxA complex contoured to 1σ around RJPXD33 (magenta; stick) with amino acids from LpxA (gray; stick) that surround the bound ligand. Though the full density of the methionine side chain from RJPXD33 could not be visualized, His160 of LpxA kinks away from the hydrophobic cleft allowing space for the methionine side chain to occupy the binding pocket.

RJPXD33 binds to LpxA in a unique fashion when compared to P920, despite a similar primary sequence motif (YMLP v. WMLDP) between the two (22). P920 forms a β-hairpin fold where the head of the loop, isoleucine, occupies the hydrophobic cleft of LpxA and the N and C-termini face out of the pocket towards the solvent face (16). The backbone and side chains of P920 overlap into the UDP binding region when compared to the UDP-GlcNAc and UDP-3-*O*-(*R*-3-hydroxyacyl)-GlcNAc structures (17,23). In contrast, RJPXD33 has more of an extended conformation and occupies more of the hydrophobic fatty acid binding cleft, while demonstrating only a minimal overlap between the N2/Y4 side chains and the UDP binding site.

The hydroxyl moiety of the T1 side chain of RJPXD33 forms polar contacts with H122, Q73, and an active site water of LpxA. These moieties have been implicated as binding contacts to the *R*-3-hydroxymyristoyl moiety of UDP-3-*O*-(*R*-3-hydroxymryistoyl)-GlcNAc, the LpxA product (17). When the structures of RJPXD33 bound EcLpxA and the EcLpxA with bound product (PDB 2QIA) were superimposed, the T1 β-hydroxyl group was shown to occupy the same space as the *R*-3-hydroxy functional group of the myristate chain (Figure 4.2A and B). In addition to the T1 residue, the L3 and M5 side chains of RJPXD33 also occupy the fatty acyl binding region.

The co-crystal structure of EcLpxA•RJPXD33 was also superimposed onto the C-chain of the *Leptospira interrogans* LpxA-(*R*-3-hydroxylaurate)-methyl-phosphopantetheine co-crystal structure (Figure 4.2C and D; PDB 3I3A) (24). While phosphopantetheine (PPan), the post-translational modification necessary for acyl chain assembly on ACP, derivatives are not substrates for EcLpxA or EcLpxD, *R*-3-hydroxy-

lauryl-methyl-PPan has been shown to be a substrate for LiLpxA (24,25). The PPan moiety of the LiLpxA structure was modeled as two conformations due to the electron density obtained from the complex. As seen with the EcLpxA•Product structure, the T1, L3, and M5 side chains of RJPXD33 overlay with the laurate chain of the LiLpxA structure. While RJPXD33 had minimal overlap with the UDP-GlcNAc functionality in the EcLpxA•product structure, the peptide backbone of RJPXD33 occupied the same space as the acyl-PPan substrate (conformation 1). This was highlighted at the amide bond between T1 and N2 of RJPXD33, which superimposes almost identically with the thioester bond between the acyl-chain and the PPan moiety.

Of the four complexes named above, all except the P920•LpxA complex contained a H160 (H155 of LiLpxA) residue that kinked outward, towards the solvent front. The opposite was true for H160 which faces the hydrophobic pocket in the structures of the free form of LpxA (PDB 1LXA; the molecular replacement model), and complexes bound with UDP-GlcNAc (PDB 2JF3) or inhibitory peptide 920 (PDB 2AQ9) (6,16,23). These results demonstrated that H160 of LpxA must kink outwards in a conformational change to allow the peptide or fatty acyl chain to access the hydrophobic cleft. While the full electron density of the RJPXD33 M5 side chain cannot be accounted for, these results would suggest that M5 would occupy the binding region formed when H160 is kinked outward (Figure 4.2A and C).

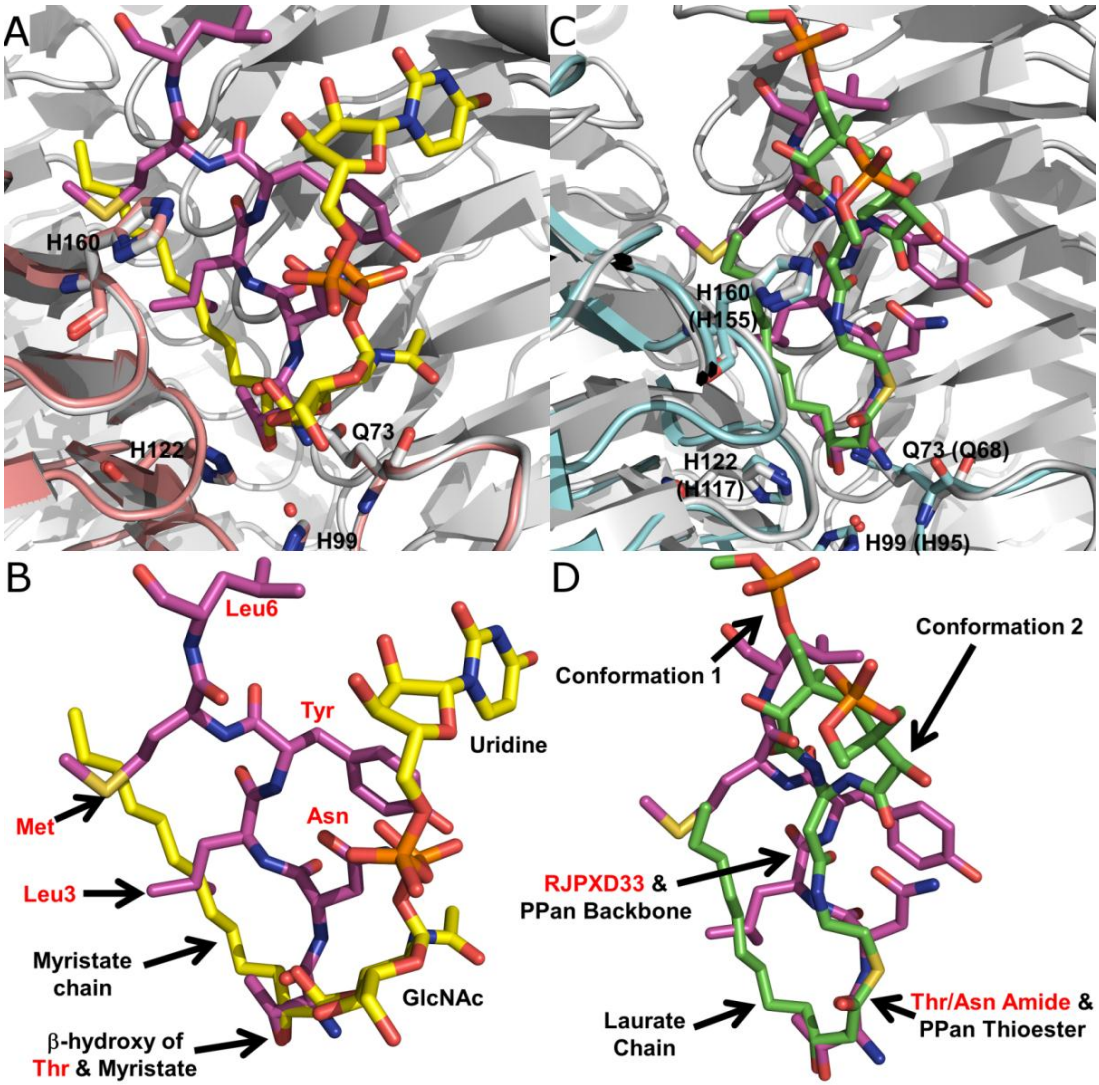

Figure 4.2. A. The RJPXD33•LpxA (magenta-gray) complex overlain against the UDP-3-*O*-(*R*-3-hydroxymyristoyl)-GlcNAc•EcLpxA complex (PDB 2QIA;yellow-pink) (27). RJPXD33, UDP-3-*O*-(*R*-3-hydroxymyristoyl)-GlcNAc, and certain side chains of LpxA (H160, H122, H99, Q73) are shown in stick diagram. The active site water which hydrogen bonds to β-hydroxymryistate and H99 is shown as a sphere (red). B. A zoomed in view of the ligands RJPXD33 (magenta) and UDP-3-*O*-(*R*-3-hydroxymyristoyl)-GlcNAc (yellow). Residues of RJPXD33 are labeled in red while UDP-3-*O*-(*R*-3-hydroxymyristoyl)-GlcNAc are labeled in black. The β-hydroxy of the threonine side chain of RJPXD33 occupies the same space where the β-hydroxy of the myristate side chain of the LpxA product is located. Furthermore, the Leu3 and Met side chains of RJPXD33 seem to occupy the hydrophobic cleft between two monomeric subunits, normally where the acyl chain of the LpxA product or acyl-ACP are suggested to bind. C. The RJPXD33•EcLpxA (magenta-grey) complex overlain against the (*R*-3-hydroxylaurate)-methyl-phosphopantetheine•LiLpxA complex (PDB 3I3A; green-cyan) (24). As in Figure 3A ligands, the active site water and certain side chains are shown in stick diagram. Residues in parenthesis represent the amino acid numbering for *L. interrogans* LpxA. D. A zoomed in view of the ligands RJPXD33 (magenta) and (*R*-3-hydroxylaurate)-methyl-phosphopantetheine (PPan). PPan was modeled into two conformations in its original structure (24). The Leu3 and Met side chains of RJPXD33 occupy the hydrophobic pocket in which the *R*-3-hydroxylaurate occupies, similar to the product complex. The amide bond between Thr and Asn of RJPXD33 overlay almost identically to the thioester bond between PPan and *R*-3-hydroxylaurate, while the peptide backbone of RJPXD33 occupies similar space in comparison to the PPan backbone in confirmation 1.

In order to validate our crystal structure and evaluate the potential for possible truncations, FITC-RJPXD33Δ6 was synthesized. FITC-RJPXD33Δ6 lacks the six terminal amino acids of full length FITC-RJPXD33. Fluorescence polarization (FP) experiments using wild-type LpxA and His_6-LpxD were performed to quantitate the binding affinity of the truncated RJPXD33 peptide (Figure 4.3). When the assay was performed with LpxA, the observed K_d for FITC-RJPXD33Δ6 was 12 $\pm$ 1 μM (Table 2). This value was in close proximity to the previously published value (K_d = 18 $\pm$ 1.6 μM) for the full length FITC-RJPXD33. This suggested that the six terminal amino acids were not making extensive binding contacts to LpxA, further validating the crystal structure.

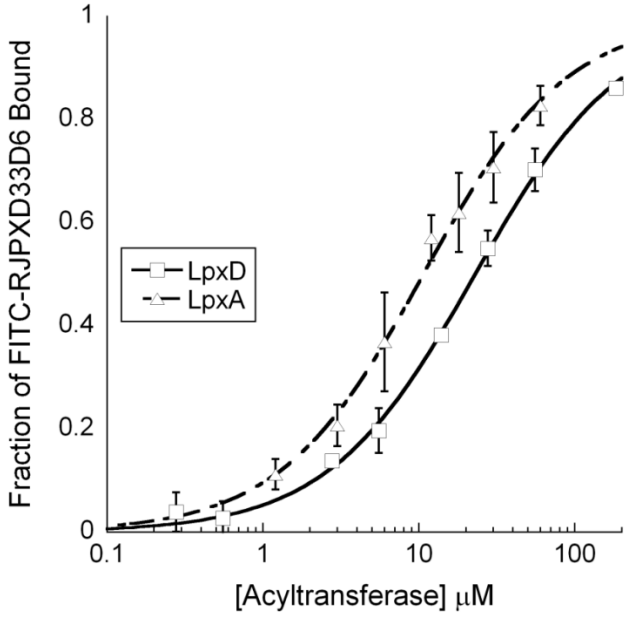

Figure 4.3. FITC-RJPXD33Δ6 binding isotherm against LpxA and LpxD. FITC-RJPXD33Δ6 (FITC-(βA)-TNLYML-$CONH_2$) was held constant (20 nM) while varying concentrations of LpxA or LpxD were titrated to generate the binding isotherm. FITC-RJPXD33Δ6 demonstrated no loss of binding affinity to LpxA (K_d = 12 $\pm$ 1 μM), when compared to FITC-RJPXD33. This suggests that the 6 C-terminal residues are not making binding contacts with LpxA which is in agreement with the crystallographic data observed. However, a significant loss of affinity for FITC-RJPXD33Δ6 was observed (K_d = 22 $\pm$ 1 μM) with respect to LpxD, suggesting that the 6 C-terminal amino acids are important for binding to LpxD. Affinities were determined from the mean of three individual experiments using the standard deviation as the calculated error.

To evaluate whether RJPXD33 bound to LpxD in a similar fashion, FITC-RJPXD33Δ6 was tested against His_6-LpxD. FITC-RJPXD33Δ6 demonstrated a binding affinity of K_d = 22 $\pm$ 1 μM. This was approximately a 30-fold decrease (FITC-RJPXD33 K_d = 0.6 $\pm$ 0.04 μM) in binding affinity compared to the full length peptide, suggesting the C-terminal residues were making substantial binding interactions to LpxD (1).

Unlabeled truncations of RJPXD33 were evaluated using a competition binding assay to identify the minimal sequence motif necessary for binding to LpxA and LpxD (Table 4.2). C-terminal truncations lacking 5, 6 or 7 amino acids demonstrated K_d's against LpxA equal to 18.6 $\pm$ 3.5 μM, 30.4 $\pm$ 2.8 μM or > 100 μM (Table 4.2). Truncations beyond the 7th amino acid displayed no appreciable binding to LpxA at concentrations up to 200 μM. RJPXD33CΔ5 demonstrated a binding affinity of 20.8 $\pm$ 1.6 μM to LpxD. RJPXD33CΔ6 bound weakly to LpxD, and C-terminal truncations beyond the 6th amino acid demonstrated no appreciable binding at concentrations up to 200 μM. These results correlated well with the direct FP binding data.

N-terminal truncations were also synthesized and tested against both LpxA and LpxD. A single truncation of RJPXD33 at the N-terminus completely abolished any binding to LpxA. Interestingly, RJPXD33NΔ1, RJPXD33NΔ2 and RJPXD33NΔ3 displayed binding affinities for LpxD equal to 1.6 $\pm$ 0.2 μM, 2.8 $\pm$ 0.4 μM and 15.3 $\pm$ 1.5 μM (Table 4.2). Truncations beyond the 3rd amino acid did not bind to LpxD.

These results suggested that the C-terminus of RJPXD33 was making extensive binding contacts to LpxD, but not to LpxA. While the first two N-terminal truncations did not adversely affect binding to LpxD, the lack of T1 completely ablated any affinity for LpxA. However, deletion of amino acids within RJPXD33's –YMLP– motif, a conserved

sequence motif identified for LpxD and LpxD/LpxA dual binding peptides (1), proved to be detrimental for binding to either target.

Table 4.2. Peptide sequences and binding affinity data for LpxD and LpxA.

Peptide	Sequence	K_d LpxD (μM)	K_d LpxA (μM)
Direct Binding Assay			
FITC-RJPXD33Δ6	FITC–β–TNLYML	22 ± 1	12 ± 1
FITC-Photo 1	FITC–β–TNXYMLPKWDIP	2.1 ± 0.3	N.T.
FITC-Photo 2	FITC–β–TNLZMLPKWDIP	D.N.B.	N.T.
FITC-Photo 3	FITC–β–TNLYMXPKWDIP	1.1 ± 0.1	N.T.
FITC-Photo 4	FITC–β–TNLYMLPKWDXP	0.8 ± 0.1	N.T.
Competition Binding Assay			
RJPXD33NΔ1	NLYMLPKWDIP	1.6 ± 0.2	D.N.B.
RJPXD33NΔ2	LYMLPKWDIP	2.8 ± 0.4	D.N.B.
RJPXD33NΔ3	YMLPKWDIP	15.3 ± 1.5	N.T.
RJPXD33NΔ4	MLPKWDIP	D.N.B.	N.T.
RJPXD33CΔ5	TNLYMLP	20.8 ± 1.6	18.6 ± 3.5
RJPXD33CΔ6	TNLYML	> 95	30.4 ± 2.8
RJPXD33CΔ7	TNLYM	D.N.B.	> 100
RJPXD33CΔ8	TNLY	D.N.B.	D.N.B.

β – β-Alanine
D.N.B – Did not bind
N.T. – Not Tested
K_d's are calculated from IC_{50} binding isotherms as described in Materials and Methods. If the IC_{50} was determined to be greater than 200 μM, the K_d's were marked > than the calculated number for an IC_{50} of 200 μM.

Numerous attempts to crystallize LpxD with RJPXD33, FITC-RJPXD33, RJPXD33Δ6 or FITC-RJPXD33Δ6 were performed, but were ultimately unsuccessful. In order to further understand how RJPXD33 binds to LpxD, derivatives of FITC-RJPXD33 containing a diazirine-based leucine derivative (14,26) or 4-azidophenylalanine were synthesized (Figure 4.4A). When irradiated with UV light these moieties can covalently cross-link to a bound protein, capturing the peptide-protein interaction. It was envisioned that a covalently linked peptide could be captured, trypsinized and the binding location could be mapped from LC/MS/MS analysis.

In order to demonstrate that the photo-affinity label did not disrupt binding, FP experiments were performed with FITC-Photopeptide 1 – 4 against LpxD (Fig 4.4B). Peptides 1, 3 and 4 containing the diazirine moiety bound to LpxD with little to no loss in binding affinity (Table 4.2, K_d's = 0.8 – 2.1 μM). The 4-azidophenylalanine substitution for tyrosine was not tolerated, as Photopeptide 2 did not show an increase in polarization with increasing concentrations of LpxD.

Owing to its binding affinity, Photopeptide 4 was chosen to undergo studies for UV time dependence (λ = 365 nm) and peptide concentration dependence of photo-labeling (Figure 4.5A and B). In a final volume of 30 μL, 10 μM of LpxD and 6 μM Photopeptide 4 were held constant while UV times were varied from 1 – 20 min. After 10 min there was no appreciable increase in fluorescence labeling of LpxD. Thus, 10 min UV irradiation was used for the remainder of the in-gel fluorescence experiments. Concentration dependence of Photopeptide 4 was tested from 0.75 – 24 μM while holding LpxD constant at 10 μM. A concentration dependent increase in fluorescence can be visualized throughout the gel, with only a slight increase from 12 to 24 μM.

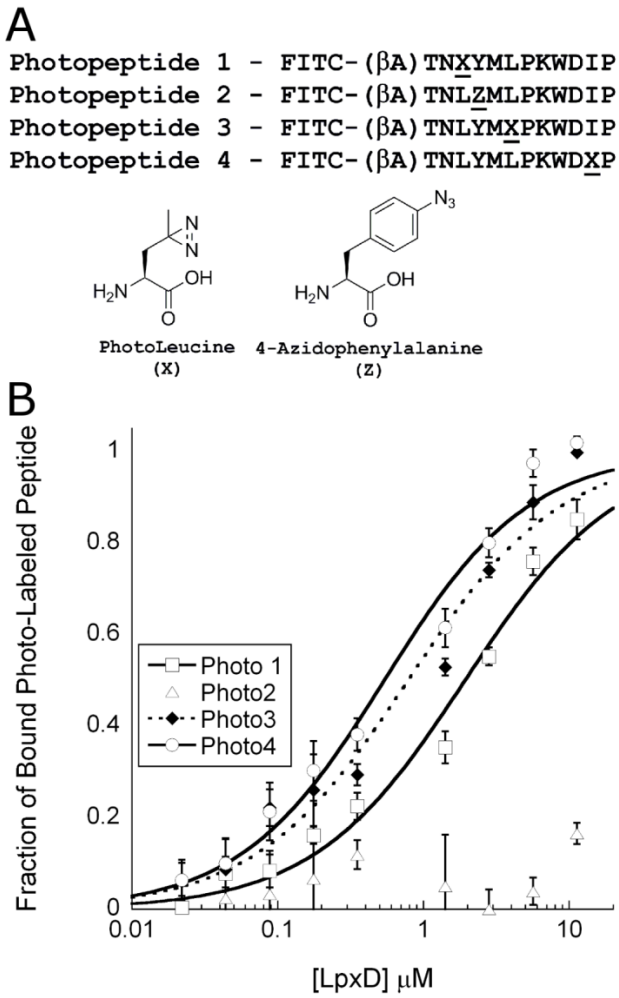

Figure 4.4. Photoactivatable peptides targeting LpxD. A. Peptide sequences containing the photo-activatable diazirine-based leucine mimic, PhotoLeu (X), or 4-azidophenylalanine tyrosine mimic (Z). B. Fluorescence polarization experiments were performed holding FITC-labeled photo-activatable peptides constant (20 nM) while varying concentrations of LpxD. All of the PhotoLeu containing FITC-labeled peptides were able to bind LpxD with only a slight loss in affinity (K_d's = 0.79 – 2.07 μM) compared to the parent peptide, FITC-RJPXD33 (K_d = 0.6 μM). However, the 4-azidophenylalanine containing peptide displayed no appreciable binding to LpxD up to ~10 μM of LpxD. Affinities were determined from the mean of three individual experiments using the standard deviation as the calculated error.

Photopeptides 1, 3 and 4 (24 μM) were subjected to UV irradiation in the presence of 10 μM LpxD with and without 150 μM of unlabeled RJPXD33 (Fig. 4.5C). When UV light was omitted no cross-linking occurred. However when the peptides and protein were irradiated with UV light peptides were covalently cross-linked to LpxD as visualized through in-gel fluorescence. Addition of unlabeled RJPXD33 significantly decreased the fluorescent signal indicating that the covalent cross-linking is due to

specific peptide•protein interactions and that the photopeptides are binding in a similar manner to the parent peptide. As a control, reactions containing LpxD without the Photopeptides were subjected to UV irradiation though no observable fluorescence was detected.

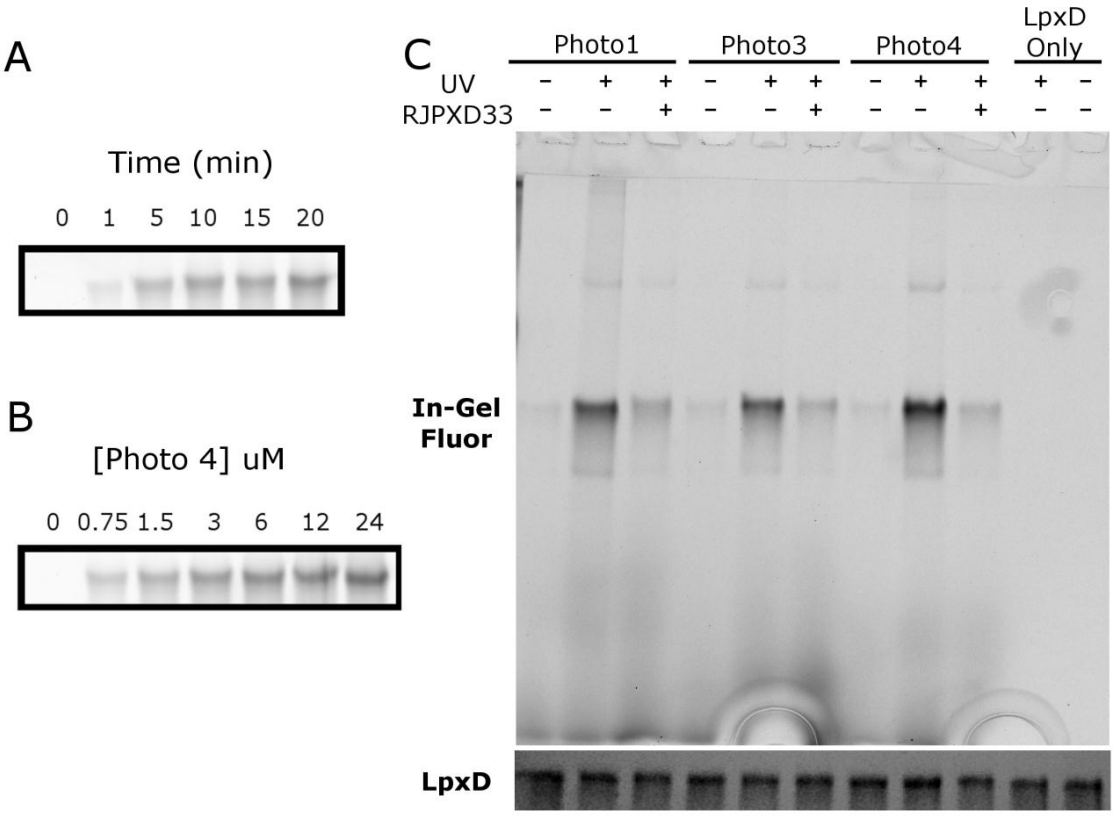

Figure 4.5. In-gel fluorescence of photo-activatable peptides. A. Time dependence of photo-crosslinking of Photo 4 to LpxD. Photo 4 and LpxD were held constant at 6 and 10 μM respectively while being irradiated with UV light (365 nm) for varying times. B. Concentration dependence of Photo 4. Concentrations of Photo 4 were varied while LpxD was held constant at 10 μM while irradiating with UV light for 10 min. C. In-gel fluorescence while holding LpxD and Photo-activatable peptides constant at 10 and 24 μM in the presence or absence of unlabeled RJPXD33 (150 μM). LpxD was stained with simply blue safe stain to demonstrate loading was constant.

Efficiency of photo cross-linking was approximated on a 1 mL scale as described in the materials and methods. Labeling efficiency of the FITC labeled photo-activatable peptides was 19%, 15.2% and 16.6% respectively for Photopeptides 1, 3 and 4. However, the FITC labeled Photopeptides could not be enriched enough to identify the binding regions via LC/MS. In order to provide enrichment of trypsinized peptides containing the

covalently linked RJPXD33 adducts, the FITC label was substituted for a cysteine-Biotin linked through a disulfide bond (Figure 4.6) (15). MS experiments and analysis are currently being performed.

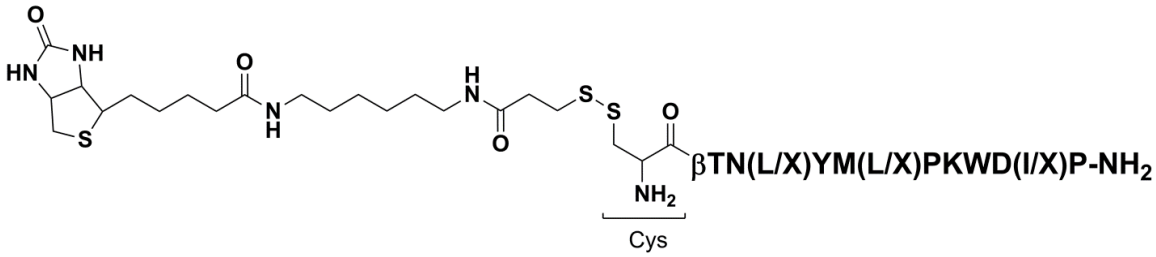

Figure 4.6. Schematic of the linkage between biotin and the Photo-activatable peptides. One of the leucine (L) or isoleucine (I) residues is substituted for PhotoLeu (X) in each of the peptides. β – β-Alanine.

Discussion

Peptides and peptidomimetics have been used as antimicrobials, some of which target bacterial membranes, DNA and RNA or proteins (27-30). In order to design potent peptidomimetic compounds one needs a fundamental understanding of the molecular interactions between the peptide and target of interest. The RJPXD33-LpxA crystal structure has assisted in elucidating the mechanism of this peptide•protein interaction. RJPXD33 binds to LpxA in an unforeseen binding mode. Consistent with our peptide truncation studies, only the N-terminal six amino acids of RJPXD33 are seen in the crystal structure. The density of the rest of this peptide could not be visualized in the structure, indicating that the six C-terminal amino acids make no binding contacts to LpxA and are highly disordered.

Though no LpxA•acyl-ACP structure is available, these current structures are suggestive that RJPXD33 would overlap with the acyl-PPan arm of acyl-ACP, thereby inhibiting acyl-ACP from binding to LpxA. This is in agreement with our previous results that demonstrated RJPXD33 was binding exclusive of acyl-ACP to LpxD and could

displace the *E. coli* LpxA inhibitory peptide 920 (P920; SSGWMLDPIAGKWSR) which was shown to be an acyl-ACP competitive ligand (1,16). While sequence similarity to P920 initially suggested that RJPXD33 may adopt a similar fold when compared to P920, the crystal structure clearly demonstrates a unique binding modality. Structural overlays of the RJPXD33•LpxA complex with UDP-3-*O*-(*R*-3-hydroxyacyl)-GlcNAc•EcLpxA and acyl-PPan•LiLpxA highlighted how the β-hydroxy of T1 and hydrophobic side chains of L3 and M5 occupied the fatty acyl binding cleft. However, the amide bond between T1 and N2 mimicked the thioester bond of acyl-PPan, while the peptide backbone of RJPXD33 occupied similar space as the PPan moiety. These findings suggest that RJPXD33 mimics the acyl-PPan moiety of acyl-ACP. This similarity to the acyl-PPan most likely accounts for the dual targeting nature of RJPXD33 owing to the fact that both enzymes utilize acyl-ACP as a substrate. Considering the diverse array of protein•protein interactions between ACP and partner proteins, other acyl-PPan mimics may find use as antimicrobial inhibitors of ACP-protein interactions.

A conformational change in H160 of the RJPXD33•EcLpxA, UDP-3-*O*-(*R*-3-hydroxyacyl)-GlcNAc•EcLpxA and acyl-PPan•LiLpxA structure can be seen, which differentiate them from other LpxA structures (17,24). While mutation of H160 to Ala reduced the activity to ~5% of the wild-type enzyme, the unfavorable nature of the LpxA reaction (K_{eq} = 0.01) and limitations of the radioactive assay prevented definitive answers with regards to the involvement of this residue in enzyme catalysis (18,19). From their mutational study, Wyckoff and Raetz hypothesized that H160's distance from the catalytic H125 residue (~12 Å) may indicate that it plays a role in substrate binding. Acidic amino acids of ACP have been implicated in binding to basic patches of partner

proteins, though there is no conserved binding motif among known ACP binding proteins (31). From previous modeling experiments, the predicted ACP binding site is within close proximity to the H160 residue, though the authors did not implicate it in binding (32). This study was also performed on apo-ACP lacking the PPan post-translational modification which may have caused subtle differences in binding to LpxA. This H160 may be forming polar contacts with the acidic residues of acyl-ACP, and thus may be important in binding. With the increase in tools to study the LpxA•ACP interaction (1,33), this issue warrants further investigation and may elucidate additional amino acids necessary for acyl-ACP binding.

The co-crystal structure of RJPXD33•LpxA and the FP experiments associated with FITC-RJPXD33Δ6 demonstrate that certain truncations can bind with minimal loss of affinity for LpxA. Such truncations would be important in developing smaller peptidomimetics capable of crossing the cell membrane. Smaller peptides such as the TNL, TNLY, and TNLYM moiety exhibited no binding at concentrations of up to 200 μM, despite T1, L3 and M5 providing extensive hydrophobic binding contacts to LpxA in the parent peptide. These data suggests that truncating the consensus sequence (YMLP) observed across the RJPXD33 series of peptides is detrimental to binding. However these results may also be explained by an increase in conformational flexibility of the truncated peptides. If this hypothesis is correct, restricted peptides could be synthesized which may display increased potency and bioavailability. One could envision substitutions at the N2 and Y4 residues to allow covalent cyclization, as these two residues appear to form an amide-π interaction. However, the hydrophobic nature of the

Y4 residue may provide energetically favorable binding within the hydrophobic cleft and thus linking strategies including a phenyl ring may need to be pursued.

It remains unclear as to how RJPXD33 interacts with *E. coli* LpxD. In order to shed light on this interaction, EcLpxD (PDB 3EH0) was superimposed on the structure of *Chlamydia trachomatis* LpxD (PDB 2IU8) with bound UDP-GlcNAc and palmitate (Figure 4.7A) to highlight the similar binding domains between the two proteins (34,35). A hypothetical binding model of the RJPXD33•LpxD was next proposed using a structural overlay between the RJPXD33•EcLpxA complex and EcLpxD (Figure 4.7B). From these overlays, it is predicted that RJPXD33 would occupy a similar fatty acyl binding groove in EcLpxD as compared to the palmitate in the CtLpxD structure. The six C-terminal residues of RJPXD33 would potentially extend into a binding groove near the C-terminal α-helical domain of EcLpxD. This would explain the role of the six C-terminal residues with respect to the increased affinity for LpxD when compared to LpxA. RJPXD33 does not occupy the UDP-GlcNAc binding domain in this model suggesting that more potent analogues may be accessed through the addition of moieties that allow for favorable binding interactions within this region.

The RJPXD33•LpxD complex was unable to be crystallized, prompting other routes to be pursued to validate this binding model. Photo-activatable amino acids have been used to map protein•protein and protein•peptide interactions, offering an alternative to crystallization (15,36). MS analysis should provide insights into the region where the peptide is interacting with LpxD. Furthermore, high resolution MS/MS may allow for the identification of the exact amino acid residue to which the photo-affinity derivative is cross-linked to. These data should provide enough evidence to validate the existing

molecular model or formulate a new model from which more potent analogues can be generated with the future goal of developing peptidomimetics compounds that are cell permeable. This model may also provide insights into how acyl-PPan of ACP binds to LpxD, providing a structural basis for the catalytic mechanism of this acyltransferase.

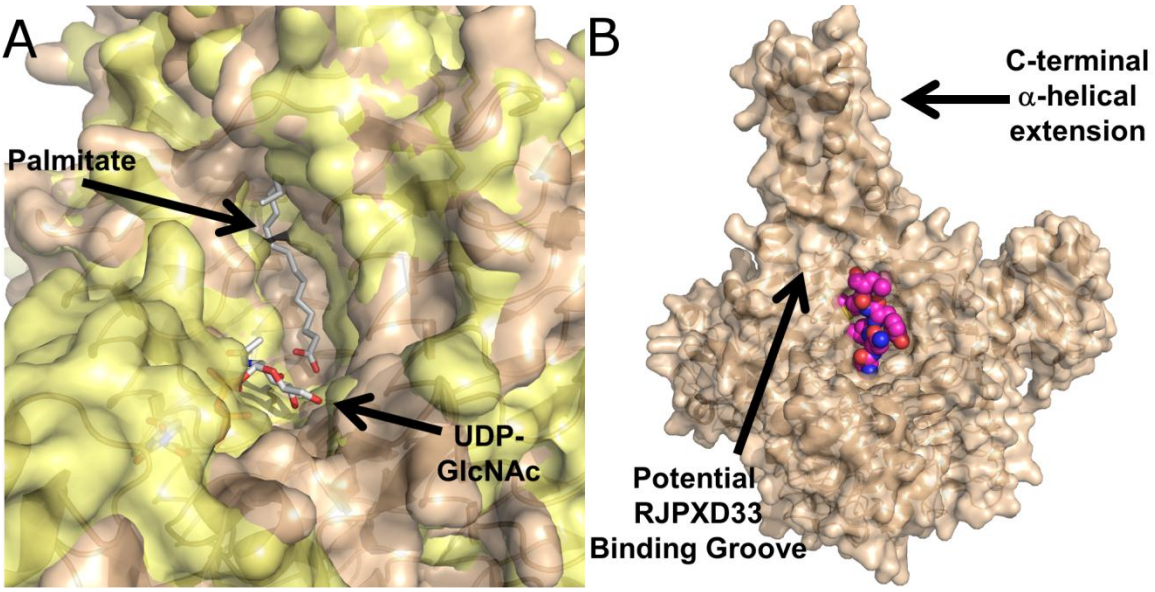

Figure 4.7. Hypothetical binding model of the RJPXD33•LpxD complex. A. Overlay of *E. coli* LpxD (wheat; PDB 3EH0) and *C. trachomatis* LpxD (yellow; PDB 2IU8). The palmitate and UDP-GlcNAc residues were co-crystallized with CtLpxD, highlighting their binding domains in comparison to the EcLpxD structure. B. The EcLpxA•RJPXD33 complex was superimposed onto EcLpxD (wheat; PDB 3EH0). RJPXD33 (magenta) would occupy the fatty acyl binding groove between two monomers in EcLpxD, similar to palmitate in CtLpxD. The six c-temrinal amino acids of RJPXD33 would potentially extend into a binding groove near the C-terminal α-helical extension of EcLpxD. This model predicts that RJPXD33 does not extend into the UDP-GlcNAc binding domain offering a way to potentially increase potency with future analogues.

Acknowledgements/Contributions

This research was supported in part by a Valteich Research Award administered by the College of Pharmacy, University of Michigan and by a Pre-Doctoral Research Grant administered by the University of Michigan Rackham Graduate School. R.J.J was supported in part by the University of Michigan Chemistry-Biology Interface (CBI) training program (NIH), grant number 5T32GM008597-14, an American Foundation for Pharmaceutical Education fellowship and a Rackham Predoctoral Research Fellowship.

This work was completed with the assistance of multiple individuals. Kyle Heslip assisted in large batch purifications of LpxD for screening, Dr. Jennifer Meagher and Dr. Jeanne Stuckey assisted with protein crystallization and data collection and analysis. Dr. Angela Walker and Dr. Phil Andrews will be performing all of the MS experiments and analysis.

References

1. Jenkins, R. J., and Dotson, G. D. (2012) *ACS Chem. Biol.* **7**, 1170-1177
2. Yin, H., and Hamilton, A. D. (2005) *Angewandte Chemie International Edition* **44**, 4130-4163
3. Jenkins, R. J., and Dotson, G. D. (2012) *Analytical Biochemistry* **425**, 21-27
4. Otwinowski, Z., and Minor, W. (1997) *Macromolecular Crystallography, Pt A* **276**, 307-326
5. McCoy, A. J., Grosse-Kunstleve, R. W., Adams, P. D., Winn, M. D., Storoni, L. C., and Read, R. J. (2007) *Journal of Applied Crystallography* **40**, 658-674
6. Raetz, C. R. H., and Roderick, S. L. (1995) *Science* **270**, 997-1000
7. Bricogne, G., Blanc, E., Brandl, M., Flensburg, C., Keller, P., Paciorek, W., Roversi, P., Sharff, A., Smart, O. S., Vonrhein, C., and Womack, T. O. (2011) *BUSTER Version 2.10.0*, (Cambridge, United Kingdom: Global Phasing Ltd.)
8. Emsley, P., and Cowtan, K. (2004) *Acta Crystallographica Section D-Biological Crystallography* **60**, 2126-2132
9. Davis, I. W., Leaver-Fay, A., Chen, V. B., Block, J. N., Kapral, G. J., Wang, X., Murray, L. W., Arendall, W. B., Snoeyink, J., Richardson, J. S., and Richardson, D. C. (2007) *Nucleic Acids Research* **35**, W375-W383
10. Chen, V. B., Arendall, W. B., III, Headd, J. J., Keedy, D. A., Immormino, R. M., Kapral, G. J., Murray, L. W., Richardson, J. S., and Richardson, D. C. (2010) *Acta Crystallographica Section D-Biological Crystallography* **66**, 12-21
11. Zucker, F., Champ, P. C., and Merritt, E. A. (2010) *Acta Crystallographica Section D-Biological Crystallography* **66**, 889-900
12. Chan, W. C., and White, P. D. (eds). (2000) *Fmoc Solid Phase Peptide Synthesis. A Practical Approach*, Oxford University Press, New York
13. Nikolovska-Coleska, Z., Wang, R. X., Fang, X. L., Pan, H. G., Tomita, Y., Li, P., Roller, P. P., Krajewski, K., Saito, N. G., Stuckey, J. A., and Wang, S. M. (2004) *Analytical Biochemistry* **332**, 261-273
14. Janz, J. M., Ren, Y., Looby, R., Kazmi, M. A., Sachdev, P., Grunbeck, A., Haggis, L., Chinnapen, D., Lin, A. Y., Seibert, C., McMurry, T., Carlson, K. E., Muir, T. W., Hunt, S., III, and Sakmar, T. P. (2011) *J. Am. Chem. Soc.* **133**, 15878-15881
15. Majmudar, C. Y., Wang, B., Lum, J. K., Håkansson, K., and Mapp, A. K. (2009) *Angewandte Chemie International Edition* **48**, 7021-7024
16. Williams, A. H., Immormino, R. M., Gewirth, D. T., and Raetz, C. R. H. (2006) *Proc. Natl. Acad. Sci. U. S. A.* **103**, 10877-10882
17. Williams, A. H., and Raetz, C. R. H. (2007) *Proc. Natl. Acad. Sci. U. S. A.* **104**, 13543-13550
18. Anderson, M. S., Bull, H. G., Galloway, S. M., Kelly, T. M., Mohan, S., Radika, K., and Raetz, C. R. H. (1993) *J. Biol. Chem.* **268**, 19858-19865
19. Wyckoff, T. J. O., and Raetz, C. R. H. (1999) *J. Biol. Chem.* **274**, 27047-27055
20. Hughes, R. M., and Waters, M. L. (2006) *J. Am. Chem. Soc.* **128**, 13586-13591
21. Imai, Y. N., Inoue, Y., Nakanishi, I., and Kitaura, K. (2009) *Journal of Computational Chemistry* **30**, 2267-2276

22. Benson, R. E., Gottlin, E. B., Christensen, D. J., and Hamilton, P. T. (2003) *Antimicrob. Agents Chemother.* **47**, 2875-2881
23. Ulaganathan, V., Buetow, L., and Hunter, W. N. (2007) *Journal of Molecular Biology* **369**, 305-312
24. Robins, L. I., Williams, A. H., and Raetz, C. R. H. (2009) *Biochemistry* **48**, 6191-6201
25. Majerus, P. W., Alberts, A. W., and Vagelos, P. R. (1965) *Proc. Natl. Acad. Sci. U. S. A.* **53**, 410-417
26. Suchanek, M., Radzikowska, A., and Thiele, C. (2005) *Nature Methods* **2**, 261-267
27. Porter, E. A., Wang, X., Lee, H.-S., Weisblum, B., and Gellman, S. H. (2000) *Nature* **404**, 565-565
28. Srinivas, N., Jetter, P., Ueberbacher, B. J., Werneburg, M., Zerbe, K., Steinmann, J., Van der Meijden, B., Bernardini, F., Lederer, A., Dias, R. L. A., Misson, P. E., Henze, H., Zumbrunn, J., Gombert, F. O., Obrecht, D., Hunziker, P., Schauer, S., Ziegler, U., Kaech, A., Eberl, L., Riedel, K., DeMarco, S. J., and Robinson, J. A. (2010) *Science* **327**, 1010-1013
29. Park, C. B., Kim, H. S., and Kim, S. C. (1998) *Biochemical and Biophysical Research Communications* **244**, 253-257
30. Kragol, G., Lovas, S., Varadi, G., Condie, B. A., Hoffmann, R., and Otvos, L. (2001) *Biochemistry* **40**, 3016-3026
31. Byers, D. M., and Gong, H. (2007) *Biochemistry and Cell Biology-Biochimie Et Biologie Cellulaire* **85**, 649-662
32. Jain, N. U., Wyckoff, T. J. O., Raetz, C. R. H., and Prestegard, J. H. (2004) *Journal of Molecular Biology* **343**, 1379-1389
33. Gong, H., Murphy, A., McMaster, C. R., and Byers, D. M. (2007) *J. Biol. Chem.* **282**, 4494-4503
34. Bartling, C. M., and Raetz, C. R. H. (2009) *Biochemistry* **48**, 8672-8683
35. Buetow, L., Smith, T. K., Dawson, A., Fyffe, S., and Hunter, W. N. (2007) *Proc. Natl. Acad. Sci. U. S. A.* **104**, 4321-4326
36. Abe, R., Caaveiro, J. M. M., Kozuka-Hata, H., Oyama, M., and Tsumoto, K. (2012) *J. Biol. Chem.* **287**, 16477-16487

Chapter 5

Cell Permeable Inhibitors of *E. coli* UDP-3-*O*-(*R*-3-hydroxyacyl)-glucosamine *N*-Acyltransferase (LpxD)

Introduction

Acyl carrier protein (ACP) is a key component for fatty acid synthesis (FAS) in all kingdoms of life (1). ACP is post-translationally modified on a conserved serine residue with a 4'-phosphopantehtiene moiety, derived from coenzyme A (CoA) (2). Mammals utilize a type I FAS system in which each catalytic domain is encoded on a single polypeptide chain (3). The mammalian FAS machinery primarily elongates the acyl chain to a length of 16 – 18 carbons and then cleaves the thioester between the acyl chain and phosphopantetheine arm to release free fatty acids into the cytosol (4). The free fatty acids can be activated onto CoA and subsequently used as acyl donors for a variety of enzymatic reactions and regulatory functions (5) In contrast, *Escherichia coli*, and most other prokaryotes, contain a type II FAS pathway, where each functionality required for FAS is encoded on its own polypeptide chain (6). Type II ACP, and its various acylated analogs, are small soluble proteins which serve a pivotal role as substrates for the biosynthesis of a large number of vital/essential bacterial molecules, including fatty acids, phospholipids, lipopolysaccharide, lipoic acid, and acyl homoserine lactones (7-10). As such ACP must interact with a vast number of functionally different enzymes. The requirement for ACP in these diverse processes suggests that interactions between ACP and ACP-dependent enzymes must be specific. However, the transient nature of the

specific protein•protein interface between ACP and its many interactive proteins has not been delineated in most instances.

Peptidic inhibitors that have been identified against both LpxD and LpxA suggest that small molecule inhibitors could be identified that disrupt the protein•protein interaction between early acyltransferases involved in lipid A biosynthesis and acyl-ACP (11,12). While inhibition of protein•protein interactions in mammalian cells has been widely appreciated as an innovative chemotherapeutic approach (13,14), it represents an underexplored niche in the field of antimicrobial drug discovery. The ability for bacterial ACP to interact with a diverse array of essential proteins, offers the possibility that dual targeting inhibitors of ACP-dependent enzymes could be identified (15). Such dual targeting inhibitors would decrease the likelihood of mutation-mediated resistance by increasing the minimal number of gene mutations necessary to confer resistance to the microbe (16).

Previously, an LpxA/D fluorescence polarization (FP) binding assay and a continuous, fluorescence-based LpxA/D activity assay were developed (12,17). Described within, the FP binding assay was adapted to a 384-well format and utilized to screen ~120,000 small molecules. Compounds which disrupted the FITC-RJPXD33•LpxD interaction in the primary screen were tested for inhibition using the secondary fluorescent acyltransferase assay. Inhibitory molecules that were confirmed to target LpxD *in vitro* were subsequently tested for growth inhibition in multi-drug efflux pump deficient (Δ*tolC*) *E. coli.* This led to the identification of several cell permeable inhibitors with antimicrobial activity. A multi-copy suppressor approach was used to validate that inhibition of LpxD was the molecular mode of action for *E. coli* growth

inhibition. These molecules represent the first cell permeable inhibitors of LpxD identified to date, offering a significant first step towards future development of LpxD inhibitors for chemotherapeutic application.

Materials and Methods

Materials. Bio-Rad Protein assay and BioGel P2 size exclusion gel were purchased from Bio-Rad. LB (Lenox) broth and agar were purchased from Difco. Fluorescein isothiocyanate (FITC) was purchased from Acros Organics. ThioGlo1 was purchased from CalBioChem. Benzonase was purchased from Novagen. *R*-3-hydroxymyristic acid was purchased from Wako Chemicals. All buffers and antibiotics were purchased in the highest grade from Sigma Aldrich or Fisher. Inhibitor compounds were purchased from ChemDiv. MC_{207110} (Phe-Arg β-naphthylamide dihydrochloride) was purchased from Sigma Aldrich. A PheraStar spectrophotometer was used for the high-throughput screening of LpxD. A SpectraMax M5 spectrophotometer was used for all other experiments. *E. coli* strain JW5503-1 (18) was provided by the Yale *E. coli* Genetic Stock Center.

Cell Culture. Bacteria strains and plasmids have been described previously (17). For protein expression and purification, all *E. coli*/T7 RNA polymerase promoter constructs were grown in 1 L baffled flasks containing 250 mL LB media supplemented with the appropriate antibiotics. The Flasks were shaken (250 rpm) at 37 °C until the cells reached an optical density of OD_{600} = 0.6 -1.0. The cultures were then induced with 1 mM isopropyl β-D-1-thiogalactopyranoside (IPTG) (Rosetta (DE3/*pLysS*)) or 1 mM IPTG and 0.2% L-arabinose (BL21-AI), and the cultures were allowed to incubate at 37 °C for an additional 4 h. Cells were harvested at 4 °C by centrifugation at 6,000 x *g* and

lysed by French press. Crude cytosol was prepared by centrifugation of cellular lysate at 20,000 x *g* for 30 min at 4 °C.

O*verexpression and Purification of His$_6$-LpxD*. Overexpression and purification of His$_6$-LpxD were carried out as previously described (17). For His$_6$-LpxD purification, Benzonase (Novagen) was added after cell lysis and the lysate was incubated for 30 min on ice prior to cytosol preparation. Ten milliliters of crude cytosol in 20 mM HEPES, 50 mM imidazole pH 8.0 was loaded onto 3 mL of Ni-NTA resin (Qiagen) equilibrated in loading buffer. The resin was washed with 10 column volumes of loading buffer containing 500 mM NaCl and then eluted with 20 mM HEPES, 250 mM imidazole pH 8.0. Purified His$_6$-LpxD was desalted on a Bio-Gel P2 column and analyzed by SDS-PAGE. Concentration was determined by absorbance measurements at A_{280} with ε = 27305 M^{-1} cm^{-1} for LpxD.

Purification of Other Enzymes and Preparation of Substrates. Overexpression and purification of LpxA, ACP, LpxC, and AasS, acylation of ACP and preparation of UDP-3-*O*-(*R*-3-hydroxymyristoryl)-GlcN have been described previously (17).

High-Throughput Screening (HTS) Assay. HTS was carried out using the fluorescence polarization (FP) binding assay for LpxD (12). For initial screening, compounds were spotted on to 384-well, black plates (Costar) at a final concentration of 100 μM in 1 % DMSO. The final assay volume was 20 μL and contained 600 nM LpxD and 20 nM FITC-RJPXD33. Individual compounds were incubated with LpxD for 10 min prior to addition of FITC-RJPXD33 and plates were subsequently read on a PheraStar spectrophotometer, λ_{ex} = 485 nm and λ_{em} = 525 nm.

Acyltransferase Inhibition Assay. The acyltransferase reaction was monitored in the forward direction using a continuous fluorescent assay as previously described (17). The assay monitors holo-ACP formation *via* conjugation to ThioGlo1 reagent, which could be monitored as an increase in fluorescence with excitation and emission wavelengths set to λ_{ex} = 379 nm and λ_{em} = 513 nm. Assays were performed on a SpectraMax M5 microplate reader (auto cutoff set to λ = 495 nm, PMT set to low, and precesion set to 40 scans per well) using Corning black, 96-well half area plates. The assay mixture in a final volume of 100 μL contained 20 mM HEPES pH 7.5, 10 μM ThioGlo, 4.5 μM UDP-3-*O*-(*R*-3-hydroxymyristoyl)-GlcN, 9 μM *R*-3-hydroxymyristoyl-ACP, 10 nM LpxD and varying concentrations of inhibitors (1 – 100 μM). Assays contained a final concentration of 2% (*v*/*v*) DMSO from stock solutions. All components with the exception of enzyme were mixed and incubated in the dark at 30 °C for 5 min. To initiate the reaction, a fresh dilution of acyltransferase from a 1 mg/mL stock was added and the reaction was monitored for 10 min using the linear range (< 10% product formation) for initial velocities. Assays were run in triplicate with the average IC_{50} being reported. A negative control containing no inhibitor and a positive control containing no acyltransferase were used for 100% and 0% relative activity. IC_{50}'s were determined by plotting relative acyltransferase activity verses inhibitor concentration and fitting to equation 1.

$$\frac{v_i}{v_o} = \frac{1}{1 + \left(\frac{[I]}{IC_{50}}\right)^h} \quad (1)$$

Where v_i is the initial velocity in the presence of inhibitor, v_o is the initial velocity in the absence of inhibitor, [I] is the concentration of inhibitor, IC_{50} is the concentration of

inhibitor at 50% inhibition, and h is the hill slope. Data points shown represent the mean of three individual experiments and error bars represent the standard deviation.

Disk Diffusion Assay. A single colony of bacteria was selected and grown overnight at 37 °C in 5 mL of LB media. Overnight cultures were diluted to an OD_{600} = 0.2 in a final volume of 1 mL LB media. With a sterile cotton swab, the diluted culture was streaked out to completely cover an LB agar plate. The plate was allowed to dry at room temperature for 10 min. Compounds were added directly to a sterile filter disc from a 25 mM stock solution in DMSO. Filter discs containing compounds or controls were placed onto the dried plates and incubated at 37 °C overnight for a minimum of 20 h. Diameters were measured the following day. Any compound lacking a ring beyond the filter disc was annotated as <6 mm diameter. DMSO was plated as a negative control and displayed no inhibition up to 33 mg (30 μL; highest amount tested). Chloramphenicol was used as a positive control at 10 μg for each plate.

Determination of Minimal Inhibitory Concentration (MIC). A single colony of JW5503-1 with pUC18 or pUC18::*lpxD* was selected and grown at 37 °C in 5 mL of LB with 30 μg/mL kanamycin until an OD_{600} = 0.6-0.8 was reached. The culture was diluted to an OD_{600} = 0.04. 50 μL of the diluted culture was then added to 50 μL of two-fold serially diluted compound (final concentrations 0.003 – 100 μg/mL) in LB media in a 96-well, half-area, clear plate (Costar UV). The plate was covered and the cells were grown at 37 °C for 20 h at which point an OD_{600} was measured. MIC's were defined by the minimal concentration at which the bacteria did not grow. All MIC's were determined in quadruplicate and the error was within one serial dilution of the MIC. For statistical

analysis of compound 6359-0284 in JW5503-1::pUC18 and JW5503-1::pUC18-*lpxD*, the MIC's obtained for all four experiments were compared using a two tailed paired t-test.

Checkerboard Synergy Analysis. A six by six dose dependence checkerboard assay was set up as described by Orhan *et. al* (19). Cultures were set up exactly as described under MIC determinations using JW5503-1 lacking any plasmids. Fractional inhibitory concentrations (FIC) were calculated using the following equation:

$$FIC = \left(\frac{FIC_A}{MIC_A}\right) + \left(\frac{FIC_B}{MIC_B}\right)$$

Where MIC_A = MIC of compound A, MIC_B = MIC of compound B, FIC_A = fractional inhibitory concentration of compound A and FIC_B = fractional inhibitory concentration of compound B. FIC were defined as antagonistic if FIC $\geq$ 4, additive if 4 > FIC > 0.5, and synergistic if FIC $\leq$ 0.5.

Synthesis of 1-(2-methoxyphenyl)-3-(naphthalen-2-yl)urea (INF_{271}). Synthesis was carried out as previously described (20). A solution of 2-methoxyphenyl isocyante (298 mg, 2 mmol) was prepared in 2 mL of diethyl ether and added drop wise to a slurry of 2-napthylamine (286 mg, 2 mmol) in 2 mL of diethyl ether. The solution was stirred for 2 h at room temperature. Upon addition of the 2-methoxyphenyl isocyanate, the 2-napthylamine began to dissolve. Within 30 min a white precipitate formed. After 1 h, 2 mL of ether was added to the round bottom due to the exothermic reaction causing ether evaporation. After two hours there was a complete loss of starting material as monitored by TLC. The precipitate was filtered and washed three times with 15 mL of diethyl ether resulting in a 63% isolated yield. The compound is very hygroscopic and ~95% pure by analytical HPLC (see Appendix). ^{1}H NMR (400 MHz, $CDCl_3$) d 8.14 (dd, J = 7.7, 1.8, 1H), 7.94 (d, J = 1.9, 1H), 7.75 (dd, J = 11.6, 8.6, 3H), 7.47 - 7.35 (m, 4H), 7.06 - 6.94

(m, 3H), 6.87 (dd, J = 7.8, 1.5, 1H), 3.80 (s, 3H). ESI-HRMS calculated for $C_{18}H_{16}N_2O_2$ $[M+Na]^+$ 315.1104, 315.1115 observed.

Results

LpxD was screened using a 384-well fluorescence binding assay previously reported (12). The FP binding assay was optimized to 20 μL final volume to allow for an increase with respect to final inhibitor concentration and a decrease in the amounts of total protein (LpxD). From initial experiments, the Z-factor was shown to be 0.84 (Figure 5.1), with an average Z-factor per plate of 0.79, indicating an excellent assay for high-throughput screening (HTS) according to Zhang *et. al*. (21). Approximately 120,000 compounds were screened for disruption of the FITC-RJPXD33•LpxD complex. Active hits were defined as displaying inhibition greater than or equal to three standard deviations above the negative control. Compounds known to exhibit intrinsic fluorescence, promiscuity in prior HTS efforts against various protein targets and those containing chemically reactive structural groups were triaged from the active hits. A second round of screening was conducted in triplicate against ~1600 of the primary actives. In this follow up screen individual compounds were first assessed for intrinsic fluorescence, followed by fluorescence quenching upon addition of FITC-RJPXD33. Compounds were then assayed for re-confirmation of disruption of FITC-RJPXD33 binding to LpxD. Of the nearly 1600 compounds, 462 were confirmed and chosen for dose response evaluation in which several concentrations (1-100 μM) of each compound was evaluated in the LpxD FP binding assay. Additionally, these same 462 compounds were subsequently screened against LpxA using an FP binding assay with FITC-P920 to potentially identify dual targeting inhibitors (11,22).

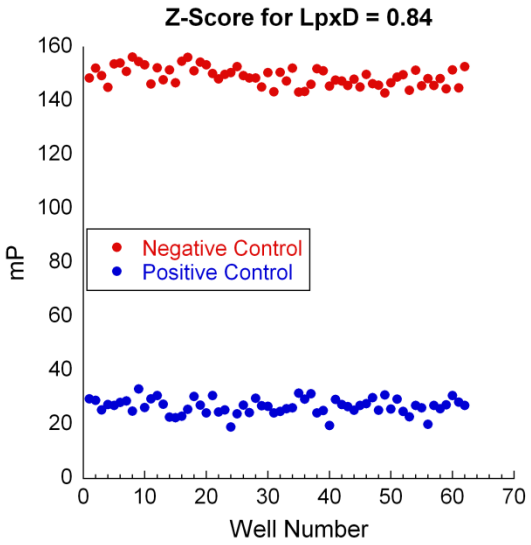

Figure 5.1. Z-score determination for the LpxD FP assay. Negative controls contain 20 nM FITC-RJPXD33 and 600 nM LpxD. Positive controls contain only FITC-RJPXD33. A Z-score of > 0.75 indicates a very good assay.

Fourteen compounds were chosen for in vitro evaluation using the acyltransferase activity assay based on their potency (pAC50; $\geq$ 3 standard deviations from the negative control), lack of promiscuity (< 10% hit rate) and hill slope (< 3) from the dose-response curves. Promiscuity and high hill slopes are indicative of aggregation-based inhibitors which are pitfalls in HTS (23,24). Of the fourteen compounds chosen, only two were inactive (one demonstrated intrinsic fluorescence which would interfere with the assay and a second was extremely insoluble). Eleven compounds (Figure 5.2) exhibited IC_{50}s ranging from low nanomolar to low micromolar (0.07 – 35 μM). Acyltransferase activity inhibition plots of the HTS hits are shown indicating the IC_{50} in micromolar and the Hill slope from the dose response of three individual assays (Figure 5.3, panel a – k). All compounds exhibited hill slopes between 0.6 and 1.4 reconfirming that these were viable hits and not promiscuous aggregation-based inhibitors.

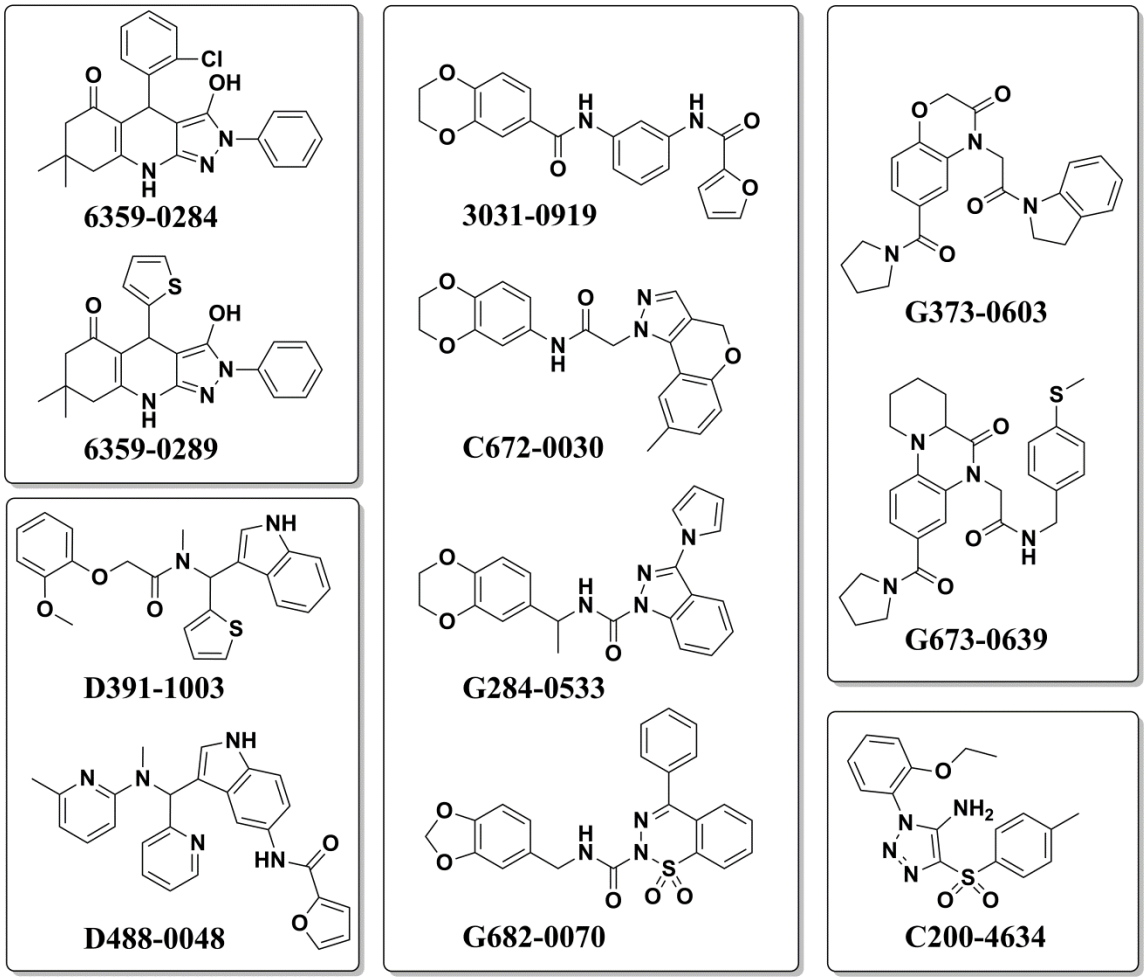

Figure 5.2. Compounds identified from the LpxD HTS that were tested in the acyltransferase assay. Compounds are boxed according to similarity to other compounds.

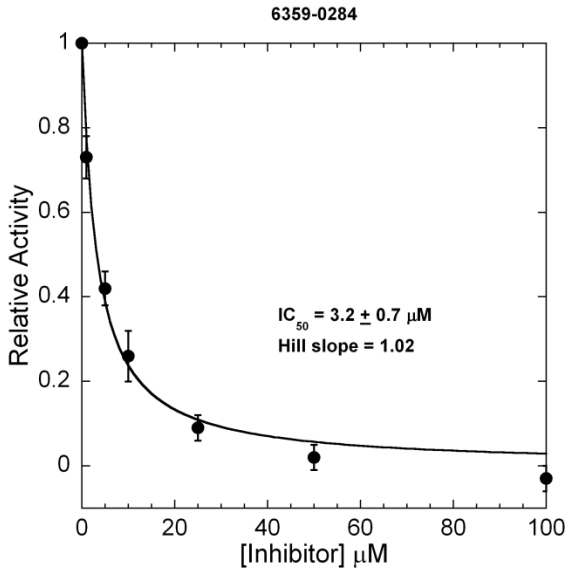

Figure 5.3a. Acyltransferase inhibition plot of *E. coli* LpxD vs 6359-0284.

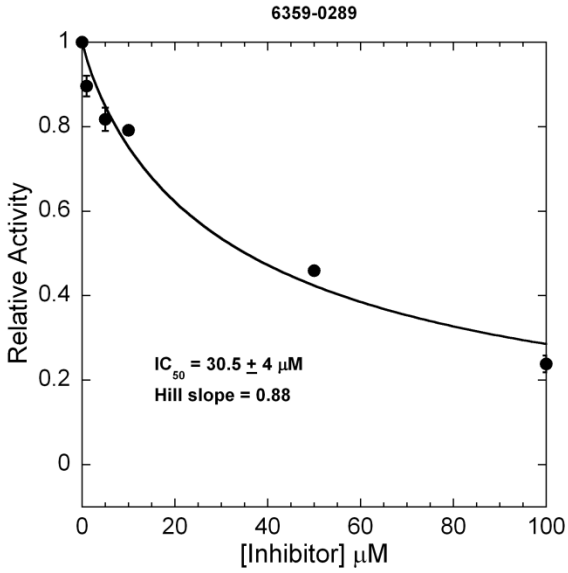

Figure 5.3b. Acyltransferase inhibition plot of *E. coli* LpxD vs 6359-0289**.**

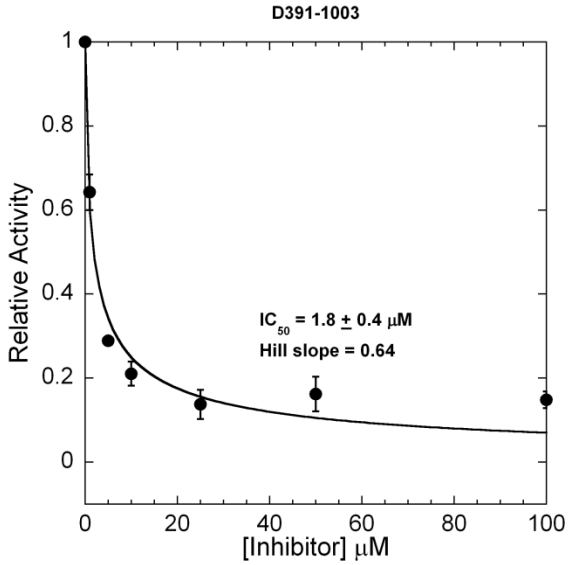

Figure 5.3c. Acyltransferase inhibition plot of *E. coli* LpxD vs D391-1003**.**

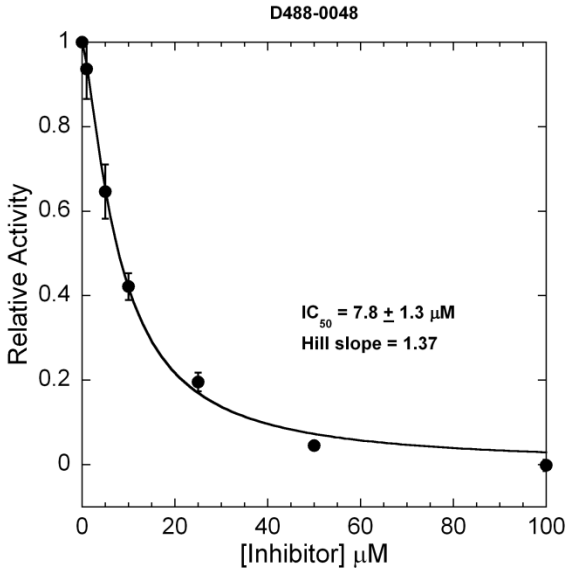

Figure 5.3d. Acyltransferase inhibition plot of *E. coli* LpxD vs D488-0048**.**

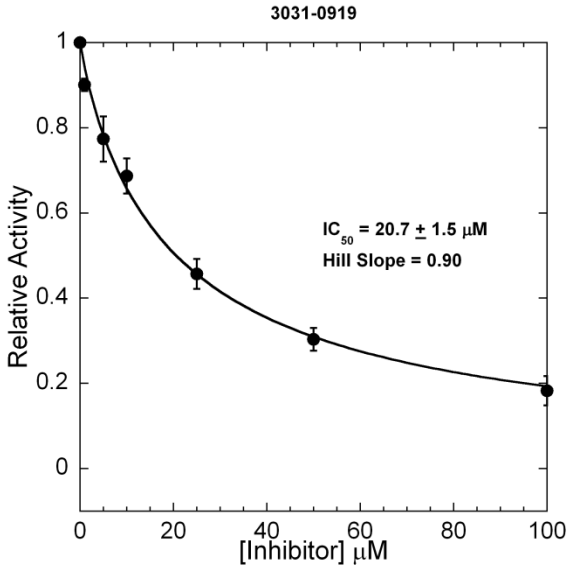

Figure 5.3e. Acyltransferase inhibition plot of *E. coli* LpxD vs 3031-0919.

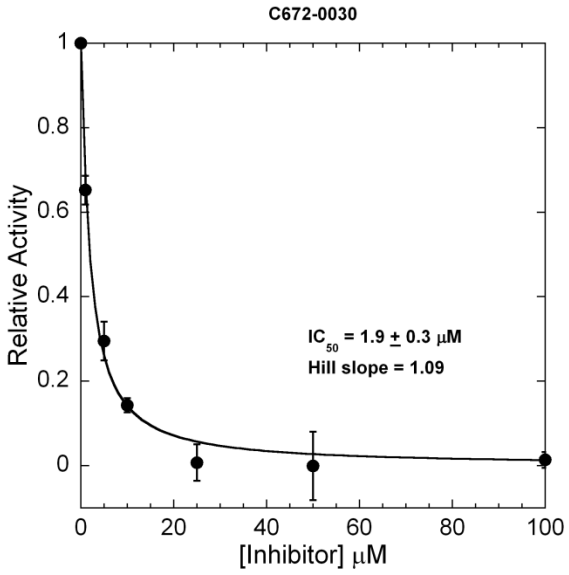

Figure 5.3f. Acyltransferase inhibition plot of *E. coli* LpxD vs C672-0030**.**

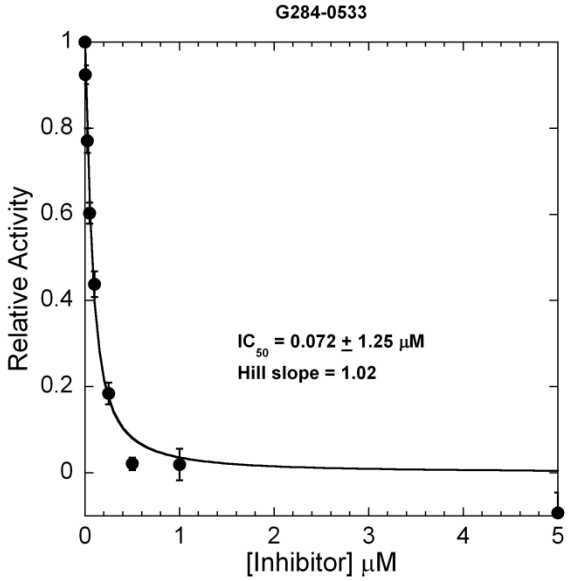

Figure 5.3g. Acyltransferase inhibition plot of *E. coli* LpxD vs G284-0533**.**

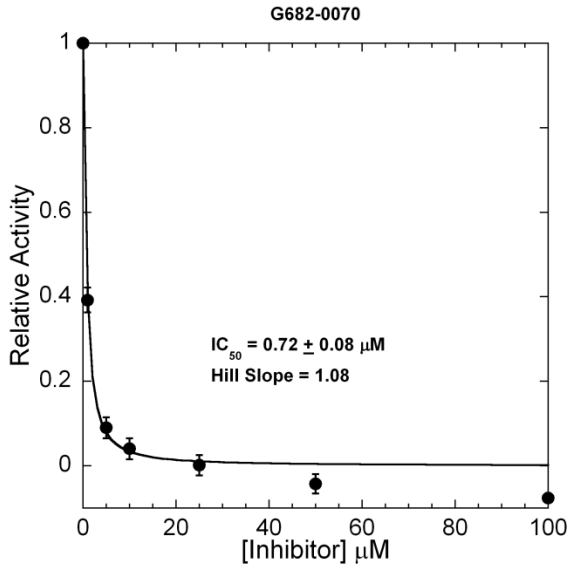

Figure 5.3h. Acyltransferase inhibition plot of *E. coli* LpxD vs G682-0070**.**

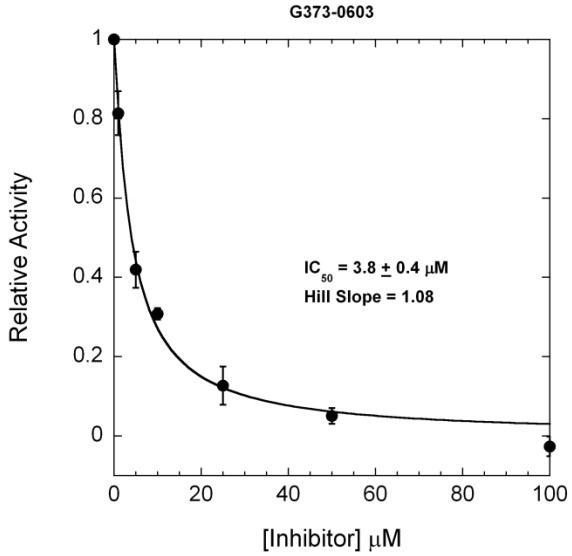

Figure 5.3i. Acyltransferase inhibition plot of *E. coli* LpxD vs G373-0603**.**

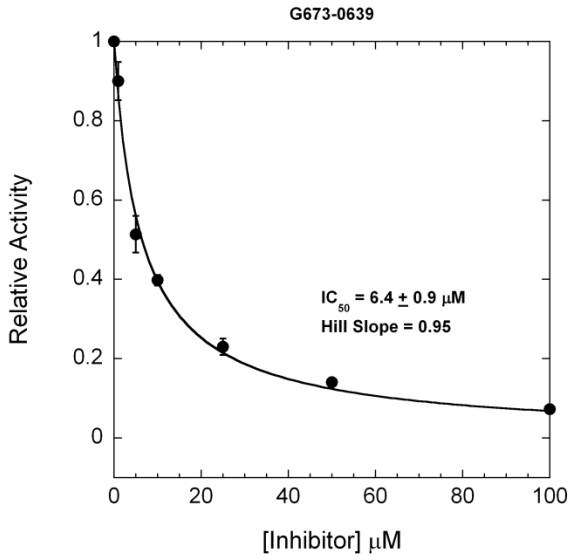

Figure 5.3j. Acyltransferase inhibition plot of *E. coli* LpxD vs G673-0639**.**

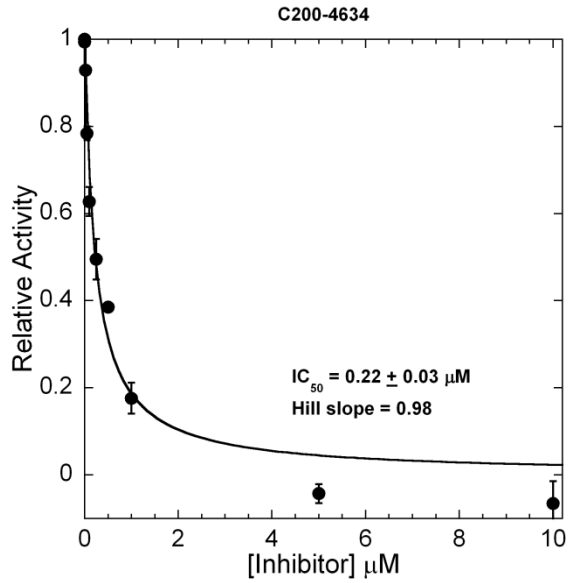

Figure 5.3k. Acyltransferase inhibition plot of *E. coli* LpxD vs C200-4634**.**

All compounds were tested for bioactivity using a disc diffusion assay to determine growth inhibition an *E. coli* MG1655 mutant (JW5503-1) (18). This strain is lacking the multi-drug efflux transport system (Δ*tolC*) which contains a kanamycin cassette in place of *tolC*. Three of the fourteen compounds demonstrated the ability to

inhibit growth of the Δ*tolC* mutant (Figure 5.4 & Table 5.1). Figure 5.3 represents a single plate, though compounds were tested in triplicate and similar data were obtained for each plate. Compounds C200-4634 and 6359-0289 demonstrated modest to high growth inhibition (10 – 20 mm diameter) at 300 μg. However, compound 6359-0284 at 25 μg demonstrated growth inhibition comparable to 10 μg of either ampicillin (Amp) or chloramphenicol (Cam).

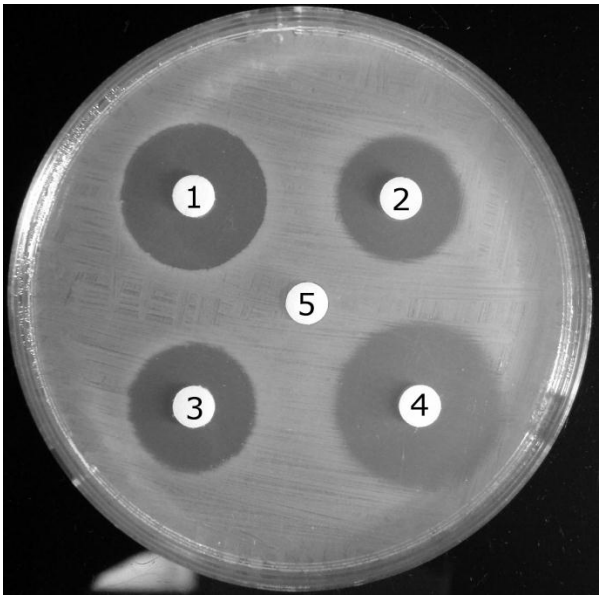

Figure 5.4. Representative disc diffusion assay for 6359-0284 & 6359-0289 against JW5503-1 in comparison to commonly used antibacterial inhibitors. Inhibition rings were measured for 1) 6359-0284 (25 μg), 2) 6359-0289 (300 μg), 3) Ampicillin (10 μg), 4) Chloramphenicol (10 μg) and 5) DMSO (33 mg; highest amount of DMSO used). Inhibition diameters are shown in Table 5.1. Plates were run in triplicate.

Compound	Amount (μg)	Diameter (mm)
6359-0284	25	25
Ampicilin	10	22
Chloramphenicol	10	28
6359-0289	300	21
6359-0289	25	8
C200-4634	300	10

Table 5.1. Disc diffusion growth inhibition data. Disc diffusion assays were performed against the *E. coli* JW5503-1.

Compounds 6359-0284 and 6359-0289 bearing a common molecular substructure, were further tested for minimal inhibitory concentration (MIC) in liquid growth medium. 6359-0284 demonstrated an MIC = 3.13 μg/mL against JW5503-1, while 6359-0289 demonstrated an MIC = 100 μg/mL. This correlated well with our enzyme inhibition results, as 6359-0284 displayed 10-fold higher inhibition (IC_{50} = 3.2 $\pm$ 0.7 μM) for LpxD than 6359-0289 (IC_{50} = 30.5 $\pm$ 4 μM).

In order to determine whether JW5503-1 growth inhibition was dependent on LpxD, a multi-copy suppression experiment was performed. JW5503-1 was transformed with an empty pUC18 vector (JW5503-1::*pUC18*) or a pUC18 vector carrying the *lpxD* gene (JW5503-1::*lpxD*). These two strains were then tested against 6359-0284 and a variety of known antibiotics which target different cellular processes. Rifampin inhibits RNA transcription, Nalidixic Acid targets DNA synthesis, Chloramphenicol blocks protein synthesis, Triclosan inhibits FAS, Fosfomycin inhibits early steps of peptidoglycan biosynthesis within the cytoplasm and Cefixime is a third generation cephalosporin (inhibits peptidoglycan cross-linking in the periplasm) which is resistant to hydrolysis by many β-lactamases, such as the one carried by the pUC18 plasmid. As observed in Table 5.2, only compound 6359-0284 was susceptible to overexpression of LpxD. Rifampin is one of many hydrophobic antibiotics that have been shown to be more potent against LPS-deficient mutants, owing to the inherent permeability barrier imparted by LPS (25,26). Overexpression of LpxD had no effect on the potency of Rifampin, suggesting that overexpression of LpxD was not simply increasing LPS production and causing a decrease in bioavailability of the antimicrobials. This would ultimately suggest

that 6359-0284 was directly inhibiting LpxD as seen by the suppression of toxicity only with this compound.

	MIC (μg/mL)		
Compound	JW5503-1::*pUC18*	JW5503-1::*lpxD*	Fold Difference
6359-0284	3.13	100	32
Rifampin	6.25	6.25	1
Nalidixic Acid	0.78	1.56	2
Chloramphenicol	1.56	1.56	1
Triclosan	0.002	0.001	0.5
Fosfomycin	12.5	12.5	1
Cefixime	3.13	6.25	2

Table 5.2. MIC data for JW5503-1::*pUC18* and JW5503-1::*lpxD*. MIC's are representative of four individual experiments. Errors of the MIC's are within a 2-fold dilution of the defined value.

While 6359-0284 demonstrated toxicity in multi-drug efflux deficient *E. coli*, no activity was seen in wild-type *E. coli* MG1655. From the above results, we hypothesized that TolC inhibitors could potentially be used in combination with 6359-0284 to inhibit the growth of MG1655. Compound MC_{207110} was identified against the *Pseudomonas aeruginosa* MexAB-OmpR multi-drug efflux system and has shown broad spectrum applicability (27,28). MC_{207110} has been used in combination with a TolC inhibitor, INF_{271}, for increased potency of antimicrobials that are substrates for efflux pumps (28). MC_{207110} was commercially available and compound INF_{271} was synthesized in a single step from napthylamine and 2-methoxyphenyl isocyanate (Figure 5.5) (20,27,28). In the presence of 20 μg/mL of MC_{207110}, compound 6359-0284 displayed an MIC = 50 μg/mL. While the MIC of 6359-0284 was > 100 μg/mL in combination with 10 μg/mL of INF_{271}, when both 10 μg/mL of INF_{271} and 20 μg/mL of MC_{207110} were utilized in combination with 6359-0284, the MIC was observed to be 25 μg/mL. As a control, MC_{207110} and INF_{271} were tested for growth inhibition aginst *E. coli* MG1655 and did not inhibit

growth at concentrations up to 5 times the concentration utilized with 6359-0284. MC_{207110} did not inhibit growth at concentrations up to 200 μg/mL, while INF_{271} displayed no inhibition up to 50 μg/mL. These results in combination with the Δ*tolC* mutant highlight that 6359-0284 is the first cell permeable inhibitor of LpxD.

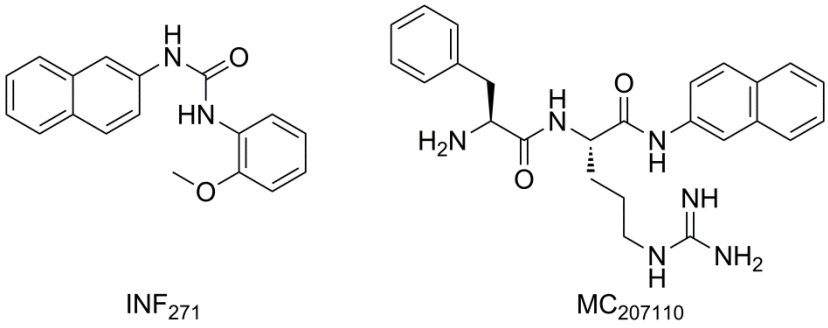

INF_{271} MC_{207110}

Figure 5.5. Multi-drug efflux pump inhibitors, INF_{271} and MC_{207110}.

One of our initial hypotheses was that inhibitors of LpxD would demonstrate a synergistic increase in potency when combined with other antibacterial compounds. This hypothesis stemmed from the fact that mutants deficient in LPS have demonstrated increased potency to clinically relevant antimicrobials (25,26,29,30). To test whether LpxD inhibitors would demonstrate synergy in potency with other antibiotics, a checkerboard synergy analysis (Figure 5.6) was performed on JW5503-1 utilizing 6359-0284 in combination with a variety of commercially available antibiotics Table 5.3 (19). Multiple compounds demonstrated a synergistic increase in potency in combination with 6359-0284, including the hydrophobic antimicrobial, Rifampin (RNA synthesis inhibitor). Despite the hydrophobicity of Triclosan (ClogP = 5.53), it only demonstrated an additive effect. While this may be surprising, our analysis represents the first synergy experiments using Triclosan in combination with chemical or genomic disruption of lipid A biosynthesis. The synergistic effect seen in combination with Nalidixic acid and Chloramphenicol are in agreement with an increased potency of DNA gyrase inhibitors

(Novobiocin) and protein synthesis inhibitors (Chloramphenicol) in lipid A defective mutants (25). Previous studies have shown conflicting effects (an increase or no increase in potency) on lipid A deficient mutants using various cephalosporins (25), and Cefixime did not show synergism with 6359-0284. Interestingly, 6359-0284 demonstrated the highest synergy with Fosfomycin, despite only an additive effect with a peptidoglycan cross-linking inhibitor (Cefixime).

	1	2	3	4	5	6	7	8	9	10	11	12
A	Pos	Pos	Pos	Pos	Pos	Pos	Pos	Pos	x	x	x	x
B	Neg	Neg	Neg	Neg	Neg	Neg	Neg	Neg	x	x	x	x
C	2x	2.13	2.25	2.5	3	4	2x	2.13	2.25	2.5	3	4
D	1x	1.13	1.25	1.5	2	3	1x	1.13	1.25	1.5	2	3
E	1/2x	0.63	0.75	1	1.5	2.5	1/2x	0.63	0.75	1	1.5	2.5
F	1/4x	0.38	0.5	0.75	1.25	2.25	1/4x	0.38	0.5	0.75	1.25	2.25
G	1/8x	0.25	0.38	0.63	1.13	2.13	1/8x	0.25	0.38	0.63	1.13	2.13
H	0	1/8x	1/4x	1/2x	1x	2x	0	1/8x	1/4x	1/2x	1x	2x

Figure 5.6. Checkerboard synergy analysis experimental set up in a 96-well plate. Compound 6359-0284 was titrated along the ordinate of a 96 well plate at concentrations of 2x MIC, 1x MIC, 1/2x MIC, 1/4x MIC, and 1/8x MIC (yellow). Other antimicrobials were titrated along the abscissa at varying concentrations from 2x to 1/8x MIC (yellow). FIC's of individual wells are denoted in blue and calculated as described in the Materials and Methods. The well with the lowest FIC displaying no growth determined the FIC. Positive controls (green) contained only LB media lacking JW5503-1, while negative controls (red) contained LB media and JW5503-1 without any compounds. X's mark wells that were not utilized in the experiments.

Synergy Analysis with 6359-0284		
Compound	FIC	Activity
Rifampin	0.38	Synergy
Triclosan	0.75	Additive
Nalidixic Acid	0.38	Synergy
Chloramphenicol	0.38	Synergy
Cefixime	0.75	Additive
Fosfomycin	0.25	Synergy

Table 5.3. Synergy analysis data using compound 6359-0284.

Discussion

Utilizing our previously described assays as a toolbox, we have discovered and validated the first cell permeable inhibitors of LpxD. Through a multi-copy suppressor

approach and growth inhibition of *tolC* knockouts, we validated that the intracellular target was LpxD. Furthermore, additional synergy data confirmed our initial hypothesis that such compounds could find use in combination therapies with existing antimicrobials to cause a synergistic increase in potency of these compounds. One of the large questions still remaining is the fundamental understanding of how these inhibitors bind to LpxD. This information will be critical in the design of more potent and bioavailable analogs. Structural work complemented with structure-activity relationship (SAR) should assist in answering this important question.

The most potent compound, G284-0533 (IC_{50} = 72 nM), displayed structural similarity to compounds 3031-0919, C672-0030 and G682-0070 (Figure 5.2). All compounds contained a phenyl dioxane or phenyl dioxolane ring system followed by an amide linkage leading to a heteroaromatic ring system. The heteroaromatic ring system is where all compounds differ, perhaps leading to the variation in affinity (0.72 – 20.7 μM). While C200-4634 does not contain a phenyl dioxane ring, the 4-amino-5-tosyl motif connected to the triazole ring is highly similar to the 1,2,3-Benzothiadiazine heterocyclic ring in compound G682-0070. The fact that C200-4634 was cell permeable and approximately 3 times more potent than G682-0070 raises the question of whether synthesizing only the heteroaromatic ring system of the dioxane series would provide potent cell permeable inhibitors of LpxD. The heteroaromatic ring system may be mimicking the uridine ring of UDP-3-*O*-(*R*-3-hydroxyacyl)-GlcN, which may allow for additional hydrophobic groups to be placed off of the ring to mimic the fatty acyl chain. However, this is simply one hypothesis and a fundamental understanding of how these compounds binds is necessary before drawing such conclusions.

The most potent biologically active compounds contained a pyrazolo-quinolone scaffold. Other compounds containing the pyrazolo-quinolone scaffold similar to 6359-0284 and 6359-0289 were also found within the screening library, but were not tested in the continuous enzyme assay. From the HTS binding data, the gem dimethyl moiety off of the C7 of the quinolone ring was not necessary for binding, but did increase binding affinity (Figure 5.7). Substitutions to or deletion of the 3-hydroxyl of the pyrazole ring were not tolerated as this aided in constraining the aryl ring off of the C4 of the quinolone ring. Only six membered aryl rings substituted at the C2 position (X) or five-membered heterocyclic aryl rings with a heteroatom at the second position (Y) were tolerated, further highlighting the necessity to constrain the aryl ring system. The stereochemistry at the C4 position was racemic and the chlorine substitution of the aryl ring may adopt an exo or endo geometry, further complicating the mechanism of binding.

Substitutions at the phenyl moiety of the pyrazole ring can be achieved using an aryl hydrazine and ethyl cyanoacetate (31). The newly synthesized aryl pyrazole ring can be added to a one-pot reaction with an aryl aldehyde and a 1,3-cyclohexanedione derivative for the one step synthesis of novel pyrazolo-quinolone compounds (32). SAR around the aryl aldehyde, the aryl pyrazole, and the 1,3-cyclohexanedione may identify compounds with increased potency that are not substrates for TolC.

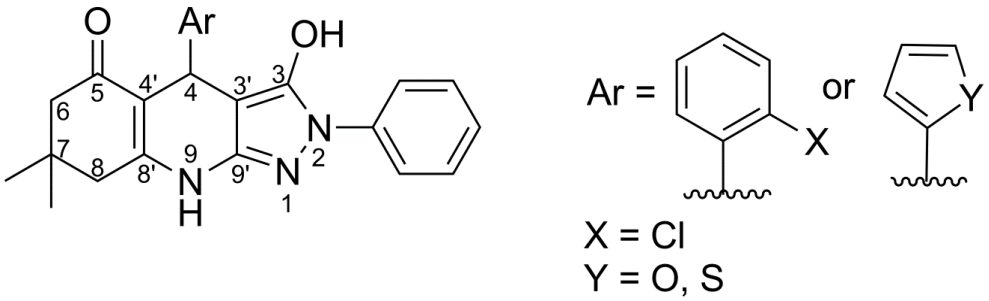

Figure 5.7. Pyrazolo-Quinolone structure. Substitutions at position X or off the phenyl moiety of the pyrazole ring may lead to more potent inhibitors of LpxD that are not substrates for the multi-drug efflux pump, TolC.

The synergy seen between 6359-0284 and Fosfomycin (a phosphonate-based antimicrobial) suggested that decrease in lipid A content may increase the bioavailability of Fosfomycin. This possibility is interesting since normally Fosfomycin must be actively transported into the cell via the glycerol phosphate transporter (33). Lipid A inhibitors may open a window of opportunity for the use of phosphate-based chemotherapeutics which would otherwise have little chance of traversing the outer cell membrane without some sort of active transport mechanism (34). Thus, further synergy experimentation with phosphate containing compounds should be conducted in combination with 6359-0284, as well as with other inhibitors of lipid A biosynthesis.

An alternative hypothesis for the synergy may be caused by an increase of toxic lipid A intermediates beyond the first committed step (LpxC). Fosfomycin is a natural product inhibitor of MurA (33,35), the first step in peptidoglycan biosynthesis (Figure 5.8). Inhibition of MurA would result in the build-up of UDP-GlcNAc, the common precursor for lipid A and peptidoglycan, which may be shunted towards lipid A biosynthesis. Since LpxD is beyond the first committed step, inhibition of this enzyme would sequester intermediates derived from UDP-GlcNAc, and accumulate detergent-like compounds (UDP-3-*O*-(*R*-3-hydroxyacyl)-GlcN) that are hypothesized to be toxic to the microbe. This scenario also raises questions of if, and how the processes of peptidoglycan biosynthesis and lipid A are regulated with regards to one another? Ogura *et. al*. displayed that the FtsH protease regulates LpxC with regards to fatty acid biosynthesis and phospholipid biosynthesis (36), but similar questions regarding peptidoglycan and lipid A biosynthesis have not been asked.

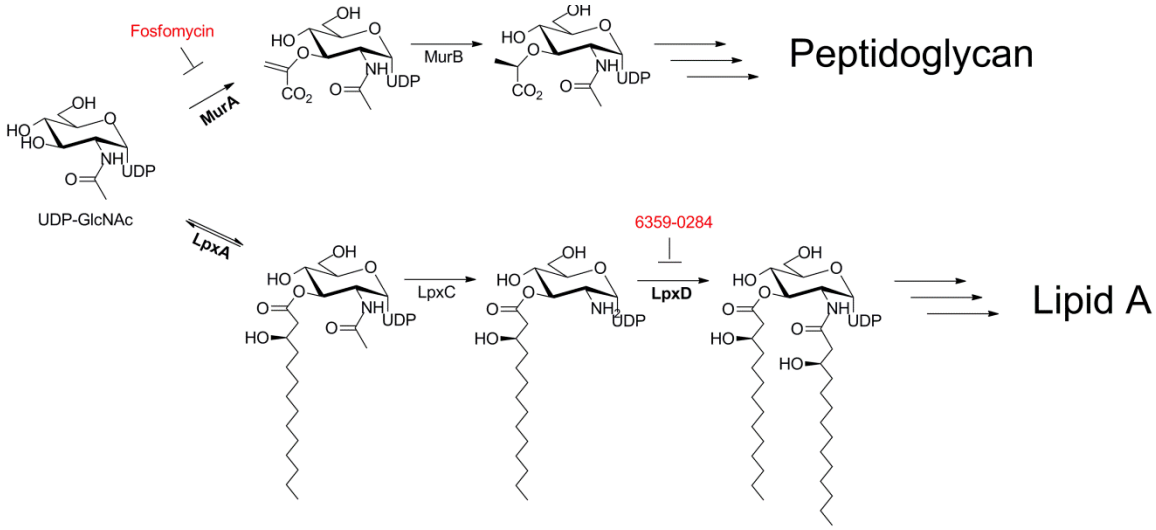

Figure 5.8. Lipid A and peptidoglycan biosynthesis. Both lipid A and peptidoglycan are synthesized from the precursor UDP-GlcNAc. Fosfomycin (red) inhibits the first step of peptidoglycan biosynthesis, whereas 6359-0284 (red) inhibits the third step of lipid A biosynthesis. LpxD is beyond the first committed step (LpxC) and may sequester UDP-GlcNAc away from peptidoglycan.

Our observations warrant further research and exploration with regards to the regulation between the peptidoglycan and lipid A biosynthetic pathways. While temperature sensitive mutants have been a boon in identifying the genes within the lipid A pathway, they require a global physiological change to decrease the quantities of lipid A (37-40). The membrane stress response is intimately tied to the heat shock response, and thus increasing temperature could adversely affect the integrity of these experiments (41,42). These inhibitors could be utilized to address the effects on peptidoglycan when lipid A biosynthesis is decreased, without a global physiological change. In combination with LpxC inhibitors, this question could further be elaborated on to explore how peptidoglycan is affected when lipid A is inhibited before and after the first committed step. This would be an important experiment as inhibition of LpxC may alter the flux of UDP-GlcNAc towards the peptidoglycan biosynthetic pathway, whereas 6359-0284 may alter the flux away from peptidoglycan biosynthesis.

The inhibitors discovered in this study should allow for a fundamental understanding of whether UDP-3-*O*-(*R*-3-hydroxyacyl)-GlcN associates with the inner membrane at high concentrations. It has been previously shown that inner and outer membrane ratios of lipid A are altered with lipid A lacking all secondary acyl chains (43). These mutants can grow below 32 °C, but have a drastic increase in the ratio of lipid A to phospholipids in the inner membrane. However, it is poorly understood how lipid A precursors affect inner membrane protein folding and activity. Inhibitors of early lipid A biosynthesis could be utilized in conjunction with these mutants to probe the effect of the accumulation of lipid A intermediates on inner membrane proteins. *In vitro* studies on the function of *E. coli* membrane proteins reconstituted in lipid nanodiscs supports the notion that catalytic activity is heavily dependent on the type of lipid introduced into the disc (44,45). Therefore, studying the accumulation of these intermediates may provide novel insights into both protein structure and function, as well as how microbes regulate membrane homeostasis through activation or deactivation of various membrane proteins under different lipid conditions. Thus, while our inhibitors will find utilization towards future medicinal chemistry efforts, they may also be used to answer intriguing biological questions.

Acknowledgements/Contributions

This research was supported in part by a Valteich Research Award administered by the College of Pharmacy, University of Michigan and by a Pre-Doctoral Research Grant administered by the University of Michigan Rackham Graduate School. R.J.J was supported in part by the University of Michigan Chemistry-Biology Interface (CBI)

training program (NIH), grant number 5T32GM008597-14, an American Foundation for Pharmaceutical Education fellowship and a Rackham Predoctoral Research Fellowship.

This work was completed with the assistance of multiple individuals. Kyle Heslip assisted in large batch purifications of LpxD for screening, Steve vander Roest assisted in the plating of the compounds for screening, Dr. Paul Kirchoff triaged all the compound hits, Martha Larsen assisted in planning experiments and triaging all the compounds and Aaron Beeler and John Porco synthesized and provided compound CMLD00031 and its stereoisomer for testing beyond the HTS.

References

1. Rock, C. O., and Cronan, J. E., Jr. (1979) *J. Biol. Chem.* **254**, 9778-9785
2. Pugh, E. L., and Wakil, S. J. (1965) *J. Biol. Chem.* **240**, 4727-&
3. Smith, S., Witkowski, A., and Joshi, A. K. (2003) *Progress in Lipid Research* **42**, 289-317
4. Chakravarty, B., Gu, Z., Chirala, S. S., Wakil, S. J., and Quiocho, F. A. (2004) *Proc. Natl. Acad. Sci. U. S. A.* **101**, 15567-15572
5. Faergeman, N. J., and Knudsen, J. (1997) *Biochem. J.* **323**, 1-12
6. White, S. W., Zheng, J., Zhang, Y.-M., and Rock, C. O. (2005) *Annu. Rev. Biochem.* **74**, 791-831
7. Zhang, Y.-M., and Rock, C. O. (2008) *Journal of Lipid Research* **49**, 1867-1874
8. Campbell, J. W., and Cronan, J. E. (2001) *Annual Review of Microbiology* **55**, 305-332
9. Staunton, J., and Weissman, K. J. (2001) *Natural Product Reports* **18**, 380-416
10. Parsek, M. R., Val, D. L., Hanzelka, B. L., Cronan, J. E., and Greenberg, E. P. (1999) *Proc. Natl. Acad. Sci. U. S. A.* **96**, 4360-4365
11. Williams, A. H., Immormino, R. M., Gewirth, D. T., and Raetz, C. R. H. (2006) *Proc. Natl. Acad. Sci. U. S. A.* **103**, 10877-10882
12. Jenkins, R. J., and Dotson, G. D. (2012) *ACS Chem. Biol.* **7**, 1170-1177
13. Yin, H., and Hamilton, A. D. (2005) *Angewandte Chemie International Edition* **44**, 4130-4163
14. Minter, A. R., Brennan, B. B., and Mapp, A. K. (2004) *J. Am. Chem. Soc.* **126**, 10504-10505
15. Byers, D. M., and Gong, H. (2007) *Biochemistry and Cell Biology-Biochimie Et Biologie Cellulaire* **85**, 649-662
16. Charifson, P. S., Grillot, A.-L., Grossman, T. H., Parsons, J. D., Badia, M., Bellon, S., Deininger, D. D., Drumm, J. E., Gross, C. H., LeTiran, A., Liao, Y., Mani, N., Nicolau, D. P., Perola, E., Ronkin, S., Shannon, D., Swenson, L. L., Tang, Q., Tessier, P. R., Tian, S.-K., Trudeau, M., Wang, T., Wei, Y., Zhang, H., and Stamos, D. (2008) *Journal of Medicinal Chemistry* **51**, 5243-5263
17. Jenkins, R. J., and Dotson, G. D. (2012) *Analytical Biochemistry* **425**, 21-27
18. Baba, T., Ara, T., Hasegawa, M., Takai, Y., Okumura, Y., Baba, M., Datsenko, K. A., Tomita, M., Wanner, B. L., and Mori, H. (2006) *Mol Syst Biol* **2**
19. Orhan, G., Bayram, A., Zer, Y., and Balci, I. (2005) *Journal of Clinical Microbiology* **43**, 140-143
20. Beaver, D. J., Roman, D. P., and Stoffel, P. J. (1957) *J. Am. Chem. Soc.* **79**, 1236-1245
21. Zhang, J.-H., Chung, T. D. Y., and Oldenburg, K. R. (1999) *Journal of Biomolecular Screening* **4**, 67-73
22. Benson, R. E., Gottlin, E. B., Christensen, D. J., and Hamilton, P. T. (2003) *Antimicrob. Agents Chemother.* **47**, 2875-2881
23. Coan, K. E. D., and Shoichet, B. K. (2008) *J. Am. Chem. Soc.* **130**, 9606-9612
24. McGovern, S. L., Caselli, E., Grigorieff, N., and Shoichet, B. K. (2002) *Biochemistry* **41**, 8967-8967
25. Vuorio, R., and Vaara, M. (1992) *Antimicrob. Agents Chemother.* **36**, 826-829

26. Vaara, M., and Nurminen, M. (1999) *Antimicrob. Agents Chemother.* **43**, 1459-1462
27. Renau, T. E., Léger, R., Flamme, E. M., Sangalang, J., She, M. W., Yen, R., Gannon, C. L., Griffith, D., Chamberland, S., Lomovskaya, O., Hecker, S. J., Lee, V. J., Ohta, T., and Nakayama, K. (1999) *Journal of Medicinal Chemistry* **42**, 4928-4931
28. Tegos, G., Stermitz, F. R., Lomovskaya, O., and Lewis, K. (2002) *Antimicrob. Agents Chemother.* **46**, 3133-3141
29. Vaara, M. (1993) *Antimicrob. Agents Chemother.* **37**, 2255-2260
30. Vaara, M. (1993) *Antimicrob. Agents Chemother.* **37**, 354-356
31. Weissberger, A., and Porter, H. D. (1942) *J. Am. Chem. Soc.* **64**, 2133-2136
32. Quiroga, J., Mejia, D., Insuasty, B., Abonia, R., Nogueras, M., Sanchez, A., Cobo, J., and Low, J. N. (2001) *Tetrahedron* **57**, 6947-6953
33. Kahan, F. M., Kahan, J. S., Cassidy, P. J., and Kropp, H. (1974) *Annals of the New York Academy of Sciences* **235**, 364-386
34. Patrone, J. D., Yao, J., Scott, N. E., and Dotson, G. D. (2009) *J. Am. Chem. Soc.* **131**, 16340-+
35. Skarzynski, T., Mistry, A., Wonacott, A., Hutchinson, S. E., Kelly, V. A., and Duncan, K. (1996) *Structure* **4**, 1465-1474
36. Ogura, T., Inoue, K., Tatsuta, T., Suzaki, T., Karata, K., Young, K., Su, L.-H., Fierke, C. A., Jackman, J. E., Raetz, C. R. H., Coleman, J., Tomoyasu, T., and Matsuzawa, H. (1999) *Molecular Microbiology* **31**, 833-844
37. Galloway, S. M., and Raetz, C. R. H. (1990) *J. Biol. Chem.* **265**, 6394-6402
38. Kelly, T. M., Stachula, S. A., Raetz, C. R. H., and Anderson, M. S. (1993) *J. Biol. Chem.* **268**, 19866-19874
39. Babinski, K. J., Kanjilal, S. J., and Raetz, C. R. H. (2002) *J. Biol. Chem.* **277**, 25947-25956
40. Takayama, K., Qureshi, N., Mascagni, P., Nashed, M. A., Anderson, L., and Raetz, C. R. (1983) *J. Biol. Chem.* **258**, 7379-7385
41. Dartigalongue, C., Missiakas, D., and Raina, S. (2001) *J. Biol. Chem.* **276**, 20866-20875
42. Missiakas, D., Mayer, M. P., Lemaire, M., Georgopoulos, C., and Raina, S. (1997) *Molecular Microbiology* **24**, 355-371
43. Vorachek-Warren, M. K., Ramirez, S., Cotter, R. J., and Raetz, C. R. H. (2002) *J. Biol. Chem.* **277**, 14194-14205
44. Amin, D. N., and Hazelbauer, G. L. (2012) *J. Biol. Chem.* **287**, 41697-41705
45. Dalal, K., Chan, C. S., Sligar, S. G., and Duong, F. (2012) *Proceedings of the National Academy of Sciences* **109**, 4104-4109

Chapter 6

Conclusion & Future Directions

Conclusion

My thesis work has encompassed the development of novel tools to study the lipid A biosynthetic pathway, along with the identification and molecular characterization of inhibitory probes targeting this pathway. Prior to our work, Raetz and co-workers had identified the first inhibitor of lipid A biosynthesis that targeted LpxC (1). With the exception of the identification of the *E. coli* LpxA selective peptide 920 (2,3), much focus in the field has involved the optimization of LpxC inhibitors (4-8). Most of the pathway has been largely ignored due to the lack of chemical and biological tools to probe the pathway for inhibitors.

In order to remedy the lack of tools to study lipid A biosynthesis, we developed a continuous enzyme assay that could monitor the turnover of LpxA and LpxD. While developing the enzyme assay, we had identified an inhibitory peptide, RJPXD33, that was found to target both LpxD and LpxA. Such dual targeting inhibitors offer the advantage of decreasing the likelihood of mutation-mediated resistance by necessitating mutations in more than one essential gene (9,10). In the same study, RJPXD33 and P920 were turned into chemical probes by linking a fluorescent marker on the peptides and performing fluorescence polarization (FP). This assay was more advantageous for use in high-throughput screening (HTS) efforts in comparison to the

continuous enzyme assay, as it does not require large quantities of the LpxD substrates, which are difficult to obtain.

We performed structural and biochemical studies to fundamentally understand how RJPXD33 is able to bind and inhibit both LpxA and LpxD. From the co-crystal structure of RJPXD33•LpxA and biochemical validation, we identified the minimal motif –TNLYML– that was required for binding to LpxA. While development of peptidomimetics from twelve amino acids may prove to be difficult, truncation to six amino acids provides an excellent starting point for the design and development of more potent small molecule analogues with increased bioavailability. Though we were unable to crystallize LpxD bound to RJPXD33, we utilized a photo-crosslinking strategy (11) to identify where RJPXD33 was binding to LpxD.

Using our newly developed tools, we were able to screen a large library of chemical compounds for disruption of the FITC-RJPXD33-LpxD complex. This assay allowed for rapid screening (~120,000 compounds in 5-6 days) and provided the first small molecule inhibitors of LpxD. Inhibitors were validated using the continuous enzyme assay and further tested for *in vivo* inhibition in Δ*tolC* deficient *E. coli*. Through an LpxD multi-copy suppressor approach, we provided support that the intracellular target of these inhibitors was LpxD. Synergy analysis provided evidence that these inhibitors could further be utilized in combination with existing antimicrobials to provide a synergistic increase in potency.

Future Directions

A methodology which allows for rapid and large-scale synthesis of the substrates of the early enzymes of lipid A is needed. While the LpxC substrate can be purchased at

$1000/mg, this is not plausible for many academic labs. Our attempts to produce an ACP recycling system produced only limited success. The temperature sensitive mutants of LpxC, LpxD and LpxH offer an avenue for large scale purification (12-14). Such efforts have been successful in producing lipid X in 0.1 – 1 g quantities (15). However, all substrates up until lipid X contain a UDP moiety which complicates the purification. An alternative approach to the LpxD substrate would entail chemical synthesis of the LpxC substrate, followed by enzymatic deacetylation. An existing synthesis exists, but relies on separation of diastereomers upon phosphorylation of the protected glucosamine ring (16). Much effort has been placed on developing phosphorylation and sugar chemistry since the initial publication (17,18). Our lab has confirmed that the phosphorylation of the anomeric hydroxyl of GlcNAc can be performed stereospecifically. However, the synthesis would still be ardous with more than seven steps and a final UMP morpholidation reaction which are generally low yielding. Thus both directions should be pursued in order produce a reliable method that can be scaled up.

Future work with design of peptidomimetics targeting LpxA will revolve around identifying the amino acids which contribute the highest binding affinity to LpxD/LpxA. A simple alanine scan can be performed with FITC-labeled mutants (19). Subsequent mutations of residues with unnatural amino acids should provide valuable information with regards to potency. A second approach should aim at stabilizing the structure of the peptide. Our biochemical data suggested that truncations beyond the sixth amino acid of the C-terminus may be increasing the flexibility of RJPXD33 and thereby decreasing binding affinity. Identification of sites which would allow for covalent linkage to minimize the flexibility of the peptide will be essential to the development of more potent

analogues. This may be accomplished through covalent linkage of the solvent exposed residues, or potentially through a hydrophobic linker between the threonine and leucine side chains. However, the latter may be difficult to achieve while maintaining the stereo-specificity required for the peptide to bind.

A fundamental understanding of how the small molecule inhibitors are binding to LpxD will be essential for a guided structure-activity relationship (SAR) campaign for increasing potency and bioavailability. A structural approach can be pursued; however an alternative approach would be the design of small molecule probes with photo-affinity labels to provide a platform for mapping interactions to LpxD, much like the strategy utilized to map peptide binding. RJPXD33 is twelve amino acids long, thus providing a very large surface area for binding to LpxD. The small molecules identified may be binding in different areas of the groove between two monomeric subunits, and thus exploration of these small molecules may identify two unique binding modalities. Such unique binding modalities offers the potential for linking two small molecules together to increase potency, much like that of Fragment Based Drug Discovery (FBDD) (20,21).

While our studies have been limited to *E. coli*, it will be essential to perform broad spectrum studies on LpxD/A enzymes from other organisms. The photo-activatable peptides synthesized in chapter 4 could be used as a tool to quickly identify whether or not these peptides bind to LpxD/LpxA from other organisms. Rather than purifying each enzyme individually one could potentially perform such studies on whole-cell lysates. Binding affinity could then be ascertained on purified enzymes with the FITC-labeled probes. Optimization of such an assay in *E. coli* will be a prerequisite step before these

studies can be achieved. This can be further expanded to small molecule inhibitory probes, as described above.

In all, our work has provided a fundamental framework towards the future development of clinically utilized lipid A inhibitors. Our FP assays have already been recognized by the pharmaceutical industry as powerful tools for screening chemical libraries against LpxA (22). Future efforts aimed at the development of peptidomimetics and SAR around the small-molecule inhibitors identified in chapter 5 may culminate in the identification of dual-targeting, cell permeable inhibitor of LpxD/LpxA. Thus this work should leave a lasting impact on the fields of both lipid A and medicinal chemistry.

References

1. Onishi, H. R., Pelak, B. A., Gerckens, L. S., Silver, L. L., Kahan, F. M., Chen, M. H., Patchett, A. A., Galloway, S. M., Hyland, S. A., Anderson, M. S., and Raetz, C. R. H. (1996) *Science* **274**, 980-982
2. Benson, R. E., Gottlin, E. B., Christensen, D. J., and Hamilton, P. T. (2003) *Antimicrob. Agents Chemother.* **47**, 2875-2881
3. Williams, A. H., Immormino, R. M., Gewirth, D. T., and Raetz, C. R. H. (2006) *Proc. Natl. Acad. Sci. U. S. A.* **103**, 10877-10882
4. Barb, A. W., Jiang, L., Raetz, C. R. H., and Zhou, P. (2007) *Proc. Natl. Acad. Sci. U. S. A.* **104**, 18433-18438
5. Barb, A. W., Leavy, T. M., Robins, L. I., Guan, Z. Q., Six, D. A., Zhou, P., Bertozzi, C. R., and Raetz, C. R. H. (2009) *Biochemistry* **48**, 3068-3077
6. Cole, K. E., Gattis, S. G., Angell, H. D., Fierke, C. A., and Christianson, D. W. (2011) *Biochemistry* **50**, 258-265
7. Jackman, J. E., Fierke, C. A., Tumey, L. N., Pirrung, M., Uchiyama, T., Tahir, S. H., Hindsgaul, O., and Raetz, C. R. H. (2000) *J. Biol. Chem.* **275**, 11002-11009
8. McClerren, A., Endsley, S., Bowman, J., Andersen, N., Guan, Z., and Rudolph, J. (2005) *Biochemistry* **44**, 16574-16583
9. Charifson, P. S., Grillot, A.-L., Grossman, T. H., Parsons, J. D., Badia, M., Bellon, S., Deininger, D. D., Drumm, J. E., Gross, C. H., LeTiran, A., Liao, Y., Mani, N., Nicolau, D. P., Perola, E., Ronkin, S., Shannon, D., Swenson, L. L., Tang, Q., Tessier, P. R., Tian, S.-K., Trudeau, M., Wang, T., Wei, Y., Zhang, H., and Stamos, D. (2008) *Journal of Medicinal Chemistry* **51**, 5243-5263
10. Cheng, J., Thanassi, J. A., Thoma, C. L., Bradbury, B. J., Deshpande, M., and Pucci, M. J. (2007) *Antimicrob. Agents Chemother.* **51**, 2445-2453
11. Majmudar, C. Y., Wang, B., Lum, J. K., Håkansson, K., and Mapp, A. K. (2009) *Angewandte Chemie International Edition* **48**, 7021-7024
12. Kelly, T. M., Stachula, S. A., Raetz, C. R. H., and Anderson, M. S. (1993) *J. Biol. Chem.* **268**, 19866-19874
13. Young, K., Silver, L. L., Bramhill, D., Cameron, P., Eveland, S. S., Raetz, C. R. H., Hyland, S. A., and Anderson, M. S. (1995) *J. Biol. Chem.* **270**, 30384-30391
14. Babinski, K. J., Kanjilal, S. J., and Raetz, C. R. H. (2002) *J. Biol. Chem.* **277**, 25947-25956
15. Raetz, C. R. H. (1992) [54] Lipid A disaccharide synthase from Escherichia coli. in *Methods in Enzymology* (Edward, A. D., and ennis, E. V. eds.), Academic Press. pp 455-466
16. Anderson, M. S., Robertson, A. D., Macher, I., and Raetz, C. R. H. (1988) *Biochemistry* **27**, 1908-1917
17. Sim, M., Kondo, H., and Wong, C. (1993) *J. Am. Chem. Soc.* **115**, 2260-2267
18. Ha, S., Chang, E., Lo, M.-C., Men, H., Park, P., Ge, M., and Walker, S. (1999) *J. Am. Chem. Soc.* **121**, 8415-8426
19. Haase, H. S., Peterson-Kaufman, K. J., Levengood, S. K. L., Checco, J. W., Murphy, W. L., and Gellman, S. H. (2012) *J. Am. Chem. Soc.* **134**, 7652-7655
20. Hajduk, P. J., Meadows, R. P., and Fesik, S. W. (1997) *Science* **278**, 497-&

21. Shuker, S. B., Hajduk, P. J., Meadows, R. P., and Fesik, S. W. (1996) *Science* **274**, 1531-1534
22. Shapiro, A. B., Ross, P. L., Gao, N., Livchak, S., Kern, G., Yang, W., Andrews, B., and Thresher, J. (2012) *Journal of Biomolecular Screening*

Appendix A

Peptide and Protein Purification Data

The following are protein purification gels for proteins used throughout our studies.

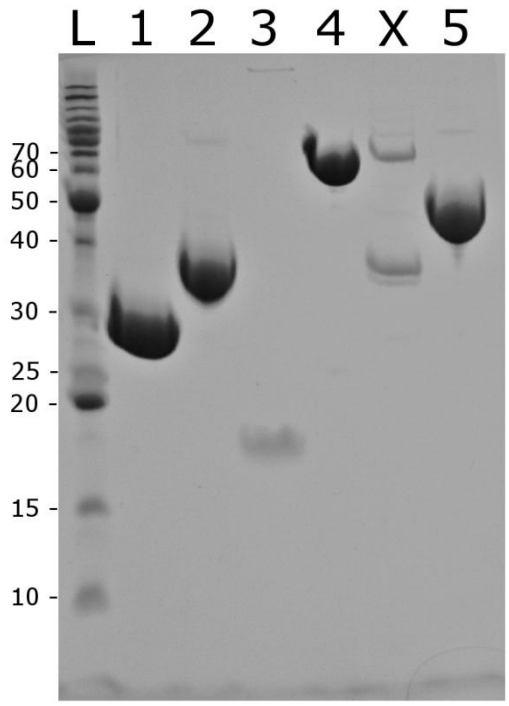

Figure A.1. Various urified proteins. L. Ladder (numbers indicate mass in kDa), 1. LpxA (8 μg) 2. N-His_6 LpxD (8 μg) 3. ACP (~0.8 μg) 4. *Vibrio harveyi* AasS (8 μg) 5. MurA (8 μg). Bands above 70 kDa in order: 80, 90, 100, 120, 160, 220 kDa.

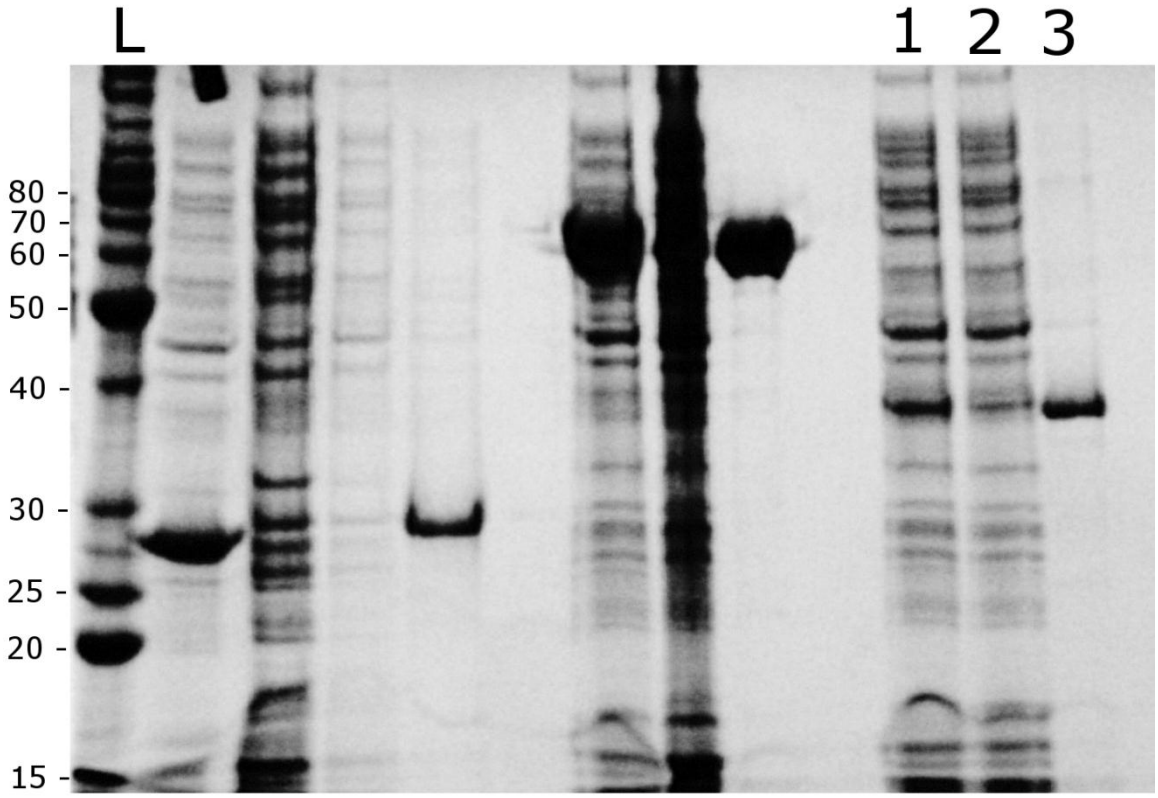

Figure A.2. LpxC protein purification. L. Ladder (numbers indicate mass in kDa) 1. Whole cell lysate before IMAC column. 2. Flow through of IMAC column. 3. Purified LpxC (~2.0 μg). Other proteins visualized are purifications for LpxA and *V. harveyi* AasS. Bands above 80 kDa in order: 90, 100, 120, 160, 220 kDa.

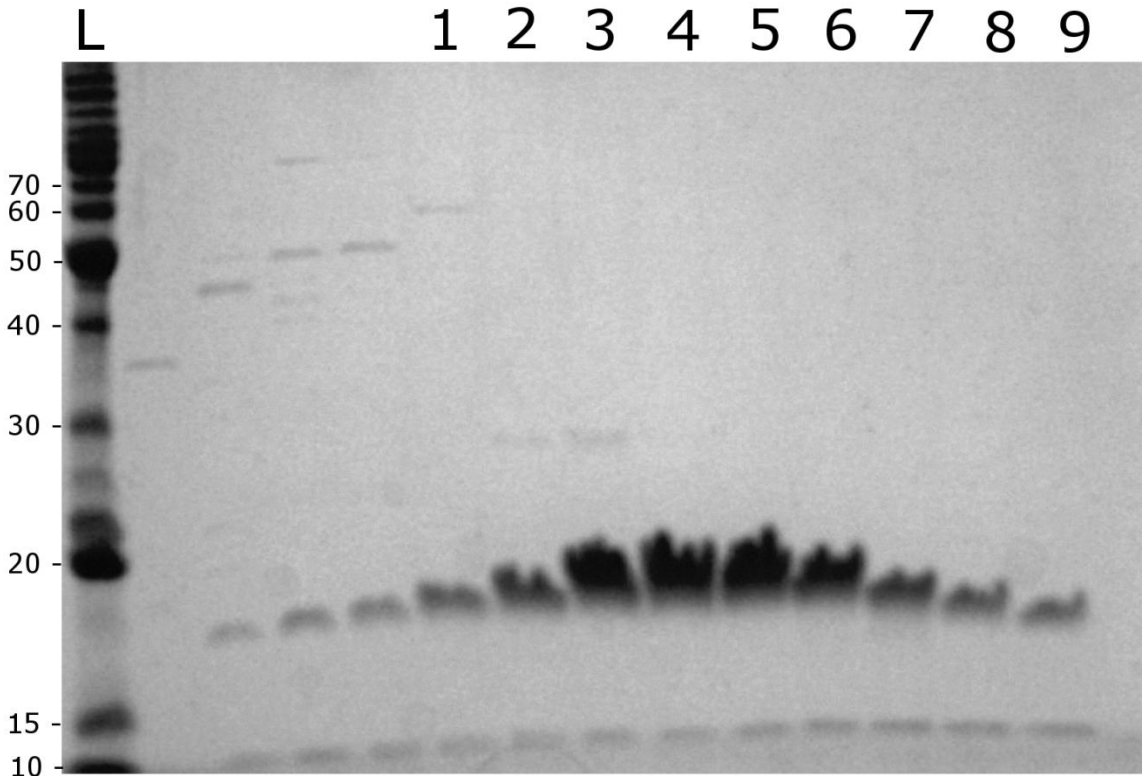

Figure A.3. ACP fractions following anion exchange. L. Ladder (numbers indicate mass in kDa) Fractions 1 – 9 were pooled and utilized for acylation reactions. Bands above 70 kDa in order: 80, 90, 100, 120, 160, 220 kDa. ACP is an 8.8 kDa protein that has been shown to run at approximately 19 – 20 kDa due to an extended stokes radius (1). ACP molecular weight was verified by MS.

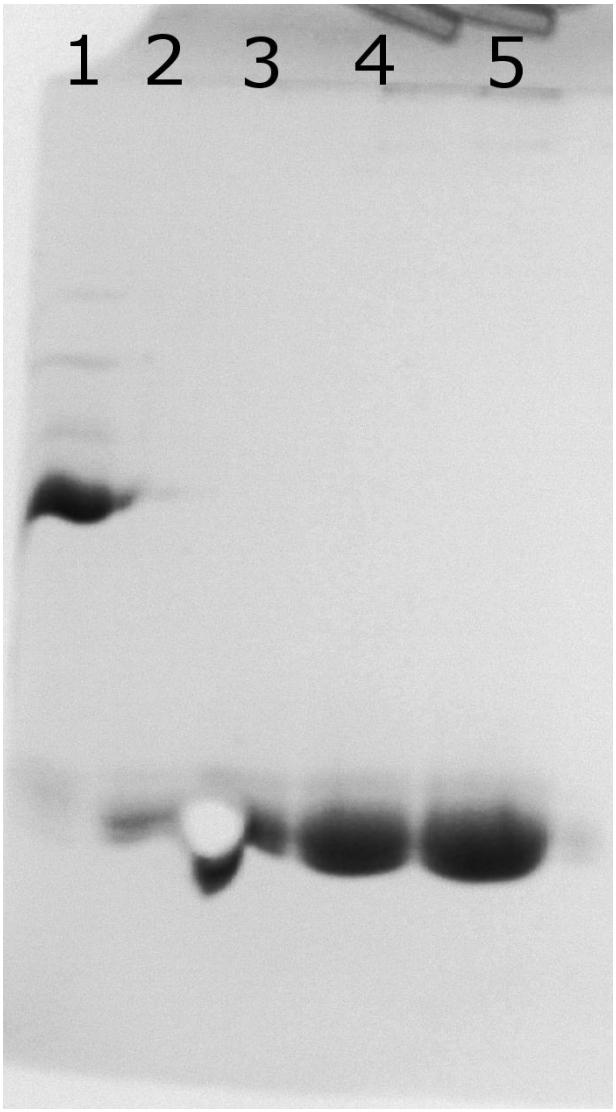

Figure A.4. Native Urea Gel for ACP acylation reaction. Conditions used were 15% native polyacrylamide gel containing 2 M Urea. 1. Holo-ACP (5 mg) 2. *R*-3-hdroxyacyl-ACP (1 μg) 3. *R*-3-hdroxyacyl-ACP (2.5 μg) 4. *R*-3-hdroxyacyl-ACP (5 μg) 5. *R*-3-hdroxyacyl-ACP (10 μg)

Table A.1. Peptide Sequences and Masses

Name	Sequence	$[M+H]^+$ (Calc)	$[M+H]^+$ (Obs)
RJPXD31	QHFMVPDINDMQ-NH_2	1473.6613	1473.6605
RJPXD33	TNLYMLPKWDIP-NH_2	1489.7871	1489.7864
RJPXD34	SENNFMLPLLPL-NH_2	1386.7449	1386.7467
FITC-RJPXD33	FITC-β-TNLYMLPKWDIP-NH_2	1949.8600	1949.8535
FITC-P920	FITC-β-SSGWMLDPIAGKWSR-NH_2	2149.9258	2149.9299
FITC-RJPXD33Δ6	FITC-β-TNLYML-NH_2	1213.4692	1213.4682
RJPXD33CΔ5	TNLYMLP-NH_2	850.4491	850.4498
RJPXD33CΔ6	TNLYML-NH_2	753.3964	753.3965
RJPXD33CΔ7	TNLYM-NH_2	640.3123	640.3119
RJPXD33CΔ8	TNLY-NH_2	509.2718	509.2712
RJPXD33CΔ9	TNL-NH_2	346.2085	346.2082
RJPXD33NΔ1	NLYMLPKWDIP-NH_2	1388.7395	1388.741
RJPXD33NΔ2	LYMLPKWDIP-NH_2	1274.6965	1274.6964
RJPXD33NΔ3	YMLPKWDIP-NH_2	1161.6125	1161.6118
RJPXD33NΔ4	MLPKWDIP-NH_2	998.5491	998.5481
RJPXD33NΔ5	LPKWDIP-NH_2	867.5087	867.5079
RJPXD33NΔ6	PKWDIP-NH_2	754.4246	754.4246
FITC-Photo1	FITC-β-TNXYMLPKWDIP-NH_2	1961.8349	1961.8309
FITC-Photo2	FITC-β-TNLZMLPKWDIP-NH_2	1974.8665	1974.8640
FITC-Photo3	FITC-β-TNLYMXPKWDIP-NH_2	1961.8349	1961.8320
FITC-Photo4	FITC-β-TNLYMLPKWDXP-NH_2	1961.8349	1961.8298
Biotin-Photo1*	Biotin-C-β-TNXYMLPKWDIP-NH_2	2103.9998	2104.0001
Biotin-Photo3*	Biotin-C-β-TNLYMXPKWDIP-NH_2	2103.9998	2103.9959
Biotin-Photo4*	Biotin-C-β-TNLYMLPKWDXP-NH_2	2103.9998	2103.9957

β – β-alanine.

*Biotin is linked through a disulfide bond with the Cysteine side chain (*Chapter 4*).

References

1. Rock, C. O., and Cronan, J. E., Jr. (1979) *J. Biol. Chem.* **254**, 9778-9785